

Diss. ETH No.16336

# **One-dimensional Atomic Gases**

A dissertation submitted to the  
SWISS FEDERAL INSTITUTE OF TECHNOLOGY  
ZURICH

for the degree of  
Doctor of Natural Sciences

presented by  
HENNING MORITZ  
Dipl.-Phys., University of Heidelberg, Germany  
born 25.10.1974  
citizen of Germany

accepted on the recommendation of  
Prof. Dr. Tilman Esslinger, examiner  
Prof. Dr. Thierry Giamarchi, co-examiner

2006



---

# Kurzfassung

In dieser Arbeit werden Experimente vorgestellt, in denen es gelungen ist, die Quantenphysik eindimensionaler Systeme mit ultrakalten atomaren Gasen zu untersuchen. Mithilfe von optischen Gittern wird die Bewegungsfreiheit der Atome auf eine Dimension beschränkt, während in den transversalen Richtungen nur quantenmechanische Grundzustandsbewegungen erlaubt sind. Zusätzlich zur Dimensionalität kann auch die Stärke und das Vorzeichen der Wechselwirkung zwischen den Atomen verändert werden. Diese einzigartige Flexibilität erlaubt die präzise Untersuchung grundlegender Fragen der Festkörper- und Quantenphysik.

Der Zustand eines kinematisch eindimensionalen Bose Gases wurde durch die Messung der kollektiven Moden charakterisiert. Diese geben Auskunft über den Quantenzustand des Vielteilchensystems und belegen, daß ein eindimensionales Bose-Einstein Kondensat erzeugt wurde. Indem wir ein zusätzliches periodisches Potential entlang der Bewegungsrichtung anlegten, konnten wir in das Regime stark korrelierter Systeme vordringen: wir beobachteten den Übergang von einer eindimensionalen Supraflüssigkeit in den Mott-Isolator Zustand und charakterisierten ihn durch Messungen des Anregungsspektrums sowie der Kohärenzeigenschaften. Dabei fanden wir Anzeichen für verstärkt auftretende Quanten-Fluktuationen, die in eindimensionalen Systemen eine besondere Rolle spielen.

Die Verwendung von Feshbach-Resonanzen eröffnet die Möglichkeit, die Molekülbildung und die Streueigenschaften der Atome in einer Dimension zu untersuchen. In einer Dimension wurden schwach gebundene Dimere sowohl für positive als auch für negative Streulänge erzeugt und charakterisiert, während im dreidimensionalen Fall gebundene Zustände grundsätzlich nur für positive Streulänge existieren. Die gebundenen Zustände bei negativer Streulänge sind Besonderheiten des niederdimensionalen Systems und werden durch den starken radialen Einschluss im optischen Gitter stabilisiert. Neben der Molekülbildung ändern sich auch die Streueigenschaften drastisch. In diesem Zusammenhang wurde die  $p$ -Wellenstreuung untersucht, die aufgrund ihrer anisotropen Wechselwirkung besonders interessant ist. Durch die Spinausrichtung und Dimensionalität konnten gezielt einzelne Streukanäle unterdrückt werden. Die Experimente zu den Streueigenschaften und der Molekülbildung zeigen, daß sich die Zweikörperphysik in einer Dimension in grundlegender Weise von der in höheren Dimensionen unterscheidet.

---

Eindimensionale System nehmen einen besonderen Platz in der Vielteilchenphysik ein, da Wechselwirkung und Quantenfluktuationen eine dominierende Rolle spielen. Mit der Untersuchung des bosonischen Mott-Isolator Übergangs haben wir dieses faszinierende Gebiet betreten. Die in dieser Arbeit entwickelte Apparatur eignet sich in idealer Weise dazu, auch stark korrelierte fermionische Systeme zu erforschen. Eine besonders spannende Herausforderung stellt in diesem Zusammenhang die Beobachtung des BEC-BCS Übergangs in einer Dimension dar, der dort durch ein exakt lösbares Modell beschrieben wird.

---

# Abstract

In this thesis I present experiments which enabled us to explore the quantum physics of one-dimensional systems with ultracold atomic gases. Using optical lattices the motion of the atoms was restricted to one dimension, permitting only ground state oscillations in the transverse directions. In addition to the dimensionality, the strength and the sign of the interaction are adjustable. This unique tunability facilitates the investigation of fundamental issues of solid state and quantum theory.

A one-dimensional Bose gas was realised and characterised by measuring its lowest lying collective oscillations. The collective oscillations are a very sensitive probe of the state of the gas, proving that a one-dimensional Bose condensate was created. By applying a periodic potential in the direction of motion the regime of strongly correlated systems was entered: we observed the transition from a one-dimensional superfluid to a Mott insulator and characterised it by studying its excitation spectrum as well as the coherence properties. We detected signatures for increased fluctuations which are characteristic for one-dimensional systems.

Feshbach resonances offer the possibility to explore the effects of reduced dimensionality on the formation of molecules and the scattering properties of the atoms. We created and studied weakly bound dimers in one dimension which exist irrespective of the sign of the scattering length, contrary to the situation in free space. These confinement induced molecules are peculiar to the low dimensional system and are stabilised by the confining potential. The reduced dimensionality has also a profound influence on the scattering properties. We investigated the  $p$ -wave scattering, which is especially intriguing due to its anisotropic character. By controlling the symmetry and the dimensionality of the system a selective suppression of individual  $p$ -wave scattering channels was achieved.

One-dimensional systems occupy a special place in many-body physics because interactions and quantum fluctuations play a dominant role. With our studies of the bosonic Mott insulator transition we have entered this fascinating regime. The apparatus that was constructed in the course of this thesis is ideally suited to study also strongly correlated fermionic systems. A particularly exciting challenge in this context is the observation of the BCS-BEC crossover for which exactly solvable models exist in one dimension.



# Contents

<b>1</b>	<b>Introduction</b>	<b>1</b>
<b>2</b>	<b>Quantum degenerate gases in optical lattices</b>	<b>5</b>
2.1	Bose-Einstein condensation . . . . .	5
2.1.1	Bose-Einstein condensation in lower dimensions . . . . .	7
2.1.2	Interactions in Bose gases . . . . .	9
2.1.3	Experimental demonstration . . . . .	11
2.2	Degenerate Fermi Gases . . . . .	14
2.3	Optical lattices . . . . .	16
2.3.1	The dipole force . . . . .	17
2.3.2	Standing wave potentials . . . . .	18
2.3.3	Quantum mechanics in periodic potentials . . . . .	21
<b>3</b>	<b>The experimental setup</b>	<b>27</b>
3.1	Design considerations . . . . .	27
3.2	Magneto-optical trap . . . . .	30
3.2.1	Vacuum chamber . . . . .	31
3.2.2	Laser system . . . . .	32
3.3	Magnetic transport . . . . .	35
3.4	Evaporative cooling . . . . .	37
3.5	The lattice . . . . .	40
3.5.1	The lattice lasers . . . . .	40
3.5.2	The optical setup . . . . .	40

3.6	One experimental cycle . . . . .	42
3.6.1	Experiments with bosonic $^{87}\text{Rb}$ . . . . .	43
3.6.2	Experiments with fermionic $^{40}\text{K}$ . . . . .	45
<b>4</b>	<b>Realisation and characterisation of a 1D Bose gas</b>	<b>49</b>
4.1	Regimes of quantum degeneracy in 1D . . . . .	50
4.1.1	Phase diagram in a harmonic trap . . . . .	50
4.2	Creating a 1D Bose gas . . . . .	53
4.3	Collective excitations in 1D . . . . .	55
4.3.1	Theoretical prediction . . . . .	55
4.3.2	Experimental observation . . . . .	57
<b>5</b>	<b>Strongly interacting 1D Bosons – the Mott insulator</b>	<b>61</b>
5.1	Bose-Hubbard model . . . . .	61
5.2	Observing the superfluid to Mott insulator transition . . . . .	63
5.2.1	Excitation spectra . . . . .	63
5.2.2	Coherence properties . . . . .	66
5.3	A dimensional crossover . . . . .	68
5.4	Prospects for 1D Bose gases . . . . .	69
<b>6</b>	<b>Confinement induced molecules in a 1D Fermi gas</b>	<b>71</b>
6.1	Scattering Theory . . . . .	72
6.1.1	Feshbach resonances . . . . .	74
6.1.2	Molecule formation in the presence of 1D confinement . . . . .	77
6.2	Preparation of the strongly interacting 1D gas . . . . .	79
6.3	Radio-frequency spectroscopy . . . . .	80
6.4	Observation of confinement induced molecules . . . . .	81
6.5	Conclusion . . . . .	85
<b>7</b>	<b><math>p</math>-Wave interactions in low-dimensional Fermi gases</b>	<b>87</b>
7.1	$p$ -Wave Feshbach resonance . . . . .	88



## CONTENTS

---

7.1.1	Multiplet structure . . . . .	88
7.1.2	Scattering properties . . . . .	89
7.2	Geometric suppression of collisions . . . . .	90
7.2.1	Preparation of a spin-polarised 1D Fermi gas . . . . .	91
7.2.2	Three-dimensional Fermi gas . . . . .	93
7.2.3	Two-dimensional Fermi gas . . . . .	93
7.2.4	One-dimensional Fermi gas . . . . .	94
<b>8</b>	<b>Fermionic atoms in a three-dimensional lattice</b>	<b>97</b>
8.1	Imaging the Fermi-surface . . . . .	98
8.2	Interaction-induced coupling between bands . . . . .	100
<b>9</b>	<b>Conclusions and outlook</b>	<b>103</b>
<b>A</b>	<b>Atomic properties</b>	<b>105</b>
A.1	$^{87}\text{Rb}$ data . . . . .	105
A.2	$^{40}\text{K}$ data . . . . .	106
A.3	Physical constants . . . . .	108
	<b>Bibliography</b>	<b>109</b>
	<b>Publications during the PhD work</b>	<b>125</b>
	<b>Curriculum Vitae</b>	<b>127</b>
	<b>Danksagung</b>	<b>129</b>



---

# 1 Introduction

When the motion of the particles in a system is restricted to one dimension instead of the usual three, the properties of the system change in a fundamental and often counterintuitive manner. One striking observation is that with decreasing particle density a one-dimensional gas becomes more strongly interacting, contrary to the three-dimensional case. Moreover, quantum fluctuations preclude the existence of long-range order such as Bose-Einstein condensation [Hoh67]. This dominant role which interactions and fluctuations play in one dimension leads to fascinating effects such as the separation of spin and charge excitations or the pinning of the atoms to a Mott insulating state in an arbitrarily weak periodic potential [Büc03b].

This thesis presents the first realisation of one-dimensional atomic and molecular gases. The quantum degenerate gases offer an unprecedented amount of control: the sign and the strength of the interactions as well as the density can be adjusted. Moreover, the atoms in a one-dimensional Fermi gas be converted into weakly bound bosonic molecules. Exploiting these possibilities of control, fundamental issues of two- and many-body physics in low dimensions were investigated.

The strict conditions for achieving one-dimensional behaviour present a considerable challenge. Traps with very high radial trapping frequencies are necessary to reduce all radial motion to zero point oscillations. Besides, very low densities need to be achieved, otherwise the chemical potential exceeds the radial level spacing. We solved these problems by trapping the atoms at the intersection of two perpendicular standing wave light fields, so called optical lattices. The resulting interference pattern features very elongated field maxima in which the particles accumulate. The great advantage of the two-dimensional standing wave pattern is manifest in the extremely tight radial confinement of only a fraction of the optical wavelength. Moreover, the geometry makes it possible to study many copies of the one-dimensional system at the same time, thereby avoiding problems arising from the detection of low particle numbers.

Although a homogeneous one-dimensional gas cannot Bose condense at finite temperature [Hoh67], it is possible in the ensembles we prepared, due to the presence of a longitudinal harmonic trapping potential: the gas has a finite size, and condensation occurs when the length scale of density and phase fluctuations exceeds this size. We created a quantum degenerate one-dimensional Bose gas and characterised it by measuring its collective excitations.

When considering the behaviour of atoms in the one-dimensional traps, several questions arise. To begin with, one wonders whether the atoms may pass each other, seeing that the motion is restricted to one dimension. Noninteracting bosons, according to the laws of quantum mechanics, may pass one another. With increasing interaction strength, however, they transform into hard-core bosons, which are impenetrable. We explored this evolution by applying an additional periodic potential along the axis of the one-dimensional trap. This increases the effective mass, thereby enhancing the role of interactions. As the gas becomes more interacting, it undergoes a crossover to a strongly correlated Mott insulator. In one dimension, the quantum fluctuations are expected to affect this transition and to shift it to lower effective interaction strength than in higher dimensions. We observed this crossover in the experiment and saw signatures of the increased fluctuations by comparing it to the three-dimensional case.

With the realisation of one-dimensional behaviour, a problem gains importance that has been academic up to now: what is the effect of the reduced dimensionality on the collisional properties and on the molecule formation that may take place during collisions? We addressed this issue by employing Feshbach resonances, which enabled us to tune the scattering length. Feshbach resonances have recently gained significance in the manipulation of cold atomic gases, e.g. in the investigation of the BEC-BCS crossover. Yet until now they were only studied in situations in which the confinement plays no significant role. In this situation weakly bound molecules are formed at positive scattering.

The reduced dimensionality has a profound influence on the molecule formation: in a one-dimensional Fermi gas we observed two-particle bound states, which exist irrespective of the sign of the scattering length, in contrast to the situation in free space. Using radio-frequency spectroscopy, we investigated these fragile entities which are stabilised only by the strong confinement. The strongly interacting Fermi gas created in the course of this investigation represents a realisation of a tunable Luttinger liquid.

When considering collisions in reduced dimensions,  $p$ -wave interactions seem particularly intriguing due to their anisotropic character. They are predicted to give rise to fascinating phenomena such as  $p$ -wave superfluidity and the mapping of strongly interacting one-dimensional fermions to noninteracting bosons. The asymptotic scattering states are restricted in reduced dimensions, and we observed that the symmetry and spin alignment affects the scattering: collisions with a particular projection of the angular momentum on the quantisation axis are completely suppressed in one dimension, whereas all  $p$ -wave scattering vanishes in a three-dimensional lattice.

It is the combination of Feshbach resonances with optical lattices which makes our experiment unique. While the optical lattices permit us to create condensed matter systems of arbitrary dimensionality, the control over the interactions opens up the path leading to the wealth of physical phenomena within the strongly correlated regime. In order to demonstrate the wide range

---

of possibilities, the first studies of a Fermi gas in a three-dimensional lattice are presented here. They reveal the great versatility of the experiment as a simulator of quantum many-body models. The particular focus of this thesis is put on one-dimensional quantum gases, whereas the related thesis of my coworker Thilo Stöferle concentrates more on the investigation of strongly correlated phenomena in 3D lattices.

## Outline of this thesis

- A short introduction to the theory of ultracold gases in optical lattices is given in chapter 2. It deals with Bose-Einstein condensation in three and one dimensions as well as with degenerate Fermi gases. Furthermore, the theory of optical dipole potentials and quantum mechanics in optical lattices is presented. The experimental setup built in the course of this thesis is described in the third chapter. It includes a step by step account of the experimental procedure used to cool atomic gases to quantum degeneracy and to load them into optical lattices.
- The experiments with one-dimensional bosonic atoms are reported in chapters 4 and 5. These include the creation of a one-dimensional Bose condensate and its characterisation by measuring its collective excitations as well as the observation of the transition to the Mott insulator state. The complementary methods which are employed to study the transition are explained and the results discussed.
- From the sixth chapter onwards, all the experiments are performed with fermionic  $^{40}\text{K}$  atoms. Using Feshbach resonances, which are explained in detail, confinement induced molecules in a one-dimensional Fermi gas are formed. The unique properties of these dimers are investigated in chapter 6 with radio-frequency spectroscopy and compared to the predictions of two-body theory. Chapter 7 focuses on  $p$ -wave scattering in low dimensions, where distinct structures are observed, depending on the dimensionality and symmetry of the system,
- Chapter 8 does not deal with a one-dimensional gas: instead, the properties of a Fermi gas in a three dimensional optical lattice are investigated and its Fermi surfaces are imaged. This chapter is meant to broaden the scope of the thesis and point out capabilities of our setup which will be important for the future direction of research.



---

## 2 Quantum degenerate gases in optical lattices

As the temperature is decreased, the quantum mechanical properties of dilute gases begin to play an important role. At sufficiently low temperatures the wave packets of the individual atoms start to overlap and the gas becomes quantum degenerate. For atoms in a harmonic trap the occupation probability of low-lying trap states approaches unity.

Ultimately, the cooling of dilute alkali gases has led to the spectacular observation of Bose-Einstein condensation [And95, Dav95a] in 1995. In this novel state of matter, which was already predicted by Einstein [Ein25] in 1925, following on the work on photons by Bose [Bos24], the occupation of the ground state of the system becomes macroscopic and the corresponding wavefunction displays long-range coherence. Unmatched control over momentum and position of the atoms is attained, limited only by the uncertainty principle.

Recently, quantum degenerate gases have been loaded into the periodic potential of a standing wave produced by laser light. The physics of the cold gas in the crystal structure of such an optical lattice changes fundamentally, and concepts from solid state physics such as the Bloch functions become relevant. This chapter deals with the essential theoretical prerequisites for understanding the behaviour of quantum degenerate gases in optical lattices. For further details the reader is referred to the textbooks by Pitaevskii and Stringari [Pit03] as well as by Pethick and Smith [Pet02].

### 2.1 Bose-Einstein condensation

Bose-Einstein condensation is an important paradigm of statistical mechanics. For a Bose gas in a trap, the occupation probability of each energy level  $E_i$  is determined by the Bose distribution function

$$N(E_i, \mu) = \frac{1}{e^{\frac{E_i - \mu}{k_B T}} - 1}, \quad (2.1)$$

where the chemical potential  $\mu$  is determined by the condition that the sum over all possible energy levels be normalised to the total particle number  $N = \sum_i N(E_i, \mu)$ . The chemical

potential must always be smaller than the energy of the lowest trap level  $E_0$ , with the latter being set to zero. As the temperature  $T$  is lowered, the chemical potential  $\mu$  must approach zero from below in order to fulfill the condition; consequently the occupation number of the ground state becomes macroscopic. If the temperature  $T$  greatly exceeds the energy level spacing, the changes in the Bose distribution function become small and the sum can be replaced by the integral

$$N = N_0 + \int_0^\infty D(\varepsilon) N(\varepsilon, \mu) d\varepsilon. \quad (2.2)$$

Here  $D(\varepsilon) = \frac{\varepsilon^2}{2(\hbar\omega)^3}$  is the density of states for the isotropic three-dimensional harmonic oscillator with trapping frequency  $\omega$ , which we will consider in the following. As the density of states vanishes for  $\varepsilon \rightarrow 0$ , the ground state contribution  $N_0 = N(E_0 = 0, \mu)$  has to be accounted for separately. The integral represents the number of excited atoms and its maximum value, which is reached for  $\mu = 0$ , is finite and decreases with temperature. Once the temperature is reduced below the critical value  $T_c$  given by

$$N = \int_0^\infty \frac{\varepsilon^2}{2(\hbar\omega)^3} \frac{1}{e^{\frac{\varepsilon}{k_B T_c}} - 1} d\varepsilon = \zeta(3) \left( \frac{k_B T_c}{\hbar\omega} \right)^3, \quad (2.3)$$

the excited states cannot accommodate all the atoms any more and the ground state occupation becomes macroscopic. The transition temperature can be found by solving equation (2.3):

$$T_c = \frac{\hbar\omega}{k_B} \left( \frac{N}{\zeta(3)} \right)^{1/3}. \quad (2.4)$$

### A macroscopic wavefunction with long-range order

At zero temperature and for weak interactions all particles are condensed into the ground state and each particle is described by the same single particle wavefunction  $\phi(\mathbf{r})$ . The resulting many-body wavefunction can be written as a product wavefunction

$$\psi_N(\mathbf{r}_1, \mathbf{r}_2, \dots, \mathbf{r}_N) = \prod_{i=1}^N \phi(\mathbf{r}_i). \quad (2.5)$$

It is convenient to describe the Bose-Einstein condensate by a macroscopic wavefunction which also represents the order parameter of the system [Leg01]

$$\psi(\mathbf{r}) = \sqrt{N_0} \phi(\mathbf{r}). \quad (2.6)$$

This is just the wavefunction of a single particle in the ground state with the normalisation adjusted so that the particle density is given by  $n(\mathbf{r}) = |\psi(\mathbf{r})|^2$ . Alternatively the wavefunction can be written as  $\psi(\mathbf{r}) = \sqrt{n(\mathbf{r})} e^{iS(\mathbf{r})}$  with  $S(\mathbf{r})$  being the phase of the condensate.



Penrose and Onsager [Pen56] proposed a general criterion for Bose-Einstein condensation which is of fundamental importance for the understanding of macroscopic quantum phenomena. It states that the existence of a condensate implies a non-vanishing value of the single particle density matrix  $\rho$  at large distances:

$$\rho(\mathbf{r}', \mathbf{r}) = \langle \hat{\psi}^\dagger(\mathbf{r}') \hat{\psi}(\mathbf{r}) \rangle \xrightarrow{|\mathbf{r}' - \mathbf{r}| \rightarrow \infty} \langle \hat{\psi}^\dagger(\mathbf{r}') \rangle \langle \hat{\psi}(\mathbf{r}) \rangle, \quad (2.7)$$

where  $\hat{\psi}$  and  $\hat{\psi}^\dagger$  are the bosonic field operators. In the framework of the “spontaneously broken gauge symmetry” [And66, Leg91, Leg95],  $\langle \hat{\psi}(\mathbf{r}) \rangle$  can be replaced by  $\psi(r)$ . To gain an intuitive understanding of this so-called “off-diagonal long range order”, we consider Bose-Einstein condensation in a homogeneous system. The macroscopic wavefunction in this case is  $\psi(\mathbf{r}) = \sqrt{n_0} e^{i\varphi}$ , where  $n_0$  is the condensate density and  $\varphi$  the spatially constant condensate phase. Consequently, the single particle density matrix  $\rho(\mathbf{r}, \mathbf{r}') = n_0$  does not vanish for large separations. The existence of off-diagonal long-range order according to equation (2.7) is equivalent to the phase coherence of the condensate at long distances, which is described by the first order correlation function  $g^{(1)}(\mathbf{r}', \mathbf{r}) \propto \langle \hat{\psi}^\dagger(\mathbf{r}') \hat{\psi}(\mathbf{r}) \rangle$ .

A Bose-Einstein condensate constitutes a coherent matter wave, and with the experimental realisation of Bose-Einstein condensation it has become possible to demonstrate the wavelike properties in a compelling set of experiments. Interference of two condensates was observed [And97] and the spatial coherence measured [Blo00]. In another experiment, a coherent atom laser beam was extracted from a Bose-Einstein condensate, the temporal coherence of which was demonstrated [Köh01].

### 2.1.1 Bose-Einstein condensation in lower dimensions

We have seen above that Bose-Einstein condensation seems feasible for a gas trapped in a three-dimensional harmonic oscillator potential; yet in other geometries the density of state changes. It has been proven by Hohenberg [Hoh67] that for a homogeneous one- or two-dimensional system long-range order and consequently a true Bose-Einstein condensate does not exist for finite temperature. Phase fluctuations gain importance in low-dimensional systems and destroy the long-range order.

The energy of each mode of the phase fluctuations with wavevector  $k$  is given by  $E_k \propto \omega(k)^2 |S_k|^2$  [Pit03]. The amplitudes  $S_k$  of the modes are the Fourier components of the phase  $S(\mathbf{r})$  of the wavefunction, where we assume  $S(\mathbf{r}) = 0$  without fluctuations. To estimate the total phase deviation we note that the energy residing in each mode is  $k_B T \propto \omega(k)^2 |S_k|^2$  due to equipartition and that the excitation spectrum is linear in  $k$  with  $\omega(k) = c k$  for low momenta.

The variance of the phase is then given by

$$\langle |S|^2 \rangle = \sum_k |S_k|^2 \propto \int_0^{k_{cut}} \frac{k_B T}{k^2} k^{d-1} dk, \quad (2.8)$$

where only low momenta smaller than a cutoff  $k_{cut}$  are relevant for the integral because at higher momenta  $\omega(k) \propto k^2$ . The integral diverges at its lower boundary  $k \rightarrow 0$  if the dimension  $d \leq 2$ . Hence, long wavelength phase fluctuations destroy the phase coherence at any  $T > 0$  in homogeneous two- or one-dimensional Bose gases.

A system of particular interest for this work is the trapped one-dimensional Bose gas. Due to the finite size of the system, the maximum wavelength of phase fluctuations is limited to the harmonic oscillator ground state extension  $a_r = \sqrt{\hbar/(m\omega)}$ , with  $m$  being the particle mass. Consequently, the divergence in the integral (2.8) is cut off. At sufficiently low temperatures phase fluctuations die out and long-range order on the length scale of the trapped sample is established.

To calculate the transition temperature and the number of particles in the ground state, we must evaluate the integral (2.2) with the density of states of the one-dimensional harmonic oscillator  $D(\varepsilon) = 1/(\hbar\omega)$ . This yields

$$N(T, 0) - N_0 = \int_{E_0}^{\infty} \frac{1}{\hbar\omega} \frac{1}{e^{\frac{\varepsilon}{k_B T}} - 1} d\varepsilon = -\frac{k_B T}{\hbar\omega} \ln(1 - e^{-\frac{E_0}{k_B T}}), \quad (2.9)$$

which diverges logarithmically with  $E_0 \rightarrow 0$ . In the harmonic oscillator the ground state has  $E_0 = \hbar\omega/2$  and the divergence is cut off. The ground state becomes macroscopically occupied below a transition temperature which is determined by

$$N(T, 0) = \frac{k_B T_c}{\hbar\omega} \ln \left( \frac{2k_B T_c}{\hbar\omega} \right), \quad (2.10)$$

assuming that  $\hbar\omega \ll k_B T$ . In contrast to the 3D case, the 1D transition temperature

$$k_B T_c \approx \frac{N}{\ln N} \hbar\omega \quad (2.11)$$

is significantly lower than the degeneracy temperature  $T_d \approx N\hbar\omega$ , at which the deBroglie wavelength equals the mean interparticle separation. The above results were first obtained by Ketterle and van Druten [Ket96] and extended to interacting gases by Petrov et al. [Pet00b, Pet04a].

To summarise, we have seen that despite the non-existence of a true Bose-Einstein condensate in a homogeneous 1D gas at finite temperature, condensation in a trapped 1D gas is possible.

### 2.1.2 Interactions in Bose gases

In a real atomic gas, particles interact with each other via the van der Waals forces. At the low temperatures considered here, the kinetic energy is too small to allow for any scattering process involving angular momentum. Only  $s$ -wave scattering occurs, which is independent of collision energy and angle. The information relevant for the scattering is contained in the  $s$ -wave scattering length  $a$ . In the Born approximation the interaction potential can be replaced by an effective contact interaction of the form

$$V_{int}(\mathbf{r}-\mathbf{r}') = g \delta(\mathbf{r}-\mathbf{r}') \quad \text{with } g = \frac{4\pi\hbar^2 a}{m}. \quad (2.12)$$

Until recently most experiments have been conducted with weakly interacting Bose gases where the scattering length is significantly smaller than the interparticle separation  $n^{1/3}$ . In this regime only the interactions between pairs of atoms have to be considered while simultaneous interactions between more than two atoms can be safely ignored. Nevertheless, the interaction energy exceeds the kinetic energy as the latter is exceedingly small in a condensate. Most properties of the condensate can be accounted for by incorporating the interactions into the Schrödinger equation with a mean-field term.

#### Gross-Pitaevskii equation

In a weakly interacting gas only binary interactions between atoms need to be considered. The Hamiltonian in second quantisation is

$$\begin{aligned} \hat{H} = & \int \hat{\psi}^\dagger(\mathbf{r}) \left( -\frac{\hbar^2}{2m} + V_{ext} \right) \hat{\psi}(\mathbf{r}) d\mathbf{r} \\ & + \int \hat{\psi}^\dagger(\mathbf{r}) \hat{\psi}^\dagger(\mathbf{r}') V_{int}(\mathbf{r}-\mathbf{r}') \hat{\psi}(\mathbf{r}') \hat{\psi}(\mathbf{r}) d\mathbf{r} d\mathbf{r}', \end{aligned} \quad (2.13)$$

where  $V_{ext}$  is the external trapping potential and  $\hat{\psi}(\mathbf{r})$  is the bosonic field operator. Bogoliubov [Bog47] introduced an important approximation by assuming that the condensate contribution to the bosonic field can be described by a classical field  $\psi(\mathbf{r})$  and fluctuations  $\delta\hat{\psi}$ . The former is the condensate wavefunction or order parameter already mentioned in earlier in this chapter. In the framework of a broken gauge symmetry the condensate wavefunction is the expectation value  $\psi(\mathbf{r}) = \langle \hat{\psi}(\mathbf{r}) \rangle$  of the field operator. The meaning of this approximation is that we neglect the quantum nature of the field operator and set its commutator to zero. In the limit of large the particle numbers  $N_0$ , this is reasonably well justified as the commutator  $[\hat{\psi}^\dagger, \hat{\psi}] = 1$  while  $\langle \hat{\psi} \rangle \simeq \sqrt{N_0}$ . In other words, the classical limit emerges for large particle numbers.

We can find the condensate wavefunction  $\psi(\mathbf{r})$  by minimising the energy (2.13) for  $\hat{\psi}(\mathbf{r}) = \psi(\mathbf{r}) + \delta\hat{\psi}(\mathbf{r})$  and enforcing particle conservation [Leg01]. We treat  $\delta\hat{\psi}(\mathbf{r})$  only as the variation

subject to which the energy has to be minimised, and set it to zero in the end. This yields the Gross-Pitaevskii equation [Gro61, Pit61]

$$\mu\psi(\mathbf{r}, t) = \left[ -\frac{\hbar^2}{2m}\nabla^2 + V_{ext}(\mathbf{r}) + g|\psi(\mathbf{r}, t)|^2 \right] \psi(\mathbf{r}, t). \quad (2.14)$$

The interactions appear in this nonlinear Schrödinger equation in a mean-field term proportional to the condensate density  $n(\mathbf{r}) = |\psi(\mathbf{r})|^2$ . The Gross-Pitaevskii equation has been very successful and describes many features of the condensate, for example the ground state extension, vortices and collective modes. To find the density distribution in the trap, the kinetic energy term, which is usually small compared to the interaction energy, is neglected. In this Thomas-Fermi approximation the wavefunction has the inverse form of the trapping potential

$$\psi(\mathbf{r}) = \max \left( \sqrt{\frac{\mu - V_{ext}(\mathbf{r})}{g}}, 0 \right) \quad (2.15)$$

However, the Gross-Pitaevskii formalism assumes that all particles condense into the many-body ground state  $\psi$  which is the product state of  $N$  single particle states. Therefore the microscopic correlations between particles are disregarded.

### Bogoliubov excitations

In the Gross-Pitaevskii equation all fluctuations  $\delta\hat{\psi}$  were ignored. The Bogoliubov theory (see [Pet02, Pit03]) takes these fluctuations in equation (2.13) into account and can therefore describe the elementary excitations of the Bose-Einstein condensate. The excitations behave like noninteracting quasi-particles which obey the dispersion relation

$$\epsilon(p) = \sqrt{(cp)^2 + \left( \frac{p^2}{2m} \right)^2}. \quad (2.16)$$

At small momentum they are phonon-like and the interactions determine the sound velocity  $c = \sqrt{gn/m}$ . At higher momenta the quasi-particles behave similar to free particles with  $\epsilon(p) \approx \sqrt{p^2/(2m) + gn}$ . The higher the temperature, the more of the elementary excitations exist. Yet even at zero temperature they do not disappear, leading to a quantum depletion of the number of atoms in the condensate  $N_0$  to [Pit03]

$$\frac{N_0}{N} = 1 - \frac{8}{3\sqrt{\pi}} \sqrt{na^3}. \quad (2.17)$$

In typical experiments with bosons in a harmonic trap, the gas parameter  $na^3$  is of the order of  $10^{-6}$ , and therefore the condition for a weakly interacting condensate is fulfilled and the quantum depletion is small. Recently, two avenues have opened up to access the strongly

interacting regime: In one approach, so called Feshbach resonances are used to increase the scattering length significantly (for experiments, see e.g. [Ino98, Cor00]). We have not accessed a Feshbach resonance in our experiments with bosons but will instead discuss them in detail in connection with the molecule formation in fermions in chapter 6.

The second pathway relies on the use of optical lattices. Jaksch et al. [Jak98] first conceived that by exposing ultracold atoms to the periodic potential of an optical lattice, the role of interactions can be enhanced to the point where the gas enters the Mott insulating phase. In a seminal experiment, Greiner et al. [Gre02] observed the superfluid to Mott insulator transition. The key idea is that the kinetic energy decreases continuously with increasing periodic potential depth due to the diminishing Bloch bandwidth. At the same time, the mutual interaction energy rises as the density distribution localises in the potential minima. We have employed this technique extensively: with bosons, we used it to study the excitations of weakly and strongly interacting superfluids [Sch04] and to induce the superfluid to Mott insulator transition in one dimension (chapter 5). The relevant theory of optical lattices will be treated in section 2.3.

### 2.1.3 Experimental demonstration

This short excursion links the concepts introduced in the preceding sections to experimental observations. One of the main attractions of experiments with Bose-Einstein condensates is that fundamental properties such as condensation, coherence and superfluidity become directly visible in images of the gases. Typically the atomic cloud is suddenly released from its trap and expands freely for some time. If the interactions during this expansion are negligible, the momentum information in the trap is mapped to the spatial distribution. The spatial distribution after the expansion is probed by a resonant laser pulse which is absorbed by the atoms. The resulting shadow is imaged onto a CCD chip. We will examine a few characteristic experimental pictures.

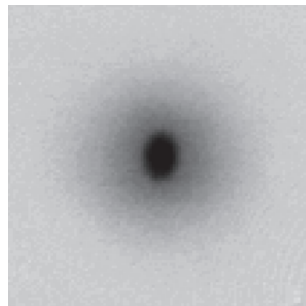


**Figure 2.1:** Absorption image of a partially condensed cloud after time of flight.

Figure 2.1 shows the spatial distribution of a partially condensed cloud after time of flight.

The condensate appears as a dense, elliptical core in the middle of the picture with a surrounding thermal cloud. Neglecting interactions, one would expect the momentum distribution of the condensate to be far smaller than observed here. However, as the interactions dominate the shape, the trapped cloud has the characteristic parabolic form given by the Thomas-Fermi distribution, which is the inverse of the trapping potential. Because the potential is anisotropic with different spatial trapping frequencies in this experiment, the condensate wavefunction takes on the form of a horizontally elongated ellipsoid. During the expansion, the repulsive interaction energy is converted into kinetic energy with faster growth in the direction in which it was initially more confined. After some time the aspect ratio is inverted. The thermal cloud, on the other hand, has a spherically isotropic momentum distribution in the trap and its interactions during the expansion are negligible. A spherical shadow in the absorption image is observed. This bimodal distribution is the standard signature for Bose-Einstein condensation.

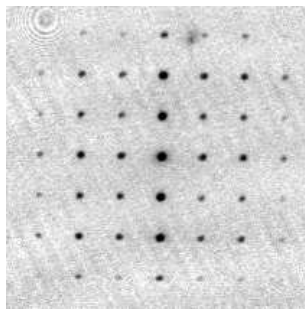


**Figure 2.2:** Diffraction of a coherent matter wave from a light grating.

The coherence of a condensate is illustrated in a striking way in figure 2.2. In this experiment, the condensate was diffracted from a potential grating prior to the expansion. In contrast to the usual diffraction of light from a solid grating, the roles of light and matter are reversed. Here, the grating is formed by the periodic potential of a standing wave light field, and the diffracted wave is a coherent matter wave, the Bose-Einstein condensate. Just before expansion, the periodic potential is switched on rapidly, giving a spatially varying phase shift to the matter wave, and the free expansion and imaging corresponds to the traditional observation of the interference pattern on a screen. The width of the interference peaks is determined by the coherence length of the condensate, although there is a minimal width given by the repulsive mean field.

Even though superfluidity and Bose-Einstein condensation are closely connected, they do not necessarily follow from one another [Hua95]. While Bose-Einstein condensation is an equilibrium property of the system, superfluidity is a kinetic property which requires the presence of interactions. Again, a direct observable for superfluidity in experiments exists: the presence of vortices provides a clear signature for superfluidity [Mat99]. In our experiment we were able

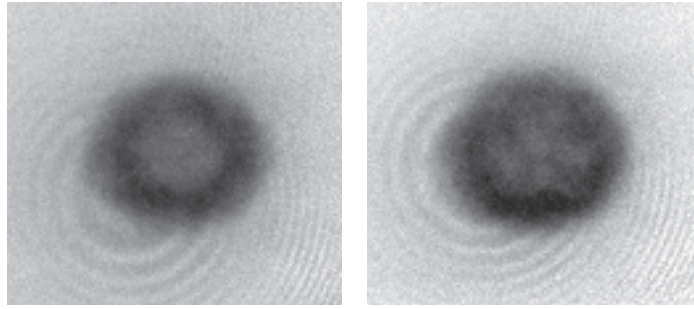


**Figure 2.3:** Vortices in a BEC. In the left panel, a giant vortex is visible, which probably has several quanta of angular momentum. In the right panel, a vortex lattice is just visible as a hexagonal pattern of lighter circles in the cloud

to produce vortices, as seen in figure 2.3.

## 2.2 Degenerate Fermi Gases

While bosons and fermions behave similarly in the classical limit, the Pauli principle plays a decisive role in cold quantum gases. In a spin-polarised gas  $s$ -wave scattering is forbidden, and cooling can only be achieved either in a spin-mixture of fermionic atoms or through sympathetic cooling with bosonic atoms. Once cooling has reduced the temperature to the point where the deBroglie wavelength approaches the interparticle separation, the Pauli principle affects the distribution of the atoms in the trap noticeably: the atoms fill all available energy levels up to the Fermi energy instead of condensing into the ground state.

The exact occupation of the trap levels is governed by the Fermi distribution function

$$f(\varepsilon) = \frac{1}{e^{(\varepsilon-\mu)/k_B T} + 1}. \quad (2.18)$$

The chemical potential  $\mu$  is determined from the total particle number conservation

$$N = \int_{\varepsilon=0}^{\infty} D(\varepsilon) f(\varepsilon) d\varepsilon. \quad (2.19)$$

In a cylindrically symmetric harmonic trap with a radial trapping frequency  $\omega_r$  and an axial trapping frequency  $\omega_z$  the density of states is given by  $D(\varepsilon) = \frac{\varepsilon^2}{2(\hbar\bar{\omega})^3}$  with  $\bar{\omega} = (\omega_z\omega_r^2)^{1/3}$ . The chemical potential changes with temperature and its value at  $T = 0$  is called the Fermi energy  $E_F$ . Integrating (2.19) at  $T = 0$  and solving for  $E_F$  yields

$$E_F = k_B T_F = \hbar\bar{\omega}(6N)^{1/3}, \quad (2.20)$$

which also defines the Fermi temperature  $T_F$ .

The momentum distribution of a noninteracting Fermi gas in a harmonic trap is always isotropic because the operators  $\hat{p}_x$ ,  $\hat{p}_y$  and  $\hat{p}_z$  enter the Hamiltonian

$$\hat{H} = \frac{1}{2m}(\hat{p}_x^2 + \hat{p}_y^2 + \hat{p}_z^2) + \frac{1}{2}m(\omega_r^2\hat{x}^2 + \omega_r^2\hat{y}^2 + \omega_z^2\hat{z}^2) \quad (2.21)$$

with the same coefficient. The coefficients of the position operators, on the other hand, reflect the symmetry of the trap, in this case cylindrical. Consequently the spatial distribution can be anisotropic. In the scaled coordinate  $\rho$  with magnitude  $\rho^2 = x^2 + y^2 + (\omega_z/\omega_r)^2 z^2$  this anisotropy is taken care of. The functional dependence of the distributions can be found when assuming a semi-classical phase space distribution  $w(\mathbf{r}, \mathbf{p})$  to describe the many-body wavefunction [But97, DeM01a]. The state of each atom is assigned a point  $\mathbf{r}$  and momentum  $\mathbf{p}$ . The atom number distribution in phase space is given by

$$w(\mathbf{r}, \mathbf{p}) = \frac{1}{(2\pi\hbar)^3} \frac{1}{e^{(H(\mathbf{r}, \mathbf{p})-\mu)/k_B T} + 1}. \quad (2.22)$$



When looking for the momentum distribution  $\Pi(\mathbf{p})$ , the atom number distribution must be integrated over space:

$$\Pi(\mathbf{p}) = \int d^3\mathbf{r} w(\mathbf{r}, \mathbf{p}) \quad (2.23)$$

$$= \left( \frac{1}{2\pi\hbar^2} \frac{k_B T}{m(w_z w_r^2)^{2/3}} \right)^{3/2} Li_{3/2} \left( -\mathfrak{z} e^{-\frac{p^2}{2mk_B T}} \right), \quad (2.24)$$

where  $\mathfrak{z} = e^{\mu/(k_B T)}$  is the fugacity and  $Li_n(-x) := \sum_{k=1}^{\infty} (-x)^k / k^n$  is the Poly-Logarithmic function of order  $n$ . Similarly, the density distribution is

$$n(\rho) = \left( \frac{mk_B T}{2\pi\hbar^2} \right)^{3/2} Li_{3/2} \left( -\mathfrak{z} e^{\frac{m\omega_r}{2k_B T} \rho^2} \right). \quad (2.25)$$

At zero temperature, the momentum and the density distribution simplify to the form of inverted parabolas, e.g.  $n(\rho) \propto 1 - (\rho/R_{TF})^2$  [But97] with  $R_{TF} = (48N\omega_z/\omega_r)^{1/6} \sqrt{\hbar/(m\omega_r)}$ .

Changes due to finite temperature only modify the wings of the position or momentum distribution. However, with the analytic form of the momentum distribution known, the temperature can be determined experimentally. The Fermi gas is released from its trap and expands freely. After a sufficient time of flight, the spatial distribution reflects the momentum distribution in the trap. Fitting the appropriate functional dependence, which can be calculated using equation (2.24) [DeM01a], yields the fugacity  $\mathfrak{z}$ . The latter is related to the temperature as

$$\frac{T}{T_F} = -(6 Li_3(-\mathfrak{z}))^{-1/3}. \quad (2.26)$$

This relation can be derived by integrating and rearranging equation (2.19) for  $T \geq 0$  and inserting the definition for  $E_F$  (eq. (2.20)).

Ultracold fermi gases have rapidly gained importance following the first production of a quantum degenerate Fermi gas [DeM99a]. A very clean fermionic system is now at the experimentalists' disposal, in which the occurrence of superfluidity is predicted [Sto96], similarly to  $^3\text{He}$ . However, the interactions need not be as strong as in  $^3\text{He}$ ; in fact, they can even be tuned [Lof02] by means of a magnetic field Feshbach resonance (see chapter 6.1.1). Moreover, Feshbach resonances enable the creation of bosonic molecules [Reg03b] from fermionic atoms, and the last two years have seen rapid progress in the field: molecular Bose-Einstein condensates were created [Gre03, Joc03b], and the pairing gap measured at the crossover from the BEC to the BCS regime [Chi04]. The observation of vortices [Zwi05] proved the superfluidity of these strongly interacting gases.

## 2.3 Optical lattices

Standing wave light fields offer great promise for the study of ultracold quantum gases. When a degenerate gas is loaded into the crystalline structure of the trapping potential, it realises an ideal model system for the investigation of solid state physics with quantum gases. The trapping potential is perfectly periodic and its strength is adjustable. Contrary to solid state systems, all important parameters, such as the filling, the interaction strength and the tunneling rate, can be changed at will. A feature of particular interest here is the possibility to reduce the dimensionality by suppressing tunneling processes in specific directions.

Research on atoms trapped in optical lattices has been marked by a constant decrease in temperature. Initially, the cooling mechanisms in dissipative standing waves formed the focus of attention. The first experiments observing the vibrational levels of atoms confined in multi-dimensional lattices were performed in 1993 [Hem93, Gry93]. When temperatures below the recoil temperature were reached, the wavelike properties of the atoms came to light: the de-Broglie waves extended over several lattice sites, enabling the observation of Bloch oscillations [Dah96].

With the advent of Bose-Einstein condensation, it was no longer necessary to cool the gas in the lattice as an extremely cold ensemble was at hand. After adiabatic loading of the condensate into the lattice, the ground state is populated without further cooling. In a single standing wave phenomena such as Josephson oscillations, tunneling and number-squeezing were observed [Cat01, And98, Orz01]. The first strongly correlated system was created through the combination of three-dimensional lattices with Bose-Einstein condensates. The observation of the quantum phase transition from a superfluid to a Mott insulator [Gre02] heralded the unique capabilities of the novel physical system.

It is particularly interesting to study quantum degenerate Fermi gases in optical lattices because fundamental questions of condensed matter physics may be addressed. However, it is technically challenging to bring fermionic gases to quantum degeneracy, which explains why the first experiments with them have only been performed very recently.

Experiments with fermionic atoms trapped in a single standing wave have revealed the insulating behaviour of a Fermi gas [Pez04] and collisionally induced transport [Ott04]. Moreover, gravity was measured by observing the Bloch oscillations of a cold Fermi gas in a lattice [Roa04]. The first studies of Fermi gases in two- and three-dimensional lattices will be presented in chapters 6-8.

### 2.3.1 The dipole force

Atoms were first trapped in the focus of a laser beam by Chu in 1986 [Chu86]. Nowadays, optical traps form a standard technique to confine neutral atoms; a review can be found in [Gri00]. They rely on the dipole force exerted on an atom by an inhomogeneous light field. The electrons and protons in an inhomogeneous light field experience an alternating electric field gradient, which induces a dipole moment  $\mathbf{d}$ . Once induced, the dipoles experience a force towards or away from the field maximum, depending on their orientation relative to the electric field gradient.

In a simple classical approach, the valence electron of an alkali atom can be regarded as a harmonic oscillator with a characteristic frequency given by the transition frequency  $\omega_0$  of the atom to the first excited level. If the detuning  $\Delta = \omega - \omega_0$  of the light field is small with respect to the atomic transition frequency, the near resonant excitation can polarise the atom very efficiently and the complex polarisability  $\alpha(\omega)$  is high. The induced dipole moment  $\mathbf{d} = \alpha(\omega)\mathbf{E}$  oscillates with the same frequency as the electric field  $E$  but not necessarily in phase. The potential depth  $V_{dip}$  can be found by integrating the force  $F_{dip}$

$$\begin{aligned} F_{dip}(\mathbf{r}) &= \mathbf{d} \cdot \nabla \mathbf{E}(\mathbf{r}) = \text{Re}[\alpha(\omega)] \mathbf{E}(\mathbf{r}) \nabla \mathbf{E}(\mathbf{r}) \\ \Rightarrow V_{dip}(\mathbf{r}) &= \frac{1}{2\epsilon_0 c} \text{Re}[\alpha(\omega)] I(\mathbf{r}), \end{aligned} \quad (2.27)$$

where  $I(\mathbf{r})$  is the intensity at position  $\mathbf{r}$  of the atom. Only the real part of the polarisability needs to be considered because only this part of the dipole moment is in phase with the electric field. The imaginary part, on the other hand, determines the amount of scattered light, with the photon scattering rate given by

$$\Gamma_{sc}(\mathbf{r}) = \frac{\dot{\mathbf{d}} \cdot \mathbf{E}}{\hbar\omega} = \frac{1}{\hbar\epsilon_0 c} \text{Im}[\alpha(\omega)] I(\mathbf{r}). \quad (2.28)$$

The polarisability can be calculated using Lorentz's model of a classical damped oscillator. Inserting this polarisability in equations (2.27) and (2.28) yields [Gri00]

$$V_{dip}(\mathbf{r}) = \frac{3\pi c^2}{2\omega_0^3} \left( \frac{\Gamma}{\omega - \omega_0} + \frac{\Gamma}{\omega + \omega_0} \right) I(\mathbf{r}) \approx \frac{3\pi c^2}{2\omega_0^3} \left( \frac{\Gamma}{\Delta} \right) I(\mathbf{r}) \quad (2.29)$$

$$\Gamma_{sc}(\mathbf{r}) = \frac{3\pi c^2}{2\hbar\omega_0^3} \left( \frac{\omega}{\omega_0} \right)^3 \left( \frac{\Gamma}{\omega - \omega_0} + \frac{\Gamma}{\omega + \omega_0} \right)^2 I(\mathbf{r}) \approx \frac{3\pi c^2}{2\hbar\omega_0^3} \left( \frac{\Gamma}{\Delta} \right)^2 I(\mathbf{r}), \quad (2.30)$$

with  $\Gamma$  being the damping rate on resonance. On the right hand side the rotating wave approximation was employed which is only correct if the detuning is small. For a red detuned ( $\Delta < 0$ ) trapping laser the dipole potential is attractive and the atoms accumulate at maxima of the electric field, e.g. the focus of a laser beam. Conversely, a blue detuned ( $\Delta > 0$ ) laser exerts a repulsive force on the atoms.

From a quantum mechanical point of view, the origin of the dipole potential becomes apparent when treating the problem with second order perturbation theory. The incoming light wave leads to an admixture of excited states to the ground state so that the energy shift is given by

$$\Delta E_i = \sum_{j \neq i} \frac{|\langle j | \hat{H}_{int} | i \rangle|^2}{E_i - E_j}. \quad (2.31)$$

The perturbing Hamiltonian is simply  $\hat{H}_{int} = -e \hat{\mathbf{r}} \mathbf{E}$ , with  $\hat{\mathbf{r}}$  being the position operator. If the saturation is small, the population of excited states is negligible. The atom resides mainly in the ground state, and only its energy shift  $\Delta E_0$  determines the potential felt by the atom. The result for the ground state energy shift  $\Delta E_0$  is identical with the classical result in equation (2.29). Corrections to the classical model only arise from the fact that several excited levels exist in reality. However, as long as the detuning is large compared to the fine and hyperfine splitting, these corrections can be ignored.

When considering which parameters to choose for an optical trap, it is important to bear in mind that for larger detunings the potential depth decreases with a  $1/\Delta$ -functional dependence (eq. (2.29)), while the scattering rate drops off much faster with  $1/\Delta^2$  (eq. (2.30)). Consequently it is preferable to work at large detunings, provided sufficient laser power is available to create an optical potential of the desired depth.

### 2.3.2 Standing wave potentials

When a Gaussian laser beam is retro-reflected, the interference between the counterpropagating beams gives rise to a standing wave pattern. If the laser frequency is smaller than the atomic transition, atoms can be trapped at the antinodes of the standing wave, the points with the highest field intensity. The individual field maxima have a pancake-like structure with the radial profile

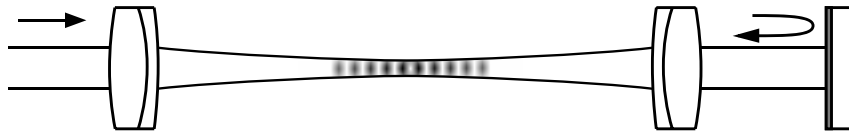


Figure 2.4:

determined by the Gaussian envelope of the laser beam. The optical lattice is created at the focus of two counterpropagating laser beams, as depicted in figure 2.4.

The lattice depth decreases when moving away from the focus position because of the increasing beam diameter. However, on the length scale of the atomic cloud this effect is usually so small that it can be ignored. The potential  $V_{1D}$  of a one-dimensional optical lattice is given

by

$$V_{1D}(x, y, z) = -V e^{-2\frac{x^2+y^2}{w^2}} \sin^2(kz) \quad (2.32)$$

with  $k = 2\pi/\lambda$  being the wavevector associated with the lattice laser wavelength  $\lambda$ .  $w$  stands for the beam waist, the radius at which the intensity has dropped of to  $1/e^2$  of its maximum value. The maximum potential depth  $V$  is four times higher than calculated with equation (2.29) for a running wave trap. This is caused by the constructive interference which doubles the electric field. In the rest of this thesis the potential depth of an optical lattice  $V = s \cdot E_r$  will always be referred to in units of the recoil energy  $E_r = \frac{\hbar^2 k^2}{2m}$ .

Higher dimensional periodic potentials can be created by adding a second or third optical lattice, which need to be at right angles to the others for cubic symmetry. Although the beams making up the different optical lattices might interfere with each other, this cross-interference usually does not have an effect on the atoms trapped in the lattices. This is due to the fact that the frequencies of the different optical lattices are chosen to be different. Then the cross-interferences change so quickly that their forces average to zero. Consequently, the potentials of several optical lattices simply add up independently.



**Figure 2.5:** The geometry of trapped 1D gases in a two-dimensional optical lattice. The spacing between the tubes is  $\lambda/2$ .

The case of two superimposed optical lattices is of particular interest here. Atoms trapped in the minima of the combined potential accumulate in elongated tubes as shown in figure 2.5. The atoms are confined radially to a fraction of the wavelength, while the relatively low longitudinal trapping frequency is caused by the lattice beam envelope. The potential  $V_{2D}$  of such a two-dimensional lattice is given by

$$V_{2D}(x, y, z) = -V_z e^{-2\frac{x^2+y^2}{w^2}} \sin^2(kz) - V_x e^{-2\frac{y^2+z^2}{w^2}} \sin^2(kx), \quad (2.33)$$

Close to the minima the potential can be accurately reproduced by a harmonic potential. If the optical lattices have the same depth in both directions with  $V_z = V_x \equiv sE_r$ , the harmonic

oscillator is characterised by a radial trapping frequency of  $\hbar\omega_r \simeq 2\sqrt{s}E_r$  and an axial trapping frequency of  $\hbar\omega_z \simeq 2\frac{\lambda}{\pi w}\sqrt{s}E_r$ . The aspect ratio  $\frac{\pi w}{\lambda}$  is determined only by the laser wavelength and the beam waist. It is important to bear in mind that the harmonic potential caused by the laser envelope is not only present in the direction of the tubes but also persists in the radial direction. Therefore the central tubes reach a lower minimum potential than the surrounding ones.

Optical lattices offer the unique possibility to change the dimensionality of a cold quantum gas. The motion in the longitudinal lattice direction can be restricted to zero point oscillations, provided the gas is cold enough. In a one-dimensional lattice the gas has two-dimensional features, whereas we manage to create one-dimensional gases in a two-dimensional lattice. Finally, the light field of three orthogonal standing waves results in point-like confinement. The array of potential wells in such a configuration resembles the cubic crystal structure known from solid state physics. The three-dimensional lattice potential is the sum of three individual optical lattices with respective depths  $V_x$ ,  $V_y$  and  $V_z$ :

$$\begin{aligned} V_{3D}(x, y, z) = & - V_x e^{-2\frac{y^2+z^2}{w_x^2}} \sin^2(kx) \\ & - V_y e^{-2\frac{z^2+x^2}{w_y^2}} \sin^2(ky) \\ & - V_z e^{-2\frac{x^2+y^2}{w_z^2}} \sin^2(kz), \end{aligned} \quad (2.34)$$

Moving away from the center, the depth of the wells decreases, which leads to a smaller oscillation frequency in each well and gives rise to an underlying harmonic potential. In our experiments, however, the radius of the region occupied by the atoms never exceeds a fifth of the laser waist. Consequently the trapping frequencies in the individual wells deviate by only a few percent over the extension of the cloud, which constitutes a negligible correction. The underlying harmonic potential, on the other hand, is important as it determines the size of the cloud in the lattice. Hence, the potential can be approximated as the sum of a homogeneous periodic potential and an additional external harmonic potential:

$$\begin{aligned} V_{3D}(x, y, z) = & - V_x \sin^2(kx) - V_y \sin^2(ky) - V_z \sin^2(kz) \\ & + \frac{1}{2}m(\omega_x x^2 + \omega_y y^2 + \omega_z z^2). \end{aligned} \quad (2.35)$$

The trapping frequency  $\omega_{\{x,y,z\}}$  in any of the three spatial directions is determined by the envelope of the two optical lattices perpendicular to it. For example,

$$\hbar\omega_x = \sqrt{2\left(\frac{\lambda}{\pi w_y} \frac{V_y}{E_r}\right)^2 + 2\left(\frac{\lambda}{\pi w_z} \frac{V_z}{E_r}\right)^2 + \omega_{ext,x}^2} E_r, \quad (2.36)$$

where  $\omega_{ext,x}$  describes a possible additional external potential.

### 2.3.3 Quantum mechanics in periodic potentials

Optical lattices constitute periodic potentials which can be treated with the methods originally developed for solid state physics. The characteristic feature of a periodic potential is the emergence of a band structure in the energy spectrum. The eigenfunctions  $\psi_{q,n}(x)$  of the Hamiltonian

$$\hat{H} = \frac{\hbar^2}{2m} \nabla^2 - V \sin^2(kx) \quad (2.37)$$

with periodicity  $d = \lambda/2$  must satisfy the Bloch theorem [Ash76]

$$\psi_{q,n}(x) = e^{iqx/\hbar} u_{q,n}(x) \quad \text{with} \quad u_{q,n}(x+d) = u_{q,n}(x). \quad (2.38)$$

The eigenfunctions are functions of the so-called quasimomentum  $q$ , which ranges from  $-k$  to  $+k$ ; there are several solutions belonging to the same  $q$ , denoted by the band index  $n$ . The wavefunctions have - up to a phase factor - the same periodicity as the lattice and are delocalised over the entire lattice. All the eigenenergies with the same band index  $n$  make up one energy band. In order to find these eigenenergies  $\varepsilon_{q,n}$ , it is useful to bear in mind that both the periodic potential and the  $u_{q,n}(x)$  share the same periodicity and can therefore be expanded into a Fourier series over all reciprocal lattice vectors  $2k \cdot \mathbb{Z}$ .

$$\psi_{q,n}(x) = e^{iqx/\hbar} \sum_{l \in \mathbb{Z}} c_l^{q,n} e^{i2lkx} \quad \text{and} \quad (2.39)$$

$$-V \sin^2(kx) = \sum_{r \in \mathbb{Z}} V_r e^{i2rkx} \quad \text{with} \quad \begin{aligned} V_{-1} &= V_1 = V/4 \\ V_0 &= -V/2 \\ V_{|r|>1} &= 0 \end{aligned} \quad (2.40)$$

Inserting these expansions into the Schrödinger equation yields

$$\frac{\hbar^2}{2m} \nabla^2 (e^{iqx/\hbar} \sum_l c_l^{q,n} e^{i2lkx}) + \sum_r V_r e^{i2rkx} e^{iqx/\hbar} \sum_l c_l^{q,n} e^{i2lkx} = \varepsilon_{q,n} e^{iqx/\hbar} \sum_l c_l^{q,n} e^{i2lkx}$$

which simplifies to

$$\sum_{l'} e^{i(q+2l'k)x} \left[ \left( \frac{(q+2l'\hbar k)^2}{2m} - \varepsilon_{q,n} \right) c_{l'}^{q,n} + \sum_r V_r c_{l'-r}^{q,n} \right] = 0. \quad (2.41)$$

Due to the orthogonality of the plane waves, each term in the sum must be zero. These terms form a set of linear equations, determining the energy bands  $\varepsilon_{q,n}$ . Three examples are displayed in figure 2.6. With rising potential depth, the energy bands flatten. For extremely deep lattices, the potential resembles an array of isolated wells, and the band structure becomes similar to the level structure of the harmonic oscillator.

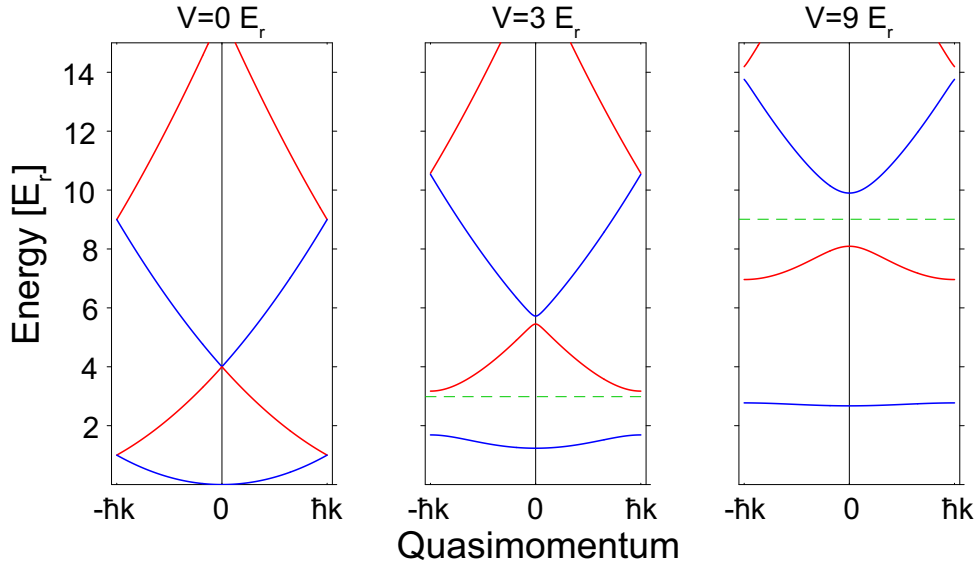


**Figure 2.6:** Band structure in a one-dimensional periodic potential. The energy of the different Bloch states  $\varepsilon_{q,n}$  is plotted as a function of the quasimomentum in the reduced zone scheme. The origin of the energy scale is chosen to be at the trap minimum, and the green dashed line marks the continuum threshold above which the atoms are untrapped.

### Probing the state in a lattice

When a very weakly interacting Bose-Einstein condensate is adiabatically loaded into a periodic potential by slowly turning on an optical lattice, nearly all particles occupy the lowest energy state  $\varepsilon_{q=0,n=0}$ . With increasing repulsive interactions, this distribution becomes unfavourable, as the perfect overlap of the single particle wavefunctions maximises the interaction energy. Instead, most atoms occupy the ground state of the interacting system and have a spread of quasimomenta. The quasimomentum distribution of the atoms may be probed experimentally: the lattice potential is ramped down adiabatically with respect to the band separation. At the same time the ramp-down is fast enough to suppress collisional processes which change the quasimomentum. When using this procedure, the single particle states follow the evolution of the eigenstates from Bloch states to free particles states. Some intermediate steps of this development can be seen when looking at the sequence of spectra in figure 2.6 from right to left. As a result of this procedure the quasimomentum is mapped to real momentum. Measured after some time of flight, the density distribution directly reflects the quasimomentum distribution in the lattice (see figure 2.7).

When the lattice is switched off quickly with respect to the tunneling time, a new picture evolves: the eigenstates within the lattice are suddenly projected onto the free atomic states  $e^{ipx/\hbar}$ , which then propagate during free expansion according to their momentum  $p$ . As the



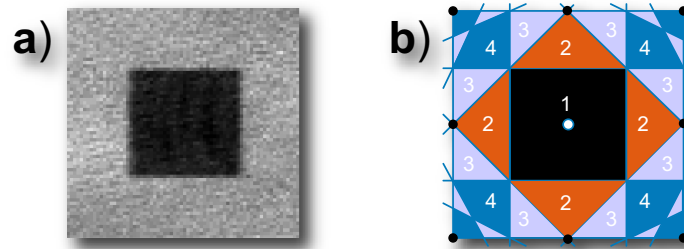


**Figure 2.7:** Quasimomentum distribution of atoms in a lattice. a) Experimental quasimomentum distribution of atoms obtained after lattice ramp-down and free expansion in an absorption image. Due to heating prior to the ramp-down, the atoms populate the entire lowest band uniformly. This is reflected in the filling of the first Brillouin zone. For reference, the corresponding Brillouin zones for a cubic lattice are drawn schematically in b).

Bloch wavefunctions  $\psi_{q,n}(x)$  are periodic with the lattice spacing, their projection onto free states has to involve contributions with higher momenta of the form  $p = q + j2\hbar k$ , where  $j$  is integer.

A weakly interacting Bose-Einstein condensate loaded into an optical lattice, for example, has only a small quasimomentum spread  $\delta q \ll \hbar k$  around  $q = 0$ . When observing the density distribution after some time of flight, several peaks appear which reflect the momentum components with  $p = 0 \pm \delta q + j2\hbar k$ , as shown in figure 2.8 a).

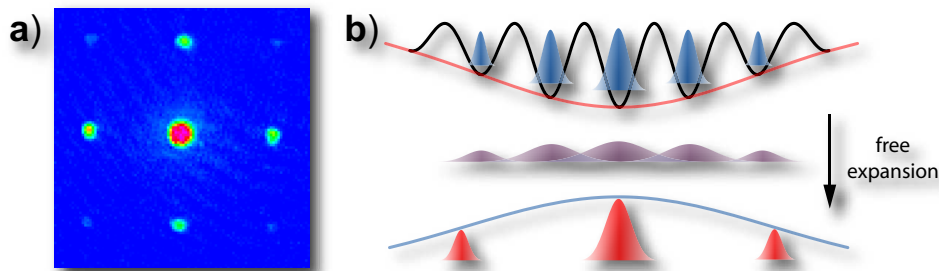


**Figure 2.8:** Expansion and interference of atomic wavepackets that are suddenly released from the lattice traps. a) Experimental absorption image of a Bose-Einstein condensate loaded into a lattice after rapid switch off and free expansion. b) Schematic drawing of the evolution of the wavepacket. In the upper section the atomic wavepackets (blue) are shown in the lattice potential (black). The individual wavepackets are assumed to be in phase, so that the coherence length is determined by the size of the matter wave (red). During expansion, the wavepackets spread out until the interference pattern reflects the momentum distribution in the trap. The size of the peaks is given by the size of the original matter wave, therefore displayed in red, while the initial size of the wavepacket governs the envelope (blue).

A more intuitive understanding of the measured momentum distribution can be gained by considering the expansion of the atomic wavepackets released from the individual wells of the lattice (see figure 2.8 b). The wavepackets expand and interfere with each other. If the atoms at the different sites all have a fixed phase relation before they are released, they represent a coherent matter wave. When released from the lattice, this matter wave spreads just like a coherent light beam passing a periodic array of slits. Interference maxima appear in the momentum distribution similarly just as they would in the far-field for the diffracted light wave. The width of the individual peaks is determined by the coherence length. The total number of peaks which is observed, on the other hand, is directly related to size to which the individual wavepackets from each site expand, because the interference peaks can only appear where several of these wavepackets interfere. This size is directly related to the kinetic energy of the atoms and consequently depends on the localisation of the atomic wavefunctions before expansion.

### Wannier functions

Although the Bloch wavefunctions form an orthogonal set of functions clearly reflecting the periodicity of the lattice, it is often useful to work with localised states. In an insulating material, for example, the particles are not delocalised over the entire lattice, as implied by the Bloch description, but are confined to a small space around a particular lattice site. The Wannier functions provide such a set of localised states, which is more appropriate for dealing with strong periodic potentials than the Bloch wavefunctions, in particular in the presence of strong interactions. The Wannier functions are linear combinations of all Bloch functions within one band of the form [Kit87]

$$w_n(x - x_j) = \mathcal{N}^{-1/2} \sum_q e^{-iqx_j} \psi_{q,n}(x). \quad (2.42)$$

Here  $x - x_j$  denotes the distance between the position of the particle  $x$  and the lattice site at  $x_j$  around which the particle is localised, and  $\mathcal{N}$  is the normalisation constant. The Wannier functions at all different lattice sites form a complete orthogonal set. An example for a Wannier function in the lowest band, which is the band we are interested in, is displayed in figure 2.9. Within the central well, a Wannier function can very well be approximated by a Gaussian function for deep lattices. The probability distribution in the neighbouring sites, however, is significantly underestimated by a Gaussian. In order to find the probability for the tunneling of a particle from one site  $j$  to its neighbouring site  $l$  along the x-axis, the integral

$$J_x = \int w_1(x - x_j) \left( \frac{\hbar^2}{2m} \nabla^2 + V(x) \right) w_1(x - x_l) \quad (2.43)$$

must be evaluated. The tunneling energy  $J_x$  quantifies the kinetic energy gained by delocalisation and the tunneling rate is given by  $J_x/\hbar$ . The tunneling energy is also directly related

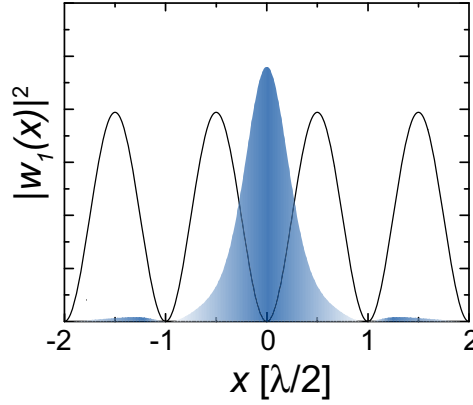


**Figure 2.9:** Occupation probability for a Wannier wavefunction in a lattice with  $V = 2 E_r$ .

to the width of the Bloch band through  $J = (\text{Maximum}(\varepsilon_{q,1}) - \text{Minimum}(\varepsilon_{q,1}))/4$ . For deep lattices ( $V/E_r \gg 1$ ) the exact solution for the bandwidth is obtained by solving the 1D Mathieu-equation 2.37, yielding a tunneling energy of [Zwe03]

$$J_x = \frac{4}{\sqrt{\pi}} \left( \frac{V}{E_r} \right)^{3/4} e^{-2\sqrt{V/E_r}} E_r. \quad (2.44)$$

For a three-dimensional optical lattice the Hamiltonian is separable and the total wavefunction is simply the product of the Wannier functions in each spatial direction. The total tunneling rate  $\tilde{J}/\hbar$  to all six neighbours in this geometry equals  $\tilde{J} = 2(J_x + J_y + J_z)$ .

The interaction energy  $U$  on a given lattice site can also be calculated once the Wannier function is known:

$$U = g \int |w(x)|^4 dx = \sqrt{\frac{8}{\pi}} ka \left( \frac{V_x V_y V_z}{E_r E_r E_r} \right)^{1/4} E_r, \quad (2.45)$$

where  $a$  stands for the scattering length and  $V_x$ ,  $V_y$  and  $V_z$  denote the lattice depths in each spatial direction. The right hand side was calculated by approximating the Wannier function by a Gaussian, which is a good approximation for deep lattices. Seeing that  $\tilde{J}$  and  $U$  characterise the kinetic and interaction energy in the lattice, respectively, it is interesting to look at their ratio, which determines when the system enters the strongly interacting regime. Figure 2.10 shows the evolution of this ratio for increasing lattice depth. In this example, two optical lattices provide very strong confinement, thereby creating one-dimensional tubes, while a third lattice is used to tune the effective interaction strength.

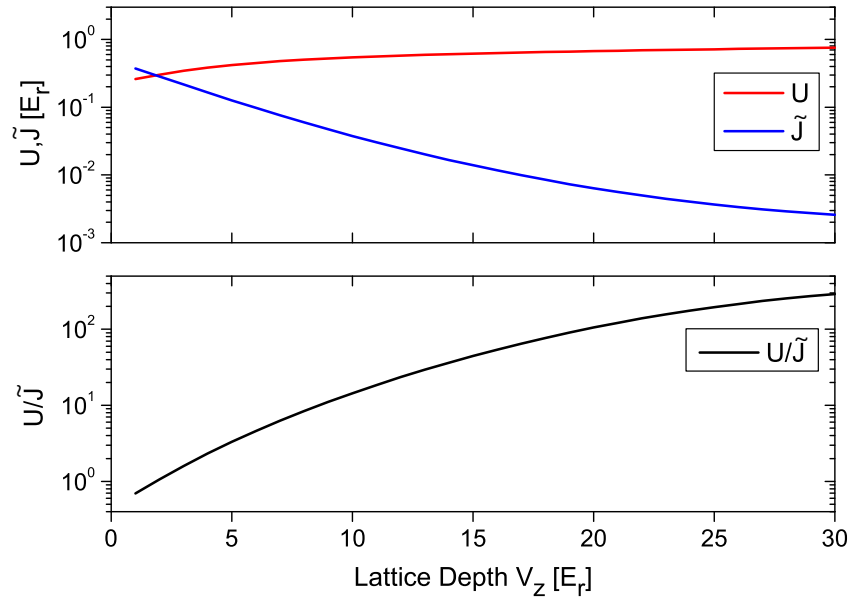


**Figure 2.10:** The interaction energy  $U$  and the kinetic energy  $\tilde{J}$  for periodic potentials along the longitudinal direction of a one-dimensional system. Two optical lattices with  $V_x = V_y = 30 E_r$  create the strong radial confinement. The third lattice with depth  $V_z$  tunes the ratio  $U/\tilde{J}$  over several orders of magnitude. The parameters chosen correspond to  $^{87}\text{Rb}$  atoms with  $a = 103 a_0$  trapped in an optical lattice with  $\lambda = 826 \text{ nm}$ .

---

## 3 The experimental setup

When this project started in the year 2001, degenerate Fermi gases had been studied for little more than a year [DeM99a, DeM01b, Tru01, Sch01] while the first use of multidimensional optical lattices had just been demonstrated with a Bose-Einstein condensate [Gre01b]. The objective of the experimental setup constructed in this thesis has been to bring these two developments together and to realise the first apparatus capable of studying *fermionic* atoms in two- and three-dimensional optical lattices. The setup has been developed based on a design by Markus Greiner [Gre01a].

Fermionic atoms are intrinsically hard to cool because the Pauli principle forbids collisions between identical fermions at low temperatures. Two approaches exist to remedy this problem: to use a spin-mixture of fermionic atoms, or to sympathetically cool a spin-polarised Fermi gas by thermal contact with a Bose gas. One of the reasons why we have chosen sympathetic cooling is the possibility to study bosons and Bose-Fermi mixtures in addition to the fermionic atoms.

In the apparatus two different technologies play a prominent role. On the one hand, ultra-high vacuum (UHV) technology provides the environment for the trapping of the atoms. On the other hand, a significant amount of laser technology is necessary to exert cooling and trapping forces on the atoms, to manipulate them and finally to perform absorption imaging on the cold cloud. The excellent optical access which is essential to perform these operations imposes strict conditions on the design of the vacuum chamber. A sophisticated arrangement of magnetic coils surrounds the vacuum chamber and creates the conservative potentials which are used to transport the atoms and to trap them during evaporative cooling.

### 3.1 Design considerations

#### Atomic species

Alkali atoms are very favourable for cooling and trapping due to their relatively simple level structure. However, only two alkali elements with stable, naturally occurring fermionic isotopes

exist,  $^6\text{Li}$  and  $^{40}\text{K}$ . We have decided to work with  $^{40}\text{K}$  for two main reasons: Firstly,  $^{87}\text{Rb}$  provides an excellent bosonic coolant with an optical transition frequency very close to  $^{40}\text{K}$ , i.e. 780 nm for  $^{87}\text{Rb}$  and 766.7 nm for  $^{40}\text{K}$ . The availability of laser diodes at these wavelengths and the small difference in frequency facilitate the experimental realisation. Secondly, it is easier to create deep optical ( $U > J$ ) lattices with  $^{40}\text{K}$  than  $^6\text{Li}$  due to its higher mass. This becomes apparent when looking at the ratio of  $U/J$  (equations (2.44) and (2.45)), which is an exponential function of the lattice depth in units of the recoil energy. Whereas the absolute lattice depth that is achievable with a far detuned laser is similar for  $^6\text{Li}$  and  $^{40}\text{K}$ , it differs considerably in units of the recoil energy since  $E_r \propto m^{-1}$ .

### Cooling strategies and the vacuum system

The trapping and cooling of the dilute atomic gases proceeds in several stages which are reflected in the components of the experimental setup (see figure 3.1). At first, the atoms are trapped from the background vapour with a combination of dissipative light fields and magnetic fields in a magneto-optical trap (MOT) [Raa87]. Only a small fraction of the background particles is trapped and cooled to  $\sim 10^{-4}$  K, because the magneto-optical trap can only capture atoms with a temperature lower than  $\sim 10$  K from the background vapour which is in thermal contact with the vacuum walls at room temperature.

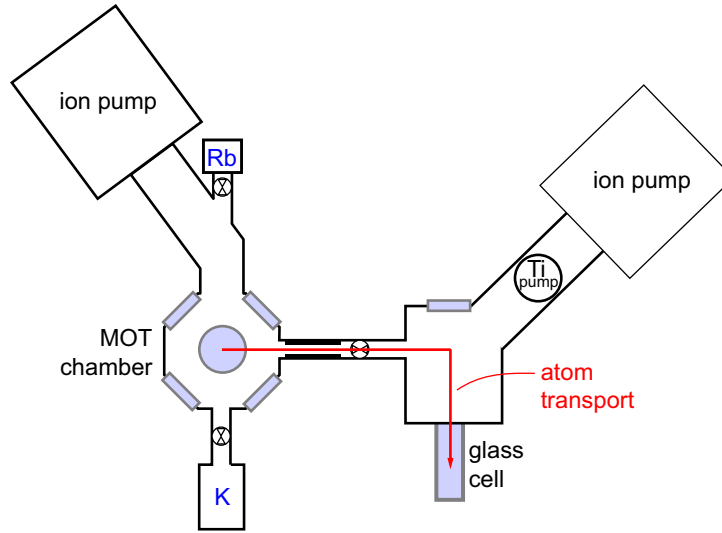


**Figure 3.1:** Schematic layout of the vacuum system.

The next step consists of evaporative cooling, in which the sample is cooled by continuous removal of the hottest atoms and simultaneous rethermalisation. The speed of the evaporative cooling is limited by the rethermalisation time, which is needed in order to repopulate the high

### 3.1. DESIGN CONSIDERATIONS

---

energy tail of the Boltzmann distribution. Evaporation from  $10^{-4}$  K to  $10^{-7}$  K, which increases the phase space density from approximately  $10^{-6}$  to unity, takes typically more than ten seconds. The atoms must therefore be trapped without losses, apart from the intentional removal of the high energy tail during this period.

This requirement is in conflict with conditions needed for a well working magneto-optical trap. In the latter, a high background pressure is necessary to provide a reservoir of atoms which can be trapped. Yet such a high background pressure entails many collisions and trap losses. The most common solution lies in a two chamber apparatus, one chamber with moderate vacuum and a second with ultra-high vacuum, where the evaporation and further experiments take place. A difficulty in such a scheme is the transport of the cold trapped cloud from one region to the other. Traditionally, the atoms were pushed to the UHV cell by light forces and a second MOT recaptured them again. The drawback of this implementation is that the second MOT blocks optical access otherwise needed, for example for the optical lattices.

We have decided to closely follow a scheme pioneered by Markus Greiner et al. [Gre01a] which employs the magnetic transport from one region to the other by a conveyor belt-like structure of magnetic coils. The excellent optical access offered by this scheme has been one of the crucial points for the success of the experiments. The magnetic field necessary to trap the atoms during evaporation is provided by a combined quadrupole Ioffe (QUIC) trap [Ess98], which combines high stability with low power consumption in a simple geometry.

Once the evaporative cooling has proceeded to the point where both species reach quantum degeneracy, the atoms are loaded into the optical lattices. For bosons, this is achieved by slowly ramping up the intensity of three retro-reflected laser beams, which generate the periodic potential. For fermions a complication arises: the cold Fermi gas produced by the sympathetic cooling is spin-polarised and no  $s$ -wave interactions are allowed. The interest in studying fermionic atoms, however, focuses mostly on interacting fermions, in particular close to a magnetic field induced Feshbach resonance.

In order to study interactions, a spin mixture must thus be created, preferably in the particular quantum states which exhibit a Feshbach resonance for collisions. These quantum states, however, cannot be trapped magnetically. Moreover, creating a spin-mixture invariably leads to an increase in the relative temperature  $T/T_F$ , where  $T_F$  is the Fermi temperature. We therefore introduce a further evaporative cooling stage in an optical trap, before loading the degenerate Fermi gas into the lattice.

## 3.2 Magneto-optical trap

In the first cooling step, atoms with  $T \sim 10$  K from the low energy tail of the room temperature Boltzmann distribution are captured from the background vapour at a pressure of  $10^{-8} - 10^{-9}$  mbar by a combination of magnetic fields and dissipative light forces. Three pairs of counterpropagating laser beams which are slightly red detuned from the atomic resonance shine on the cloud of trapped atoms from all three spatial directions as in figure 3.2. The laser

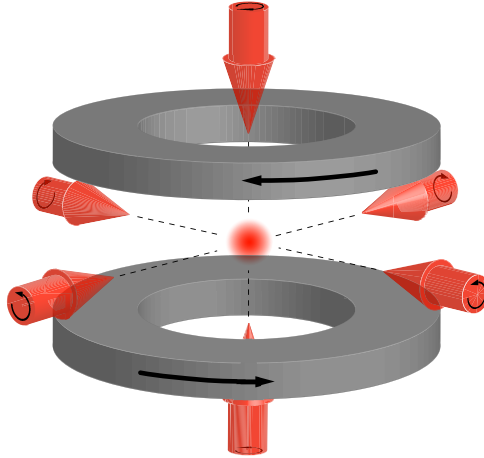


**Figure 3.2:** The magneto-optical trap. Three pairs of red-detuned laser beams intersect at the center of a quadrupole field, trapping a cloud of atoms. The arrows on the magnetic coils indicate the direction of the electric current whereas the arrows on the laser beam symbols denote the light polarisation.

beams exert a cooling force on the atoms due to the Doppler shift: whenever an atom is not stationary but moves along one of the beam directions, the counterpropagating beam is tuned into resonance with the atomic transition whereas the copropagating beam is detuned even further. The photon scattering rate from the counterpropagating beam predominates and the net momentum transfer slows down the atom.

Moreover, an inhomogeneous magnetic field is applied which causes a spatially dependent Zeeman shift of the optical transition. This shift leads to a spatially varying effective detuning of the laser beams with respect to the transition which differs for the copropagating and counterpropagating laser beams due to their different polarisations. This results in a spatially dependent light force which confines the atoms. More information on the theory of the magneto-optical trap can be found in [Phi98, Met99]. The trapped clouds have typical temperatures of a few hundred microkelvin, densities of  $10^{-11}/\text{cm}^3$  and diameters of several millimeters. We can trap both species simultaneously with atom numbers of up to  $N_{Rb} \approx 2 \cdot 10^9$  and  $N_K \approx 10^7$ .

After the end of the magneto-optical trapping phase, two cooling and manipulation stages



happen in rapid succession. The temperature is first reduced by molasses cooling [Let88] before all the atoms are optically pumped into the hyperfine states required for the subsequent magnetic trapping.

### 3.2.1 Vacuum chamber

The magneto-optical trap operates inside a stainless steel vacuum chamber (see figure 3.3) to which optical access is provided by six indium sealed windows. Six laser beams along all three spatial directions can enter through the 40 mm diameter windows and intersect at the center of the vacuum chamber. Two magnetic coils in anti-Helmholtz configuration situated directly above and below the chamber create a magnetic quadrupole field. The magnetic zero of this quadrupole field coincides with the intersection point of all laser beams and represents the center of the magneto-optical trap. An ion pump with a nominal pumping speed of 75 l/s maintains the vacuum. As we were not sure whether the pumping speed might be too high and lead to an unwanted drain of potassium and rubidium background vapour, a rotatable disk was placed in the tube connecting the MOT chamber to the ion pump. This obstruction is now in fact used to reduce the pumping diameter and consequently also the effective pumping speed.

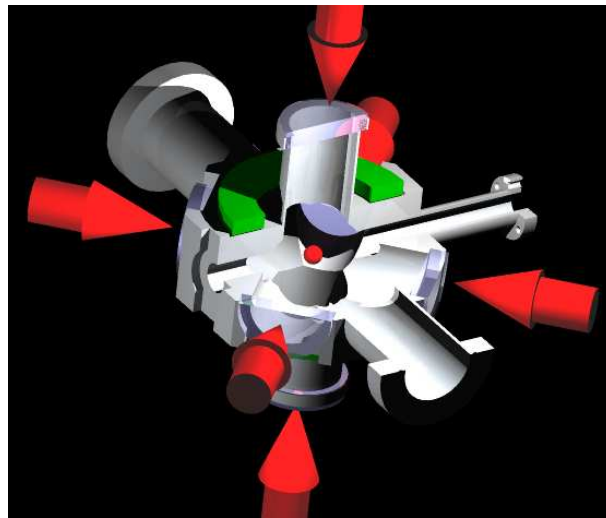


**Figure 3.3:** The vacuum chamber for the magneto-optical trap. The front and top parts have been removed in this CAD rendering in order to show more details. Six windows give optical access to the trapping beams (red arrows). The upper quadrupole coil (green) is visible whereas the lower coil is hidden beneath the chamber. After the MOT phase the cloud is transported to the right towards the UHV chamber. The vacuum tube at the back leads towards the ion pump while the one at the front is used to connect the MOT chamber to the potassium source.

## Sources

The only contaminants in the MOT chamber should ideally be  $^{87}\text{Rb}$  and  $^{40}\text{K}$  atoms at a pressure which is adjusted to supply sufficient atoms for trapping while not seriously limiting the lifetime of the trapped atoms. Rubidium and potassium atoms originate from two different sources: a glass ampule filled with 2 g of pure Rubidium is mounted in an extension of the MOT chamber, where it can be sealed off and pumped separately. It is broken under vacuum and subsequently heated. The vapour pressure rises and the atoms which evaporate diffuse throughout the MOT chamber.

The natural abundance of  $^{40}\text{K}$  in potassium is very low, only 0.012%. However, potassium enriched to 5%  $^{40}\text{K}$  is available as a salt in the form of  $\text{KCl}^1$ . We employ this salt in a dispenser source, following a design by DeMarco et al. [DeM99b]. Approximately 6 mg of enriched  $\text{KCl}$  and 15 mg of pure calcium<sup>2</sup> are finely ground, sieved and mixed under argon atmosphere. Subsequently they are filled into a small container made from folded Nichrome foil<sup>3</sup>. Mounted on an electrical feedthrough, they are placed in the vacuum system at a distance of  $\sim 20$  cm from the MOT. When running a current of 3.5 ampere through the Nichrome container, the dispenser heats up to several hundred degrees centigrade, thus enabling the chemical reaction  $2\text{KCl} + \text{Ca} \rightarrow 2\text{K} + \text{CaCl}_2$ . The K atoms escape into the vacuum chamber, where some are captured by the MOT.

### 3.2.2 Laser system

The laser system providing the light for the MOT is set up on a separate optical table (see figure 3.6). Single mode optical fibers, which are polarisation maintaining, guide the light from the laser table to the vacuum setup, spatially filtering the beams at the same time. Close to the vacuum setup, the beams are sent through a series of beam splitters and telescopes in order to create the three pairs of counterpropagating beams with a  $1/e^2$  radius of  $\sim 20$  mm which enter the MOT chamber.

In order for the MOT to work, two light frequencies per atomic species are needed (see figure 3.4). One drives the main cooling transition. This transition is not completely closed, and from time to time atoms decay from the excited state to the wrong hyperfine state. The second light frequency, the repumper, pumps those atoms back to the cooling cycle. The light is generated by external cavity diode lasers [Ric95]. Their frequencies are stabilised to features of the atomic spectra by performing frequency modulation spectroscopy [Bjo83] on rubidium and potassium vapour cells. Typically one laser, the so-called reference, is locked directly to an

<sup>1</sup>Trace Sciences International Corporation, Ontario, Canada

<sup>2</sup>ESPI, Ashland, Oregon, USA

<sup>3</sup>Advent Research Materials Ltd., Oxford, UK

### 3.2. MAGNETO-OPTICAL TRAP

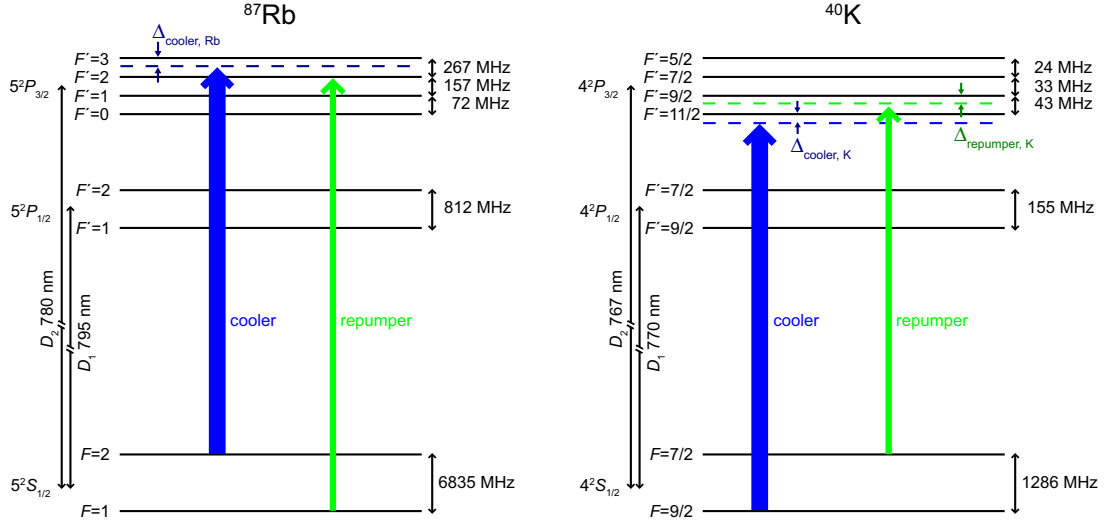


**Figure 3.4:** Level structure of  $^{87}\text{Rb}$  [Ste01] and  $^{40}\text{K}$  [Wil97]. The cooling transition in  $^{87}\text{Rb}$  which is nearly resonant with the  $F = 2 \rightarrow F' = 3$  line is almost closed due to the large splitting of 267 MHz between the excited levels  $F'=2$  and  $F'=3$ . Only rarely is an atom excited into the  $F'=2$  state, which is allowed to decay into the  $F=1$  ground state. Consequently, very little repumping light is needed to reintroduce those atoms into the cooling cycle. For  $^{40}\text{K}$ , a slightly different scenario arises. The small excited state splitting leads to high probability of excitations to the  $F'=9/2$  state and subsequent decay into the  $F=7/2$  ground state. Therefore the ratio of repumping to cooling light power is about five times higher in  $^{40}\text{K}$  than in  $^{87}\text{Rb}$ . As a result the  $^{40}\text{K}$  repumping laser is red-detuned, providing a cooling force as well as emptying out the  $F=7/2$  state.

atomic feature while a second laser generating the cooling light is locked to the first laser with a variable frequency difference [Sch99]. In order to increase the power in the cooling beam, this light is sent through a tapered amplifier which has an output of several hundred milliwatts.

In the case of  $^{87}\text{Rb}$ , the repumping light is created by an additional laser directly locked to the relevant atomic transition by frequency modulation spectroscopy. In  $^{40}\text{K}$ , the cooling beam passes through an electro-optic modulator (EOM), which generates two sidebands in the frequency spectrum, one of which provides the repumping light, while the second has no effect on the atoms.

For the molasses stage which follows the MOT phase, no additional laser frequencies are needed. The magnetic quadrupole field is simply switched off and the earth's magnetic field is compensated. The MOT laser beams remain switched on, with their detuning changed slightly to optimise the cooling. After this stage optical pumping transfers the atoms into the  $|F = 2, m_F = 2\rangle$  state for  $^{87}\text{Rb}$  and into the  $|F = 9/2, m_F = 9/2\rangle$  state for  $^{40}\text{K}$ . Circularly polarised light resonant with the  $F = 2 \rightarrow F' = 2$  and  $F = 9/2 \rightarrow F' = 9/2$ , respectively, is used in

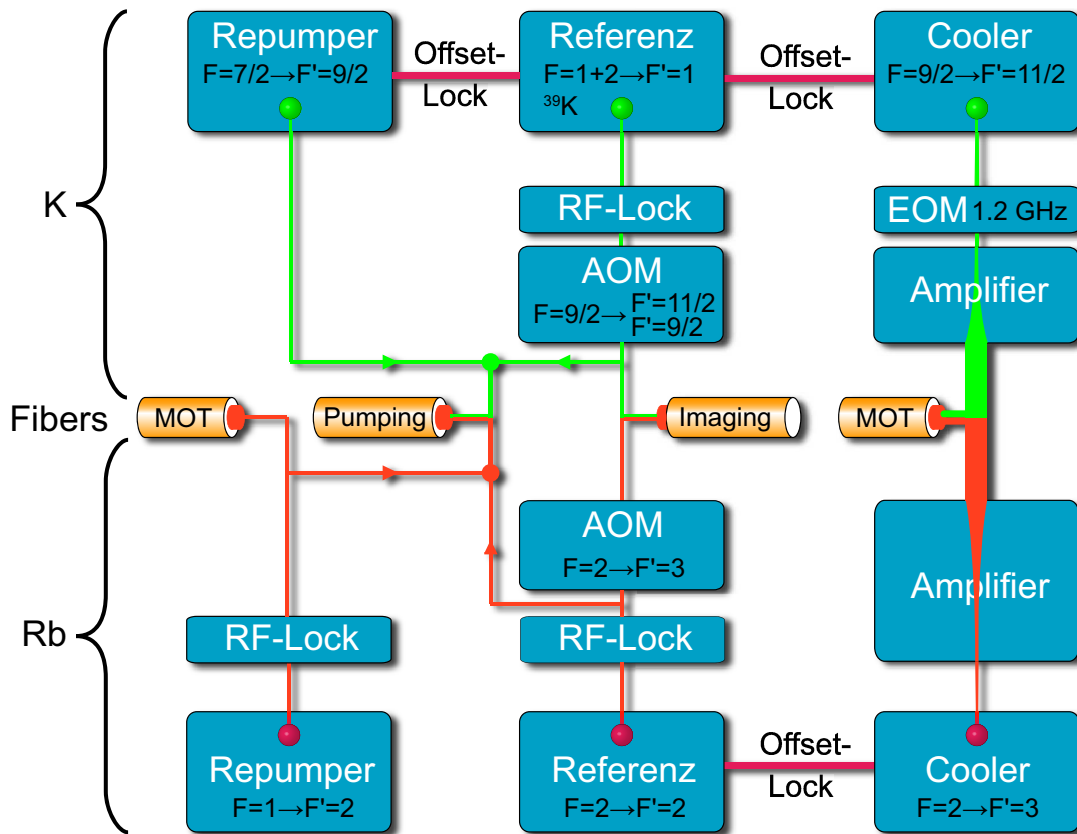


**Figure 3.5:** Laser setup with  $^{87}\text{Rb}$  lasers at the bottom (red) and  $^{40}\text{K}$  lasers at the top (green). The lasers are stabilised either to an atomic transition by radio-frequency modulation spectroscopy (RF-Lock) or to another laser with a variable frequency difference (Offset-Lock). The relevant transition frequency is given in black. In the case of the reference lasers, the frequencies are shifted with acousto-optic modulators (AOM). The modulator for the  $^{40}\text{K}$  reference laser can either produce light appropriate for imaging ( $F'=11/2$ ) or for optical pumping ( $F'=9/2$ ). Finally, the  $^{87}\text{Rb}$  and  $^{40}\text{K}$  beams are combined sent into four fibers.

combination with the repumping light. The entire MOT laser setup is summarised schematically in figure 3.5.



**Figure 3.6:** Laser setup providing the light for the double species MOT, pumping and imaging. Grating stabilised diode lasers and tapered amplifiers (in grey or translucent housings) emit light at the desired frequencies. After passing optical insulators which protect the delicate laser diodes from back-reflections, the beams are shaped and divided. The laser frequencies are stabilised by performing spectroscopy on self-made glass vapour cells and the radio-frequency modulated signal is detected on fast photodiodes. Mechanical shutters enable us to block a beam entirely while the intensity and frequency is changed very rapidly ( $\sim 1 \mu\text{s}$ ) with acousto-optic modulators. Finally, the beams are coupled into optical fibers.

### 3.3 Magnetic transport

After the atoms are pumped into the maximally polarised states  $|F_{Rb} = 2, m_F = 2\rangle$  and  $|F_K = 9/2, m_F = 9/2\rangle$ , they are trapped magnetically [Mig85]. The Zeeman energy  $E(\mathbf{r}) = g_F m_F \mu_B B(\mathbf{r})$  of these low field seeking states increases with increasing magnetic field, leading to trapping at the minimum of a magnetic quadrupole field. Here  $g_F$  is the Landé  $g$ -factor,  $\mu_B$  the Bohr magneton and  $B(\mathbf{r})$  the local magnetic field. The trapped cloud is magnetically transported 40 cm from the MOT chamber to the UHV region following a scheme developed by

Markus Greiner [Gre01a]. In this scheme, a sequence of overlapping coils<sup>4</sup> in anti-Helmholtz configuration as shown in figure 3.7 is used to realise the transport.

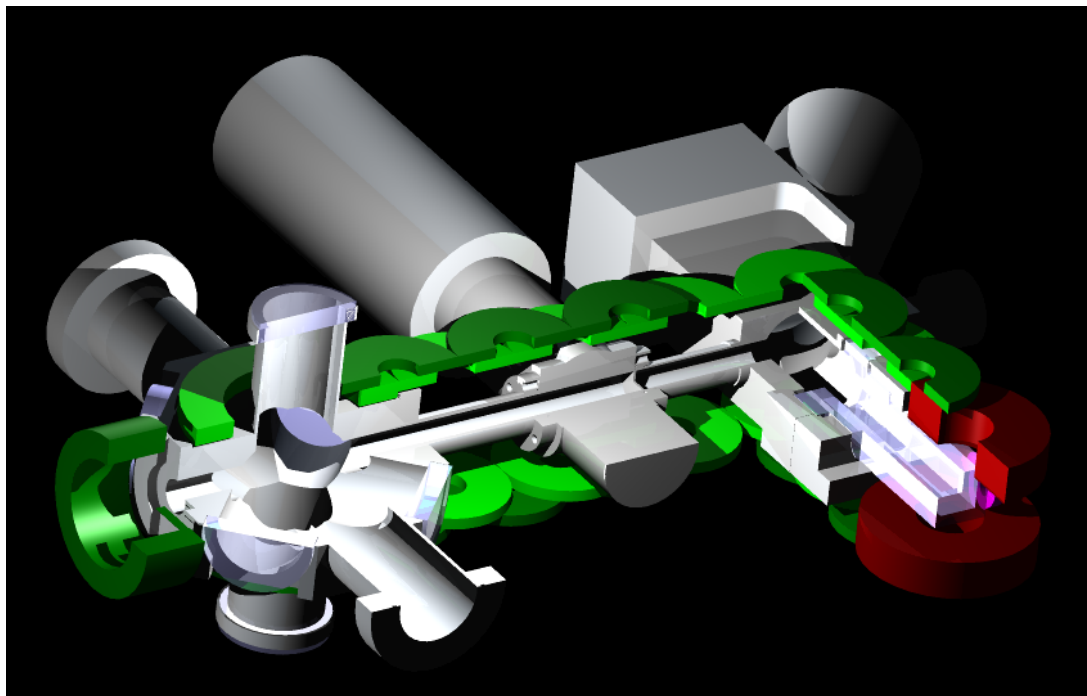


**Figure 3.7:** The transport coils (green) connecting the MOT chamber on the left with the UHV glass cell on the right. The front and top parts have been removed in this CAD rendering in order to show more details. The cloud first passes a vacuum valve, which can be used to shut off the ultra-high vacuum section from the MOT chamber. After a change of the transport direction, the atoms are moved into the glass cell, where two large quadrupole coils (red) above and below as well as a small Ioffe coil (purple) to the right generate the QUIC trap.

The basic idea is to turn on the current through one pair of coils after the other so that the minimum of the magnetic quadrupole field moves continuously from the MOT chamber to the UHV region. In order to avoid heating of the atomic cloud through constant variations of the trap geometry, the current flow through the coils is optimised to keep the aspect ratio and the changes in the gradient of the field nearly constant.

In order to understand this requirement in more detail, let us look at two limiting cases: if only one pair of coils is switched on, the trap has an aspect ratio of one with circular equipotential lines in the symmetry plane and  $\frac{\partial|B|}{\partial x} = \frac{\partial|B|}{\partial y} = \frac{1}{2} \frac{\partial|B|}{\partial z}$ . If, on the other hand, the atomic cloud is situated exactly between two pairs of coils, the trapping geometry is elongated in the x-y plane with an aspect ratio of  $\frac{\partial|B|}{\partial y} / \frac{\partial|B|}{\partial x} \simeq 1.6$  in our case. During transport, the trap geometry

<sup>4</sup>The coils were wound, cast in Araldit F resin and glued to the water cooled mounts with Stycast 2850FT by Oswald Magnettechnik, Miltenberg, Germany.



would constantly change from circular to elongated and back to circular. By running current through additional coil pairs, this heating effect is avoided: when for example the position of the atom cloud is centered exactly on the symmetry axis of a coil pair, additional current is run through the two neighbouring coil pairs, increasing the aspect ratio to  $\simeq 1.6$ . Following this idea, the current through three adjacent coil pairs must be adjusted independently to achieve transport at constant aspect ratio of  $\simeq 1.6$  and constant gradient of  $\frac{\partial|B|}{\partial z} \simeq 200 \text{ G/cm}$ .

The three adjacent coil pairs are served by independent power supplies. We use four very fast linear power supplies<sup>5</sup> which are multiplexed by banks of high-power MOSFETs to the 30 coils. During the transport, the cloud passes through a tube which is 100 mm long and 8 mm wide and serves as a differential pumping section dividing the MOT chamber from the UHV region at  $\approx 2 \cdot 10^{-11} \text{ mbar}$ . We have observed transport efficiencies higher than 80% with no detectable heating of the cloud.

## 3.4 Evaporative cooling

The quadrupole field configuration employed during the transport is unsuitable for the cooling of the gas to quantum degeneracy. At the center of the trap the magnetic field and consequently the Larmor frequency is zero. The atoms cannot follow the local magnetic field vector any more and undergo Majorana spin flips [Dav95b] to untrapped states, which are lost. We avoid this by transforming the quadrupole magnetic field configuration to a Ioffe type trap with a finite offset field  $B_0$ . The Quadrupole-Ioffe-Configuration (QUIC) [Ess98] which we use is distinguished by a simple geometry, low power consumption and high bias field stability. In addition to a coil pair in anti-Helmholtz configuration a smaller coil is placed between the pair at right angles (see figure 3.8 and 3.7). The small coil produces a field with high curvature which provides the finite offset field of  $B_0 = 3.1 \text{ Gauss}$  at 25 A at the trap minimum.

The coils are placed around a fused silica glass cell<sup>6</sup>, which serves as an UHV chamber with particularly good optical access. A mu-metal shielding<sup>7</sup> which encloses both, the glass cell and the magnetic coils, reduces static magnetic stray fields by a factor of 30 and alternating fields at 50 Hz by a factor of 7. The vacuum in the UHV section is maintained by a 75 l/s ion pump and

---

<sup>5</sup>The power supplies are a customised version of the 3000 W NLN series by F. u. G. Elektronik GmbH, Rosenheim, Germany. They are optimised to be able to ramp the current up to the maximum of 150 A and down again to zero within 2 ms with an inductive load.

<sup>6</sup>The glass cell is a custom design manufactured by Hellma GmbH & Co. KG, Mühlheim, Germany. It has been antireflection coated by Laseroptik, Garbsen, Germany. The glass to metal seal from the cell to the 304 steel chamber is provided by a gasket made by Helicoflex, Columbia, SC, USA.

<sup>7</sup>The box was laser-cut and formed by our mechanical workshop from a 1 mm thick soft-magnetic NiFe alloy from Vacuumschmelze, Hanau, Germany. Afterwards it was heated to approximately 900°C under H<sub>2</sub> atmosphere to improve the magnetic shielding at the Paul Scherrer Institute, Villingen, Switzerland.

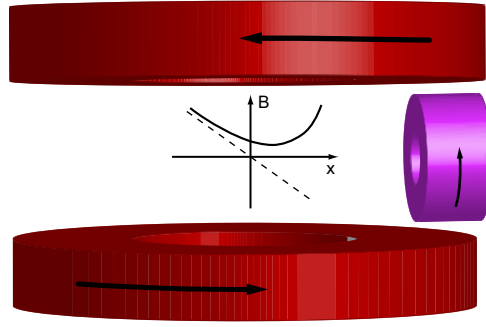


**Figure 3.8:** Comparison between a quadrupole field (dashed) created by the red quadrupole coil pair and the QUIC configuration (solid) with an additional smaller purple coil .

and a titanium sublimation pump.

In the QUIC trap the lifetime of the cloud is on the order of minutes, limited only by the background pressure. This is long enough to perform the evaporative cooling of  $^{87}\text{Rb}$ . A radio-frequency or microwave field limits the effective trap depth and leads to the loss of atoms in the high energy tail of the Boltzmann distribution. Rethermalisation and further evaporation result in a decrease of temperature. The radio-frequency field induces transitions from the trapped  $|F = 2, m_F = 2\rangle$  state via the  $|F = 2, m_F = 1\rangle$  state to the untrapped  $|F = 2, m_F = 0\rangle$  state. The energy dependence of the radio-frequency knife is caused by the Zeeman splitting between the states. When the frequency is adjusted to drive transitions at a magnetic field that is reached far from the trap minimum, only hot atoms are evaporated. For mixtures of  $^{40}\text{K}$  and  $^{87}\text{Rb}$  radio-frequency evaporation may also lead to losses of the  $^{40}\text{K}$  atoms and therefore we use microwave evaporation in this instance. The microwave field at approximately 6.8 GHz only affects the  $^{87}\text{Rb}$  atoms, inducing transitions to the untrapped  $|F = 1, m_F = 1\rangle$  state. Care is taken to remove all Rubidium atoms in the  $|F = 2, m_F = 1\rangle$  state, because we suspect that they induce inelastic losses with the  $^{40}\text{K}$  atoms.

Before going on to describe the laser system for the optical lattices, a quick overview of all the different vacuum and magnetic components needed to create the quantum degenerate Bose and Fermi gases is given. A schematic of the apparatus has already been displayed in 3.1 and a technical drawing is shown in 3.9. The actual apparatus 3.10 is more complex than the drawing, with the MOT, lattice and imaging optics closely surrounding the vacuum chamber.



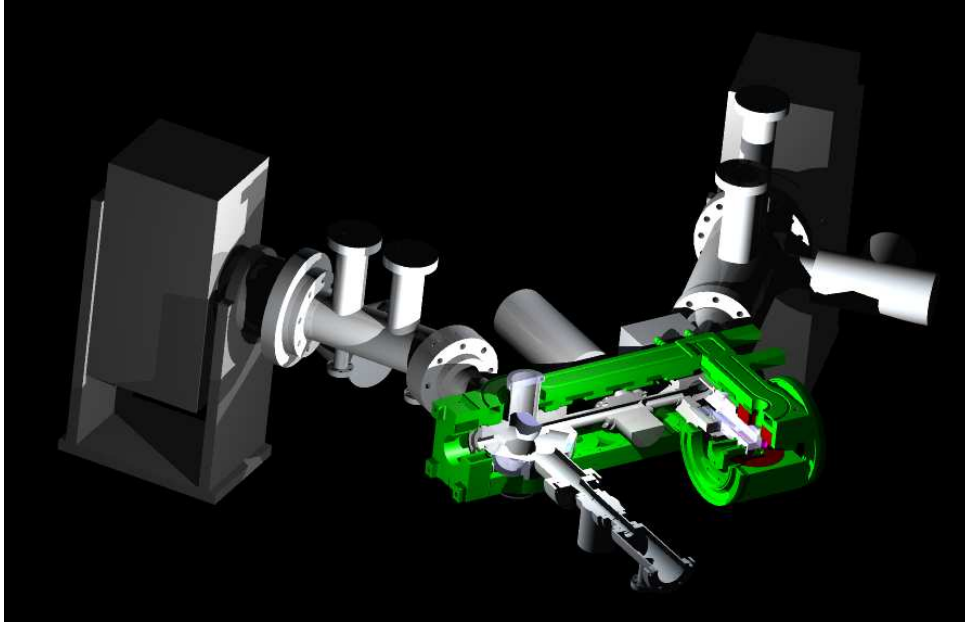


**Figure 3.9:** Overview over the vacuum setup and the magnetic transport. The front and top parts have been removed in this CAD rendering in order to show more details. The transport coils are attached to water cooled mounts shown in green. At the far left and right the two ion pumps are visible. The extension of the MOT chamber at the front houses the  $^{40}\text{K}$  dispensers.

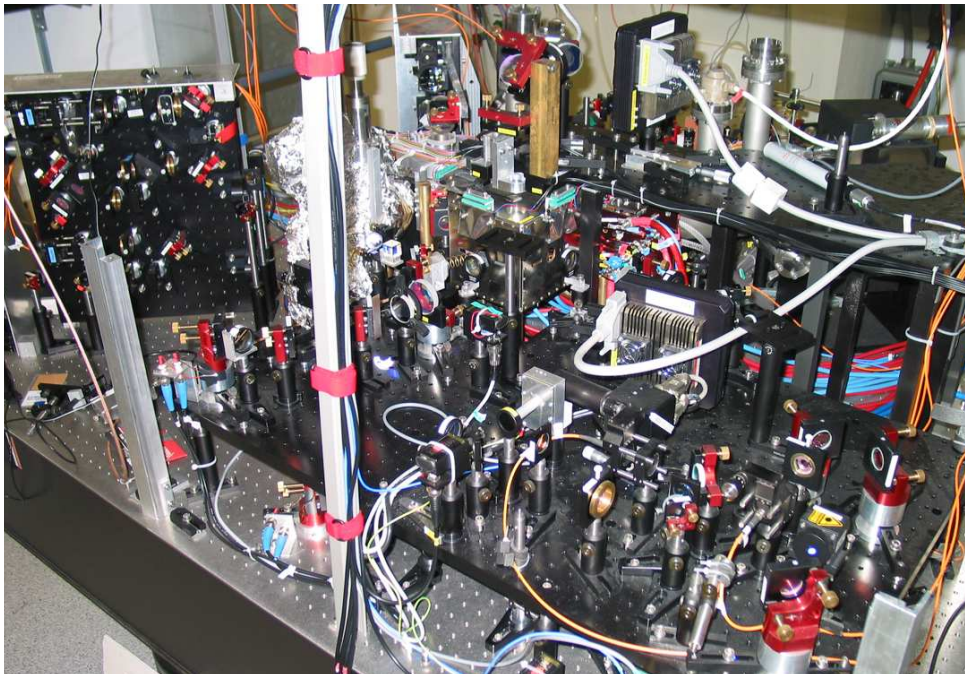


**Figure 3.10:** The vacuum setup with surrounding optics. The glass cell is hidden beneath the mu-metal shielding at the center of the image.

## 3.5 The lattice

In many ways, the optical lattice is the centrepiece of the apparatus. Every experiment described in this thesis is performed in the optical lattice potential and all previous experimental steps are precursors to create quantum degenerate gases for loading into the periodic potential. Considerable work has been spent on creating optical lattices of high quality with negligible imperfections. Detrimental effects which had to be avoided include spatial ripples in the Gaussian profile caused by reflections from the various optical elements as well as fluctuations of the intensity, frequency and position of the lattice laser light.

### 3.5.1 The lattice lasers

The three laser beams which intersect at the position of the trapped cloud (see figure 3.11) are generated by semiconductor lasers running at 826 nm. For this application, the laser diodes need to be stabilised because the frequency fluctuations of free-running laser diodes are unacceptably high. These frequency fluctuations reduce the coherence length and the corresponding wavelength variations result in position fluctuations of the lattice wells, leading to parametric heating. We stabilise one external cavity laser diode to a high finesse cavity and thereby reduce its linewidth to the order of 10 kHz. By injection locking three free-running 150 mW laser diodes to this master laser, sufficient optical power for the three lattice axes is created. In later experiments (chapter 6 and 7) the injection locked laser diodes were replaced by tapered amplifiers which yield higher output powers.

The light of each laser is frequency shifted by an acousto-optic modulator after passing through an optical isolator which protects the delicate lasers from back-reflections. The acousto-optic modulators serve two purposes: firstly, the frequency shifts which they introduce differ by more than 15 MHz for the three lattice axes. This frequency difference is sufficiently large to average out all undesirable cross-interference terms between the different lattice axes, as discussed in section 2.3.2. Secondly, they provide a means to control the lattice depth: by changing the amount of radio-frequency power which drives the modulators, the intensity of the frequency-shifted beam can be adjusted.

### 3.5.2 The optical setup

Single mode optical fibers transport the light to the vacuum setup and filter the spatial mode at the same time. The light is expanded with suitable telescopes and focused onto the atomic cloud with high quality achromatic lenses. In order to be able to perform absorption imaging, imaging light copropagates with the lattice beams. The resonant imaging light is polarised

orthogonally to the lattice beams and added to the beam path with a polarising beamsplitter cube as shown in figure 3.11. After passing the atomic cloud, the lattice beam is recollimated and then retro-reflected by a dichroitic mirror. The two counterpropagating beams form one lattice axis. Resonant enhancement of the trapping light in the cavity formed by the retro-reflecting mirror and the end-facet of the optical fiber is suppressed by an optical isolator in the beam path.

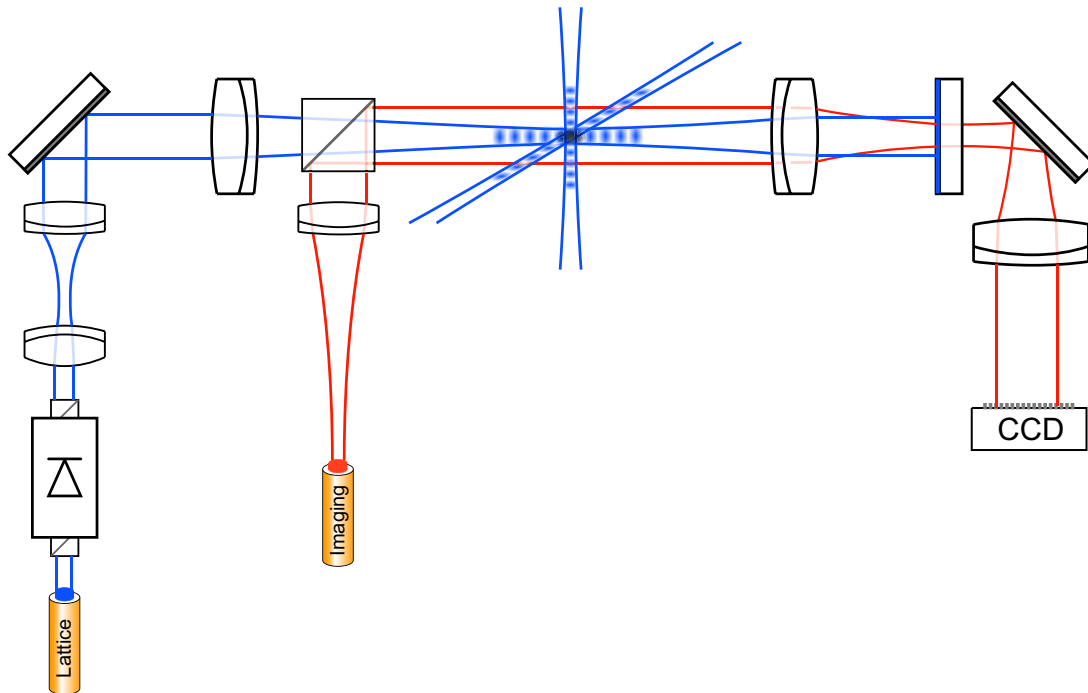


**Figure 3.11:** The lattice laser setup. In the middle of the figure, three standing waves intersect at the position of the cloud, forming a three dimensional cubic lattice. The beam path of one lattice laser (in blue) is shown in more detail. Starting from the fiber, the beam passes an optical isolator and a telescope before being combined with the imaging beam (in red). The lattice beam is focused onto the cloud, recollimated and retro-reflected. The shadow image of the atoms passes the dichroic mirror and is imaged onto a CCD camera.

The imaging light passes through the dichroitic mirror and is imaged onto a CCD camera. In this way, absorption images of the atomic sample can be taken along the lattice axis. This alignment is also very useful for the adjustment of the lattice: a small fraction of the lattice light passes the mirror and is imaged on the camera. By comparing the image of the sample in the trap with the lattice laser beam, the position of the latter adjusted. For the fine alignment of the beams, we use the atomic sample as a probe. Just before switching off the magnetic trap and time of flight imaging, the lattice beams are switched on for a few ten microseconds. If the beams are perfectly aligned with the center of the magnetic trap, the center of mass of the

atomic cloud should feel no net force. By comparing the cloud positions after time of flight with and without this laser pulse, the fine alignment is performed.

The resulting optical lattice is characterised by the power, the diameters and polarisations as well as the frequencies of the laser beams. These values are summarised in table 3.1. The lattice depth is stabilised in order to reduce the effect of fluctuations in the laser power and the fiber coupling. This is done by measuring the laser power of the lattice beams with a photodiode and feeding the signal into a servo-loop which controls the diffraction efficiency of the acousto-optic modulator.

Lattice axis	x	y	z
Beam waists for experiments in chapter 4 and 5	120 $\mu\text{m}$	120 $\mu\text{m}$	105 $\mu\text{m}$
Beam waists for experiments in chapters 6-8	50 $\mu\text{m}$	70 $\mu\text{m}$	70 $\mu\text{m}$
Polarisation	linear, but mutually orthogonal		
Laser wavelength	826 nm		
Laser linewidth	$\approx 10$ kHz		
Frequency difference	$>15$ MHz		
Lattice depth	up to 30 $E_R$		

**Table 3.1:** Summary of the optical lattice parameters.

## 3.6 One experimental cycle

After having introduced the methods and technology used in our experiment, this section summarises the experimental procedure step by step. Starting with a brief overview over the hardware which controls the experiment, the experimental sequence for studying degenerate Bose gases in optical lattices is described. This is relevant for the experiments presented in chapters 4 and 5. The experiments reported in chapters 6-8 are performed with fermionic atoms in the lattice. The sequence deviates from the one for bosons in many small details, so that it is described in a separate section.

### Experiment control

The process of creating a quantum degenerate gas, loading it into the lattice and performing imaging takes roughly a minute, while individual events of millisecond duration sometimes

follow each other in quick succession. Up to 60 digital and 10 analog outputs as well as several radio-frequency generators have to be controlled with microsecond precision. This is realised by computer control with a program developed by my coworker Thilo Stöferle and realtime capable hardware<sup>8</sup>.

At the end of each cycle the images from the CCD cameras<sup>9</sup> are transferred to the image processing software. The software is capable of automatically processing the data and fitting it to theoretical models. As the imaging is destructive, the whole sequence has to be repeated for each new data point. Therefore, the reliable reproducibility of the sequence is of paramount importance and great care has been taken to avoid thermal and other drifts.

#### 3.6.1 Experiments with bosonic $^{87}\text{Rb}$

##### MOT-phase

In the first 10 seconds of the experimental sequence we capture  $2 - 3 \times 10^9$   $^{87}\text{Rb}$  atoms in the magneto-optical trap. For high capture rates, we use about 120 mW of cooling light, which is slightly red-detuned with respect to the cooling transition by  $\Delta_{\text{cooler,Rb}} = -2.5 \Gamma_{\text{Rb}}$ , where  $\Gamma_{\text{Rb}} \approx 2\pi \times 6 \text{ MHz}$  is the natural linewidth of the rubidium  $D_2$  line. At the same time, approximately 5 mW of resonant repumping light transfer the atoms which have decayed to the “wrong” hyperfine state back to the cooling cycle. A pair of anti-Helmholtz coils generates the magnetic gradient field with a gradient of about  $7 \frac{\text{G}}{\text{cm}}$ , which causes the spatial dependence of the light forces.

In order to compress the atomic cloud, the magnetic gradient is increased by a factor of three in 10 ms at the end of the MOT-phase. After that, all magnetic fields are abruptly turned off and polarisation gradient cooling is performed for 9 ms with the detuning increased to  $\Delta_{\text{cool,Rb}} = -10 \Gamma_{\text{Rb}}$ . Finally, the atoms are optically pumped to the magnetically trappable  $|F = 2, m_F = 2\rangle$  state with a 2 ms long sequence of laser pulses.

---

<sup>8</sup>Digital output is provided by a PCI DIO-64 card from Viewpoint Systems Inc. (Rochester, NY, USA), analog output by several NI PCI-6713 and NI PCI-6733 cards from National Instruments (Austin, TX, USA). Moreover, we use a NI PCI-GPIB controller card from National Instruments to communicate with the frequency synthesizers (Agilent 33250A and Tabor 8025).

<sup>9</sup>One slow-scan CCD camera per lattice axis is used: AP1E cameras from Apogee Instruments Inc. (Auburn, CA, USA) on the  $x$ - and  $z$ -axes and a SIS SC-90 camera from Theta System Elektronik GmbH (Gröbenzell, Germany) on the  $y$ -axis.

### Magnetic transport

The magnetic field gradient is rapidly ramped up to a value of  $\frac{\partial B}{\partial z} \approx 50 \frac{\text{G}}{\text{cm}}$  for ideal transfer with minimal heating from the MOT to the magnetic trap. Subsequently, the gradient is increased linearly within 50 ms to a value of  $\frac{\partial B}{\partial z} \approx 200 \frac{\text{G}}{\text{cm}}$ , which is used during transport. The entire transport over approximately 40 cm to the glass cell takes 1.5 seconds, where another 500 ms are spent on fading to the final QUIC configuration.

### Evaporative cooling

In the QUIC trap a radio-frequency field is applied to remove the hottest atoms. After 25 s of forced evaporative cooling with a exponential radio-frequency sweep, an almost pure Bose-Einstein condensate of up to  $3 \times 10^5$   $^{87}\text{Rb}$  atoms is formed. In order to reduce inelastic three-body losses during the cooling, the magnetic trapping potential is lowered slightly during the sweep. At the end the trapping frequencies are  $\omega_{x,\text{Rb}} = 2\pi \times 20 \text{ Hz}$ ,  $\omega_{y,\text{Rb}} = 2\pi \times 122 \text{ Hz}$  and  $\omega_{z,\text{Rb}} = 2\pi \times 124 \text{ Hz}$ .

### Loading the lattice

After condensation we adiabatically change the trapping geometry to an approximately spherical symmetry with trapping frequencies of  $\tilde{\omega}_x = 2\pi \times 17 \text{ Hz}$ ,  $\tilde{\omega}_y = 2\pi \times 20 \text{ Hz}$ , and  $\tilde{\omega}_z = 2\pi \times 22 \text{ Hz}$ . This reduces the peak density by a factor of 4 and allows us to load the optical lattice more homogeneously.

Adiabatic loading into the ground state of the optical lattice is achieved by ramping up the laser intensity to the desired value with an exponential ramp with a duration of 100 ms or 150 ms, depending on the experiment. We have verified experimentally that all atoms are loaded into the lowest Bloch band of the optical lattice: we ramped down the intensity of the lattice laser beams adiabatically and observed in the time of flight image, after release from the magnetic trap, that only the lowest Brillouin zone was occupied [Gre01b].

We calibrate the potential depth of each of the optical lattice laser beams by measuring the frequency of small amplitude dipole oscillations along the axis of the laser beam. From the oscillation frequency we deduce the effective mass  $m^*/m$  at the quasi momentum  $q = 0$  in the band structure, which is a measure of the potential depth of the optical lattice [Cat01, Krä02]. The calibration error is estimated to be  $< 10\%$ . Further details on the optical lattice geometry can be found in table 3.1.

#### 3.6.2 Experiments with fermionic $^{40}\text{K}$

When working with  $^{40}\text{K}$ , the bosonic  $^{87}\text{Rb}$  cloud is used to sympathetically cool the fermions. The rubidium atoms are not transferred into the lattice, however, and therefore the procedure is optimised to maximise the number of cold potassium atoms rather than the size of the Bose condensate.

##### Two-species MOT

Both species must be trapped simultaneously in our MOT-chamber as it is necessary to transport them to the UHV section in the same moving magnetic trap. The simultaneous loading of a magneto-optical trap of  $^{40}\text{K}$  and  $^{87}\text{Rb}$  leads to losses in the potassium cloud, possibly caused by light assisted hetero-nuclear collisions [Gol02]. A strategy which has proven successful to minimise these losses consists of avoiding overlapping high densities of the both clouds. Therefore the  $^{40}\text{K}$  MOT operates for 12 seconds while the  $^{87}\text{Rb}$  light is only turned on for the last two seconds of this phase. Moreover, the densities of both clouds are reduced by employing relatively far detuned trapping light.

We use more than 300 mW of cooling and 100 mW of repumping laser power, both with a detuning of  $\Delta_{\text{cooler,K}} = \Delta_{\text{repumper,K}} = -5.5 \Gamma_{\text{K}}$  with respect to the two relevant transitions, which are indicated in figure 3.4.  $\Gamma_{\text{K}} \approx 2\pi \times 6 \text{ MHz}$  denotes the linewidth of the potassium transition. The detuning of the  $^{87}\text{Rb}$  cooling light is  $\Delta_{\text{cooler,Rb}} = -3 \Gamma_{\text{Rb}}$ . We estimate that we capture about  $10^7$   $^{40}\text{K}$  atoms and  $2 \times 10^9$   $^{87}\text{Rb}$  atoms.

The sequence continues with 6 ms of polarisation gradient cooling with  $\Delta_{\text{cooler,K}} = -3 \Gamma_{\text{K}}$ ,  $\Delta_{\text{repumper,K}} = -3 \Gamma_{\text{K}}$  and  $\Delta_{\text{cooler,Rb}} = -10 \Gamma_{\text{Rb}}$ . Finally, both species are pumped optically to the maximally polarised states  $|F_{\text{K}} = 9/2, m_F = 9/2\rangle$  and  $|F_{\text{Rb}} = 2, m_F = 2\rangle$  within 1.8 ms.

##### Magnetic transport and evaporative cooling

The magnetic transport works as well with two species as with one. The only change to the sequence is an added pre-evaporation phase because the atomic clouds are so large that normally the hottest atoms hit the inner walls of the glass cell. While this is not a problem for the rubidium atoms because it results in evaporative cooling, it reduces the potassium atom number unnecessarily. The pre-evaporation phase takes place in a QUIC trap located further away from the glass cell walls than usual. Both cloud sizes are reduced by selective evaporation on the rubidium atoms before fading to the final QUIC configuration.

Now the hottest rubidium atoms are selectively removed by a microwave field resonant with the  $|F_{\text{Rb}} = 2, m_F = 2\rangle \rightarrow |F_{\text{Rb}} = 1, m_F = 1\rangle$  transition around 6.8 GHz. The potassium

atoms, which are unaffected by this microwave field, are cooled sympathetically. After a 20 s long microwave sweep a Bose condensate with  $3 - 5 \times 10^5$   $^{87}\text{Rb}$  atoms forms in the presence of  $6 - 10 \times 10^5$   $^{40}\text{K}$  atoms at  $T = 0.35 T_F$ . No sign of a collapse induced by the attractive interspecies interaction [Mod02] is observed.

### Optical evaporation

So far we have only performed experiments with pure Fermi gases and therefore we remove all rubidium atoms with a microwave sweep before proceeding. It is particularly interesting to study interacting  $^{40}\text{K}$  atoms close to a Feshbach scattering resonance. However, the states for which resonant control of the scattering has been observed [Lof02] cannot be trapped magnetically. Moreover, the production of the desired spin mixture leads to additional heating. The experimental strategy to produce a cold spin mixture is the following: the potassium atoms are transferred into a crossed-beam optical dipole trap, in which the desired spin mixture is prepared. After further evaporative cooling, the quantum degenerate spin mixture is transferred into the optical lattice.

The experimental details of this procedure are the following: starting from the magnetically trapped pure  $^{40}\text{K}$  cloud in the  $|F_K = 9/2, m_F = 9/2\rangle$  state, the optical dipole trap is turned in 100 ms. The optical dipole trap is formed by the lattice laser beams along the  $x$ - and  $y$ -axis. In this instance, however, the retro-reflecting mirrors are blocked by mechanical shutters so that no standing wave patterns develops. The maximum trapping frequencies in the trap are  $\omega_{x,K} = 2\pi \times 93 \text{ Hz}$ ,  $\omega_{y,K} = 2\pi \times 154 \text{ Hz}$  and  $\omega_{z,K} = 2\pi \times 157 \text{ Hz}$ . Next, the current through the magnetic trapping coils is linearly ramped down in 100 ms while a homogenous offset field is simultaneously applied with a final value of approximately 13 G. A short radio-frequency pulse drives a Landau-Zener transition transferring all atoms into the  $|F_K = 9/2, m_F = -9/2\rangle$  state. The magnetic field then is increased to 232.9 G, where a 50/50 spin-mixture of  $m_F = -9/2$  and  $m_F = -7/2$  states is created with a 200 ms long radio-frequency pulse.

At this magnetic field, which is far from the Feshbach resonance at 202.1 G [Reg04] and the zero crossing of the scattering length at 210 G, optical evaporation is possible due to the relatively large scattering length between the two spin states of  $\approx 120 a_0$ . After lowering the laser power in the optical trapping beams by approximately a factor of three we end up with a spin mixture of  $5 \times 10^4$  to  $2 \times 10^5$  atoms at  $T/T_F = 0.2$  to  $0.25$ . The sample is now ready to be transferred into the optical lattice.



#### Transfer into the optical lattice

Prior to loading the atoms into the optical lattice we tune the magnetic field to  $B = (210 \pm 0.1)$  G, so that the  $s$ -wave scattering length between the two states vanishes. Due to the fact that optical trap is formed by the lattice laser beams with the retro-reflecting mirrors blocked by shutters, the loading procedure is somewhat involved. First, the standing wave laser field along the vertical  $z$ -axis is turned on. Subsequently, the optical dipole trap along the  $y$ -axis is turned off and a standing wave laser field along the same axis is turned on, and finally the dipole trap along the  $x$ -axis is ramped down. This procedure results in a one-dimensional tubes oriented along the  $x$ -axis. For the experiments in chapter 8, we use a three-dimensional lattice and therefore a standing wave along  $x$ -axis is turned on as well. In order to keep the loading of the atoms into the lattice as adiabatic as possible the intensities of the lasers are slowly increased (decreased) using exponential ramps with time constants of 10 ms (25 ms) and durations of 20 ms (50 ms), respectively.

The lattice depth is calibrated by modulating the laser intensity and studying the parametric heating. The calibration error is estimated to be  $< 10\%$ . Further details on the lattice parameters are listed in table 3.1. After having gone through the steps described above, a degenerate fermionic spin mixture in an optical lattice is at hand which can be studied at arbitrary interaction strength by making use of a Feshbach resonance.



---

## 4 Realisation and characterisation of a 1D Bose gas

An ultracold Bose gas in one spatial dimension is different from its two- or three-dimensional counterparts. One striking example is that Bose-Einstein condensation does not occur at finite temperature in a homogeneous one-dimensional system [Hoh67]. In an interacting Bose gas the constraint to one dimension leads to another remarkable and unexpected property. With decreasing atomic density the interactions become increasingly dominant and the character of the system changes. Lieb and Liniger [Lie63b, Lie63a] studied the 1D Bose gas assuming delta-functional interaction. The corresponding Hamiltonian is

$$H = \sum_j \frac{\hbar^2}{2m} \frac{\partial^2}{\partial x_j^2} + g_{1D} \sum_{i < j} \delta(x_i - x_j), \quad (4.1)$$

where the coupling constant  $g_{1D}$  specifies the interaction strength and  $m$  the atomic mass. Remarkably, they found exact solutions for the ground state and the excitation spectrum for arbitrary interaction strength. The system is characterised by the single parameter  $\gamma$ , which is the ratio between the interaction energy  $g_{1D}n_{1D}$  and the characteristic kinetic energy  $\frac{\hbar^2}{mn_{1D}^2}$  of particles with the mean separation given by the inverse density  $1/n_{1D}$ :

$$\gamma = \frac{m g_{1D}}{\hbar^2 n_{1D}}. \quad (4.2)$$

With decreasing density the kinetic energy is reduced faster than the interaction energy and the 1D gas becomes interaction dominated for small densities instead of becoming more ideal. The prospect that this unique model in many-body quantum physics might become experimentally accessible has led to an increased theoretical interest in trapped 1D gases. Assuming elongated trapping geometries in which the radial atomic motion is confined to zero point oscillations, different physical regimes could be identified [Ols98, Ho99, Pet00b, Pet04a, Dun01, Gir01, Men02, Lie03, Ped03].

---

Parts of this chapter are published in [Mor03].

## 4.1 Regimes of quantum degeneracy in 1D

Contrary to the homogeneous case, Bose-Einstein condensation in harmonically confined ideal gas is possible [Ket96]. Decreasing the temperature below  $T_c = N\hbar\omega_z/\ln(2N)$  strongly increases the occupation of the ground state. The clear crossover to a macroscopic occupation of this state is due to the discrete level structure of the trap (see section 2.1.1).

### Weakly interacting Bose gas

Interactions can change this picture. Only if the interaction among the particles in the lowest eigenstate is smaller than the trapping frequency, it is possible to distinguish the individual trap levels. Otherwise the discrete level structure is smeared out and a gradual crossover to a Bose-Einstein condensate with Thomas-Fermi profile results. While the density fluctuations are small for temperatures below the degeneracy temperature  $T_d = N\hbar\omega_z$ , phase fluctuations persist down to temperatures on the order of  $T_\phi = T_d \hbar\omega_z/\mu$  [Pet00b, Pet04a]. Below this temperature a true Bose-Einstein condensate appears, while for  $T_\phi < T < T_d$  density fluctuations are suppressed but the phase fluctuates on a length scale much smaller than the sample length. Such a condensate with fluctuating phase is usually termed a quasi-condensate.

### Strongly interacting gas

When the 1D density is lowered, the kinetic energy of the ground state is reduced and may become smaller than the interaction energy, thereby bringing the gas into the strongly interacting regime where  $\gamma > 1$ . The longitudinal motion of the particles is highly correlated and the bosons do not occupy the same positions, so that the mutual repulsion is minimised. At small interparticle distances the relative wavefunction of two particles is strongly reduced. In the limit  $\gamma \rightarrow \infty$ , often referred to as the Tonks-Girardeau regime, this repulsion mimics the Pauli principle and the Bose gas acquires fermionic properties. In particular, the density distribution and the density-density correlation functions of such a strongly interacting Bose gas are given by the corresponding properties of a noninteracting Fermi gas [Gir60].

#### 4.1.1 Phase diagram in a harmonic trap

Usually, atoms in a dilute gas can move and scatter off each other in all three dimensions. Only if they are subject to strong radial confinement does one have an effectively one-dimensional gas, as all radial motion is reduced to zero point oscillations. The 1D regime is reached when

the condition

$$\mu, k_B T \ll \hbar \omega_r \quad (4.3)$$

is fulfilled, where  $\omega_r$  denotes the radial trapping frequency and thus the strength of the radial harmonic confinement,  $\mu$  the chemical potential, and  $T$  the temperature. Yet even when the 1D regime is reached, the ground state extension in the radial direction  $a_r = \sqrt{\hbar/(m\omega_r)}$  is usually much larger than the characteristic radius of interatomic potential. Therefore the confining potential plays no significant role during the scattering process, which continues to be three-dimensional. The outgoing wavefunction, on the other hand, has to travel along the direction of the waveguide. As a result, it is possible to describe the system with a fully one-dimensional Hamiltonian:

$$H = \sum_j \frac{\hbar^2}{2m} \frac{\partial^2}{\partial x_j^2} + g_{1D} \sum_{i < j} \delta(x_i - x_j) + \sum_j \frac{1}{2} m \omega_z^2 z_j^2, \quad (4.4)$$

with  $\omega_z$  characterising a harmonic potential along the direction of motion. The 1D coupling strength  $g_{1D}$  in an atomic gas can be expressed in terms of the 3D scattering length  $a$  as [Ols98]

$$g_{1D} = \frac{2\hbar^2}{m} \frac{a}{a_r^2} \quad \text{for } a \ll a_r. \quad (4.5)$$

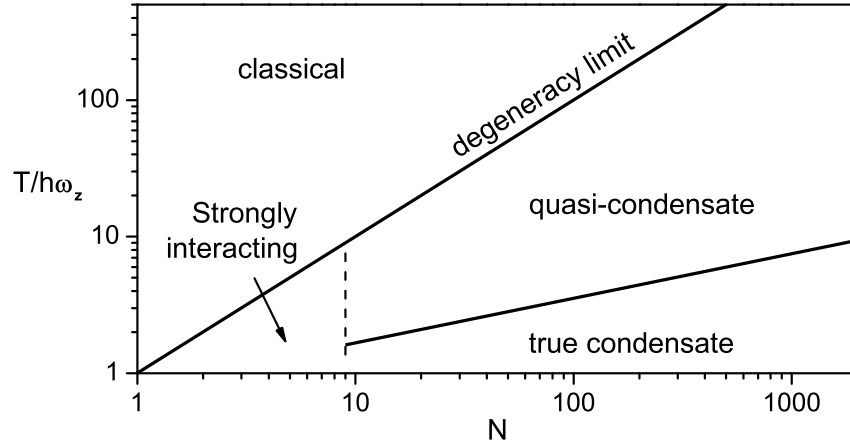


**Figure 4.1:** Phase diagram of a harmonically trapped 1D Bose gas at finite temperatures. With decreasing temperature the ideal classical gas is transformed continuously to a gas dominated by either its interaction or its quantum statistics. The parameters are chosen to match our experimental conditions. For temperatures or particle numbers above the ones displayed, the 1D condition  $\mu, k_B T < \hbar \omega_z$  is violated (figure adapted from [Pet00b]).

In the following, the phase diagram of a trapped 1D gas subject to this Hamiltonian will be discussed, following the treatment given by Petrov et al. [Pet00b]. To come to the most important point first, the phase diagram is shown in figure 4.1 for the situation pertaining to our experiments. The lines dividing the phases only indicate the presence of crossovers as no phase

transitions exist in a trapped one-dimensional gas. While temperature and particle number are the variables describing the gas, the phase diagram is also determined by the trap parameters and the atomic scattering properties. These parameters are characterised by the harmonic oscillator length in transversal and longitudinal direction, termed  $a_r$  and  $l_z$  respectively, as well as by the scattering length  $a$ . They are constrained by the particular experimental realisation.

When the trapping potential is created by a red detuned lattice, the maximum anisotropy  $(l_z/a_r)^2 = \pi w/\lambda$  (see section 2.3.2) is determined by the available laser power, which limits the waist  $w$ . For our experiment, typical values are  $l_z = 1.2 \mu\text{m}$  and  $a_r = 60 \text{ nm}$ . Moreover, the scattering length is fixed by the alkali atom trapped, here  $^{87}\text{Rb}$  with  $a = 5 \text{ nm}$ .

The starting point for finding the different phase boundaries will be a one-dimensional condensate in the Thomas-Fermi regime. Here the kinetic energy term can be omitted and the density profile takes the parabolic form typical for condensates in harmonic traps with a density in the center of  $n_{1D} = \mu/g_{1D}$ . Integrating over the density profile, one obtains [Pet04a]

$$\mu = \frac{\hbar^2}{2m} \left( 3N \frac{a}{l_z^2 a_r^2} \right)^{2/3}. \quad (4.6)$$

This equation will be employed to find the crossover to the neighbouring phases, namely the noninteracting and quasi condensate as well as the strongly interacting degenerate Bose gas.

## 1D regime

The chemical potential has to meet  $\mu \ll \hbar\omega_r$ , which is equivalent to a maximum number of  $N \ll \frac{l_z^2}{3a a_r}$  atoms. Any additional atoms would have to occupy the next transversal oscillator level and correspondingly the gas cannot be regarded as 1D any more. In the experimentally realised 1D trap that will be presented in this chapter the number of particles is therefore limited to  $N \ll 2 \cdot 10^3$ , making the experimental realisation of 1D gases challenging.

## Noninteracting condensate

In order to have a distinctly observable crossover to a nearly noninteracting Bose-Einstein condensate, the chemical potential has to be smaller than axial trapping frequency  $\mu \ll \hbar\omega_z \Rightarrow N \ll \frac{a_r^2}{3a l_z}$ , which is smaller than one for our parameters. This regime can only be accessed by reducing the scattering length  $a$  or the aspect ratio  $\omega_r/\omega_z$ . Otherwise a gradual crossover occurs, either to a weakly interacting Bose-Einstein condensate in the Thomas-Fermi regime or to an interaction dominated Bose gas.

### Crossover from weak to strong interactions

The two cases are separated by a transition region characterised by  $\gamma \approx 1$ . Assuming the validity of the Thomas-Fermi approximation, the coupling constant  $\gamma$  can be reexpressed as

$$\gamma = 8 \left( \frac{a^2 l_z^2}{3N a_r^4} \right)^{2/3}. \quad (4.7)$$

Here the definition of  $\gamma$  (eq. (4.2)) and the fact that  $n_{1D} = \mu/g_{1D}$  holds in the Thomas-Fermi regime were used. With this explicit expression for the coupling strength at hand we can estimate the crossover between weak and strong interactions to happen for  $N \approx 20$  in our experiment. Below this number the interactions dominate.

### Quasi-condensate

Even if  $\gamma < 1$ , the existence of a true Bose-Einstein condensate requires the temperature to be below  $T_\phi = T_d(\hbar\omega_z/\mu)$  [Pet00b]. Using equations (4.6) and (4.7) yields  $T_\phi/\hbar\omega_z = 2^{5/2}/(3\sqrt{\gamma})$ . This value is significantly smaller than the degeneracy temperature  $T_d/\hbar\omega_z = N$ , in particular close to the crossover to a strongly interacting gas.

## 4.2 Creating a 1D Bose gas

There has been significant progress towards the realisation of trapped 1D atomic gases over the past years. Both in a  $^6\text{Li}/^7\text{Li}$  mixture [Sch01] and in  $^{23}\text{Na}$  [Gör01], quantum degenerate gases have been created in extremely elongated traps, and features of one-dimensional condensate expansion were observed. Considering only the condensed fraction, a chemical potential of  $\mu \gtrsim 0.5 \hbar\omega_r$  was attained in these experiments. However, the thermal component, a substantial portion of the gas, was in a 3D configuration ( $k_B T > \hbar\omega_r$ ) leaving the whole sample in an interesting crossover regime. In a similar experimental regime  $^7\text{Li}$  Bose-Einstein condensates with attractive interparticle interactions were launched into 1D matter waveguides forming bright matter wave solitons [Kha02]. Moreover, a Bose-Einstein condensate of rubidium was loaded into the ground state of a two-dimensional optical lattice. The transverse oscillations were frozen out but the tunneling rate between the tubes exceeded the axial trapping frequency, resulting in an array of strongly coupled tubes [Gre01b].

In our experiment we have realised both quantum degenerate and thermal one-dimensional atomic gases with the condition (4.3) being well fulfilled: for all our experiments  $k_B T/\hbar\omega_r < 6 \times 10^{-3}$  and  $\mu/\hbar\omega_r < 0.1$ . The atoms are prepared in a 2D optical lattice which offers the advantage of an extremely tight radial confinement of only a fraction of the optical lattice wavelength. Moreover, the geometry (see figure 4.2 a) makes it possible to study many copies of

the 1D system at the same time, thereby avoiding problems arising from the detection of a very low number of particles. The parameter  $\gamma$  ranges approximately from 0.4 to 1, which is at the crossover from the mean field to the strongly correlated regime.

In our experimental setup, we produce almost pure Bose-Einstein condensates of up to  $3 \times 10^5$   $^{87}\text{Rb}$  atoms in the  $|F = 2, m_F = 2\rangle$  hyperfine ground state, as described in chapter 3.6.1. The Bose gas is adiabatically loaded into the ground state of an optical lattice by ramping

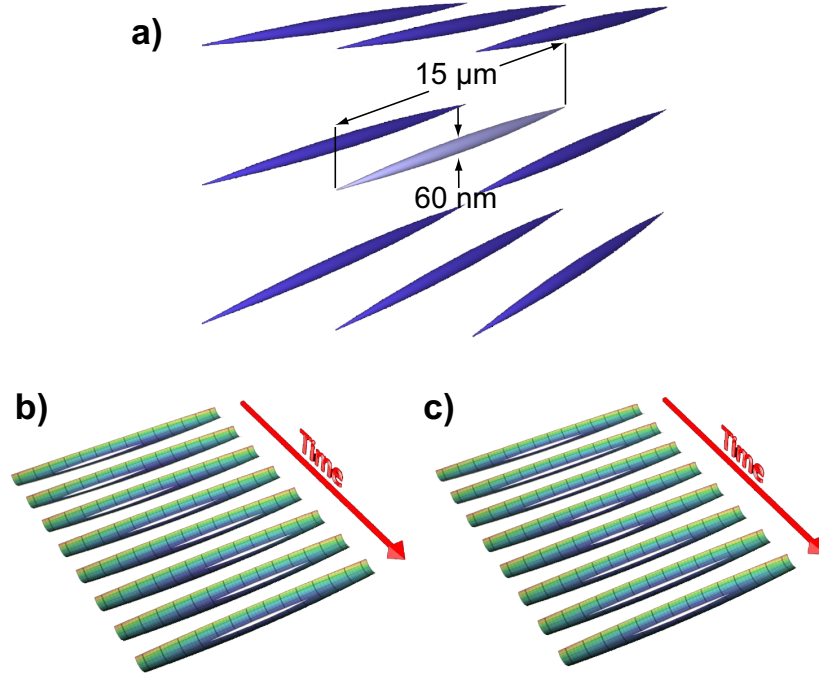


**Figure 4.2:** a) The geometry and size of trapped 1D gases in a two-dimensional optical lattice. The spacing between the 1D tubes in the horizontal and vertical direction is  $413\ \text{nm}$ . b) Dipole mode with center of mass motion. c) Breathing mode of the 1D gas.

up the laser intensity to  $V_0 = 30 E_r$  with an exponential ramp using a time constant  $75\ \text{ms}$  and a duration of  $150\ \text{ms}$ . The two-dimensional optical lattice created from two laser beams along the  $x$ - and  $z$ -axis produces an array of tubes, tightly confined in the radial direction with  $\omega_r \approx 37\ \text{kHz}$  and spaced by the periodicity of the lattice  $d = \lambda/2$  (see figure 4.2 a). Further details on the lattice laser beams can be found in the table 3.1 and in chapter 3.6.1.

The 1D systems in the optical lattice are not perfectly isolated, but the tubes are coupled by the tunneling matrix element  $J$ . For sufficiently deep lattice potentials, the tunneling becomes exponentially small and contributes only a minor correction of order  $J/\mu$  to the 1D characteristics in the individual tubes. If  $J/\mu \ll 1$  the gas acquires 1D properties and can be well described by a local Lieb-Liniger model, even though the whole sample is three-dimensional



[Ped03]. Experimentally we observe the disappearance of the matter wave interference pattern with increasing lattice depth when the atoms are suddenly released from the optical lattice. Higher order momentum peaks ( $\pm 2\hbar k, \pm 4\hbar k, \dots$ ) are usually observed at lower laser intensities [Gre01b]. We attribute this loss of coherence between the individual tubes to the very small tunnel coupling at large lattice depths, which is too small to stabilise the global phase coherence.

## 4.3 Collective excitations in 1D

Having created a one-dimensional Bose gas, we need to find a way to characterise it. Specifically, the excitation spectrum can be used to determine the different regimes of the 1D gas in the optical lattice. The frequency ratio between the lowest compressional mode (breathing mode) and the dipole oscillation ( $\omega_B/\omega_D$ )<sup>2</sup> is a sensitive measure, both for isolated 1D systems [Men02] and for atoms in an optical lattice [Ped03]. The two modes are depicted in figure 4.2 b and c.

### 4.3.1 Theoretical prediction

The easiest case to consider is that of a thermal gas, where neither interactions nor statistics play a role. Here the ratio is  $(\omega_B/\omega_D)^2 = 2^2$ , which becomes obvious if we examine the motion of two particles which initially start out in the center of the trap with opposite velocities. While they perform one oscillation (with  $\omega_D$ ), their respective separation  $|z_1 - z_2|$  exhibits two maxima, corresponding to two oscillations of the breathing mode. In the Tonks-Girardeau limit, the strongly interacting Bose gas maps to a noninteracting Fermi gas. Therefore one expects the latter to have the same collective modes as a thermal gas.

In order to understand the behaviour of the breathing mode of a 1D mean-field Bose-Einstein condensate, we study an interacting classical 1D gas. Its density distribution  $n_{1D}(z)$  is subject to the equation of motion  $F(z, t) = -\frac{\partial}{\partial z}(\frac{1}{2}m\omega_z^2 z^2 + U n_{1D}(z, t))$ , where the last term describes the mean-field interaction. The stationary distribution  $n_{1D}(z) = n_{1D}(0) - \frac{1}{2U}m\omega_z^2 z^2$  is determined by  $F(z) = 0$  and has the parabolic shape characteristic for the potential. We are interested in oscillating solutions of  $n(z, t)$  and assume that an infinitesimally small volume element moves along the trajectory  $z(t) = \lambda(t)z(0)$  given by the scaling parameter  $\lambda$ . The equation of motion becomes

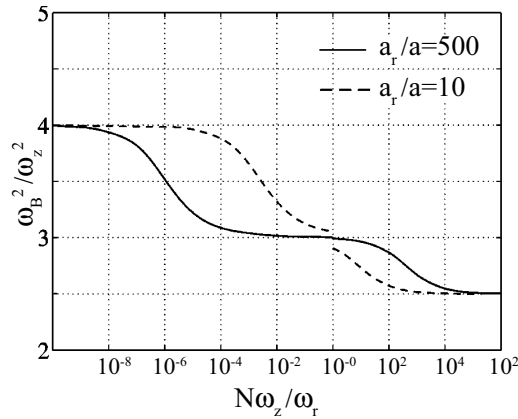
$$\begin{aligned}
 m\ddot{z}(t) &= -m\omega_z^2 z(t) - U \frac{\partial}{\partial z(t)} n_{1D}(z, t) \\
 mz(0)\ddot{\lambda} &= -m\omega_z^2 z(0)\lambda - \frac{U}{\lambda} \frac{\partial}{\partial z(0)} \frac{n_{1D}(z(0))}{\lambda} \\
 \Rightarrow \quad \ddot{\lambda} &= -\omega_z^2 \lambda + \frac{\omega_z^2}{\lambda^2}.
 \end{aligned} \tag{4.8}$$

Looking at small periodic deformations  $\lambda(t) = 1 + \epsilon \sin(\omega_B t)$  of the gas simplifies equation (4.8) to

$$\begin{aligned} -\epsilon \omega_B^2 \sin(\omega_B t) &= -\omega_z^2(1 + \epsilon \sin(\omega_B t)) + \frac{\omega_z^2}{(1 + \epsilon \sin(\omega_B t))^2} \\ &\simeq -3\epsilon \omega_z^2 \sin(\omega_B t). \end{aligned} \quad (4.9)$$

Hence, in this classical model for a gas in the 1D mean field regime, one finds  $(\omega_B/\omega_D)^2 = 3$ .

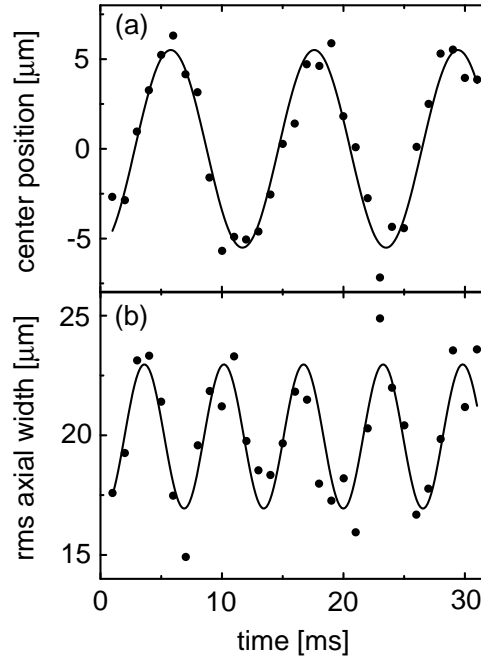
The considerations above are purely classical. In a more appropriate treatment [Men02, Ped03, Fuc03], the density of the gas is described by the hydrodynamic equations of superfluids. Oscillating solutions depend on the equation of state  $\mu(n_{1D}(z))$ , which is described locally by the Lieb-Liniger theory [Lie63b]. Analytic solutions can be found in the limiting cases of the 1D-mean field and Tonks-Girardeau regime, which coincide with the ones found with our simple models above. For a degenerate gas in the 1D mean field regime, one expects  $(\omega_B/\omega_D)^2 = 3$ , whereas in the Tonks-Girardeau regime  $(\omega_B/\omega_D)^2 = 4$ . The latter frequency ratio is the same for both a thermal gas and a gas of degenerate, noninteracting fermions. In contrast, for a three-dimensional elongated condensate in the mean field regime the ratio of the oscillation frequencies is  $(\omega_B/\omega_D)^2 = 5/2$  [Str96, Mew96, Che02]. Between these regimes, the ratio can be found numerically using a sum rule approach [Men02]; the result is displayed in figure 4.3.



**Figure 4.3:** Ratio of the two lowest collective modes  $(\omega_B/\omega_z)^2$  as a function of the parameter  $N\omega_z/\omega_r$  [Men02]. In our experiment,  $a_r/a \approx 10$ . To the right the particle number is so high that  $\mu > \hbar\omega_r$  and the gas is three-dimensional ( $\omega_B^2/\omega_z^2 = 2.5$ ). Reducing the particle number brings the gas into the 1D mean-field regime ( $\omega_B^2/\omega_z^2 = 3$ ). At the lowest particle numbers interactions dominate and the characteristic frequency ( $\omega_B^2/\omega_z^2 = 4$ ) of the Tonks-Girardeau regime is obtained. This figure is published with the kind permission of C. Menotti.

### 4.3.2 Experimental observation

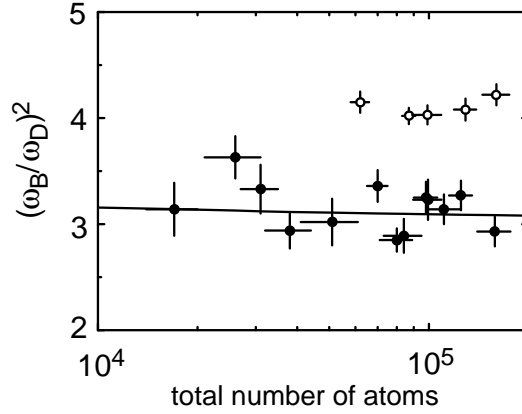
We measure the frequency of the collective excitations of the atoms in the optical lattice. The breathing mode is excited by sinusoidal intensity modulation of the optical lattice with an amplitude of  $4 E_r$  for five cycles and a frequency of 150 Hz, which is close to but does not match the expected frequency of the breathing mode. At the end of the modulation period a short (1 ms) magnetic field gradient is applied along the symmetry axis of the 1D tubes to induce a dipole oscillation of the condensate in the axial trapping potential. After a variable evolution time in the combined optical and magnetic trapping potential all confining forces are suddenly switched off<sup>1</sup> and we detect the atoms after ballistic expansion by absorption imaging. The density distribution of the atoms is fitted by a Gaussian to extract the position and width of the cloud. Figure 4.4 shows a data set of a dipole oscillation (figure 4.4 a) and a breathing mode (figure 4.4 b). In order to extract the frequencies of the modes, we fit an exponentially decaying sine function to the position of the cloud and an exponentially decaying sine function plus a linearly increasing term to the rms axial width of the cloud. The latter accounts for the observation that there is a



**Figure 4.4:** Dipole oscillation (a) and breathing mode (b) of a quantum degenerate one-dimensional Bose gas. For this data set an almost pure Bose-Einstein condensate with  $N = (9.8 \pm 0.8) \times 10^4$  atoms is loaded into the optical lattice and imaged after 15 ms of ballistic expansion. From the fits we obtain  $\omega_D = 2\pi \times (84.6 \pm 0.4)$  Hz and  $\omega_B = 2\pi \times (152.6 \pm 2.0)$  Hz.

<sup>1</sup>The switch-off time for the optical lattice is 5  $\mu$ s and for the magnetic trap 300  $\mu$ s.

slight increase in the width of the cloud with longer hold times, possibly due to technical noise. The damping coefficients vary between  $0 \text{ s}^{-1}$  and  $40 \text{ s}^{-1}$  for the dipole oscillations and between  $3 \text{ s}^{-1}$  and  $60 \text{ s}^{-1}$  for the breathing mode. We find that the damping coefficients depend critically on the alignment of the optical lattice and the quality of the beams.



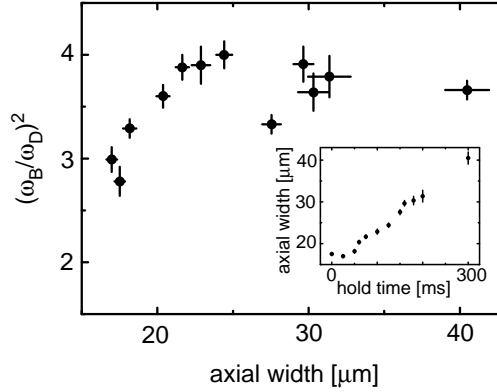
**Figure 4.5:** The measured frequency ratio  $(\omega_B/\omega_D)^2$  for a Bose condensed 1D gas (solid symbols). The solid curve is the theoretical prediction from [Ped03] using the measured dipole frequency along the 1D tubes  $\omega_z = 2\pi \times 84 \text{ Hz}$  and the frequency  $\omega$  of the slowly varying confining potential in the transverse direction with  $\sqrt{m/m^*}\omega = 2\pi \times 4 \text{ Hz}$ . Averaging all measurements, independent of the atom number, we obtain a frequency ratio of  $(\omega_B/\omega_D)^2 = 3.15 \pm 0.22$ . For a 1D gas of thermal atoms we find  $(\omega_B/\omega_D)^2 = 4.10 \pm 0.08$  (open circles). The depth of the optical lattice is  $30 E_r$ . The error bars reflect only the statistical uncertainties on the total atom number and fit errors on the frequencies.

Figure 4.5 shows the measured ratio  $(\omega_B/\omega_D)^2$  for a pure 3D-Bose-Einstein condensate loaded into a 2D optical lattice for various total atom numbers. There is no discernible thermal cloud for any data point, which allows us to estimate for the temperature  $T/T_{c,3D} < 0.3$ , where  $T_{c,3D}$  denotes the critical temperature for Bose-Einstein condensation in the final magnetic trapping configuration. We compare the measured ratio  $(\omega_B/\omega_D)^2$  to the theoretical prediction of [Ped03] (solid line) and find good agreement over the wide range of atom numbers investigated. This serves as proof that the gas is indeed one-dimensional. For the lowest total atom numbers  $N = 1.7 \times 10^4$  the parameter  $\gamma$  reaches unity in the central tube of the lattice, indicating that we are in the crossover region from the 1D mean field regime to the Tonks-Girardeau regime. We estimate the number of atoms in the central tube to be 30, assuming that the overall 3D density profile is Thomas-Fermi-like and using an effective coupling constant  $\tilde{g}$  which is modified by the optical lattice [Krä02, Krä03].

We also load thermal gases into the optical lattice and obtain an average value  $(\omega_B/\omega_D)^2 = 4.10 \pm 0.08$  without significant dependence on the total atom number  $N$  and temperature  $T$ .

over the range of  $6 \times 10^4 < N < 1.6 \times 10^5$  and  $54 \text{ nK} < T < 91 \text{ nK}$ . For thermal clouds we observe that the frequency of the dipole oscillations is up to 5% smaller than for the Bose condensed clouds. We attribute this to the larger size of the thermal clouds which therefore might experience anharmonic parts of the optical potential.

In order to study the transition from the 1D quantum degenerate gas to the 1D thermal gas we prepare atomic clouds in the optical lattice with increasing non-condensed fraction but constant atom number. We load an initially pure Bose-Einstein condensate of  $7 \times 10^4$  atoms into an optical lattice and trap it there for different hold times before exciting the collective modes. During the hold period the condensate is subjected to heating by off-resonant photon scattering with a calculated heating rate of  $70 \text{ nK/s}$  and possibly technical noise on the trapping fields. We find that together with the hold time the axial width of the atomic cloud increases (see inset of figure 4.6), whereas the radial size is unaffected. Since the timescale for thermalisation of the 1D gas is unknown it remains unclear whether the cloud is in thermal equilibrium and we refrain from calculating a temperature from the rms axial width of the cloud. Figure 4.6 shows the measured ratio  $(\omega_B/\omega_D)^2$  as a function of the rms axial width of the cloud. For increasing width the ratio  $(\omega_B/\omega_D)^2$  approaches 4, which is the value for a classical noninteracting gas. From a simple estimate we deduce that the 1D gases are in a collisional regime along the axial direction, since  $N_{1D} \cdot (1 - \mathcal{T}) \gg 1$ , where  $\mathcal{T}$  is the transmission coefficient for a 1D collision of two bosons [Ols98] and  $N_{1D} \sim 70$  is the number of atoms in a 1D tube.



**Figure 4.6:** The measured frequency ratio  $(\omega_B/\omega_D)^2$  for a Bose gas with  $7 \times 10^4$  atoms after heating in the optical lattice. The rms axial width is measured after 15 ms of time-of-flight and is an indicator of the rising temperature. The ratio increases from its initial value of approximately 3 to 4, as is expected for a transition from a 1D Bose gas to a thermal gas. The inset shows the evolution of the axial width vs. hold time in the optical lattice prior to excitation of the collective modes.

In conclusion, we have realised both thermal and quantum degenerate gases in one dimension and investigated their physics by measuring the low-lying collective excitations. Our measurements have shown that the properties of the 1D ground state are extremely sensitive to thermal excitations, and that finite temperature effects must be taken into account when studying 1D gases, in particular for the identification of the Tonks-Girardeau regime of impenetrable bosons.

---

## 5 Strongly interacting 1D Bosons – the Mott insulator

Quantum gases trapped in the periodic potential of an optical lattice have opened a new experimental window on many-particle quantum physics. Besides enabling us to change the dimensionality and study one-dimensional systems - as in the last chapter - it is possible to control the effect of interactions with optical lattices. This ability has led to the observation of the transition from a three-dimensional superfluid to a Mott insulator by Greiner et al. [Gre02]. Such strongly correlated phases lie at the heart of quantum many-body physics. By studying them in experiments where nearly all parameters can be tuned, one hopes to gain a deeper understanding of general concepts related to superfluidity and superconductivity. In one dimension quantum fluctuations play an important role, changing the transition from a superfluid to a Mott insulator significantly. By introducing a periodic potential along the direction of motion of a 1D gas, we were able to observe the transition from the superfluid to the Mott insulator in one dimension and see signatures of increased quantum fluctuations.

### 5.1 Bose-Hubbard model

Degenerate Bose gases trapped in the lowest band of an optical lattice can be modelled using the Bose-Hubbard Hamiltonian [Fis89, Jak98], in which the hopping of atoms between neighbouring lattice sites is characterised by the tunneling matrix element  $J$ , while the interaction energy for two atoms occupying the same site is given by  $U$ :

$$H = -J \sum_{\langle i,j \rangle} \hat{a}_i^\dagger \hat{a}_j + \frac{U}{2} \sum_i \hat{n}_i (\hat{n}_i - 1) + \sum_i \epsilon_i \hat{n}_i. \quad (5.1)$$

Here  $\hat{a}_i^\dagger$  and  $\hat{a}_i$  denote the bosonic creation and annihilation operators for a particle at site  $i$ , and  $\hat{n}_i = \hat{a}_i^\dagger \hat{a}_i$  is the number occupation of site  $i$ . The last term introduces a site-specific

---

Parts of this chapter are published in [Stö04, Köh04, Köh05b].

energy offset  $\epsilon_i$  related to a possible external potential. The physics of this model is governed by the ratio between  $U$  and  $J$ , i.e. between interaction and kinetic energy. This parameter can be controlled by changing the depth of the lattice potential. If the ratio  $U/J$  is below a critical value, it is favourable for the atoms to delocalise due to the large energy gain  $J$  and the ensemble becomes superfluid. The number fluctuations which are an inherent feature of superfluidity become energetically unfavourable when  $U/J$  is above the critical ratio, due to the large repulsive interaction  $U$ . Instead, the interaction energy is minimised when each site is occupied by the same number of atoms. In order to achieve this, the atoms must localise and the system becomes Mott insulating. In order to compare the phase diagram in different geometries (see figure 5.1), the total energy gain  $zJ$  due to delocalisation to all  $z$  neighbours has to be taken into account, where  $z = 2$  in 1D and  $z = 6$  in 3D.

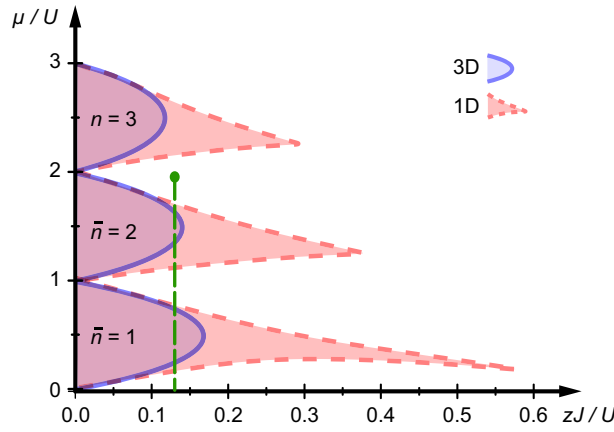


**Figure 5.1:** Schematic phase diagram at  $T = 0$  showing the Mott lobes. Within the Mott lobes the system is incompressible with a fixed particle number  $\bar{n}$  per site. Outside, the superfluid phase prevails. The phase boundaries in the three-dimensional case can be determined accurately by mean-field calculations [Fis89], while in the one-dimensional case, the increased quantum fluctuations have to be taken into account [Bat90, Fre94, Küh98]. As a consequence, the insulating phase is entered at much lower interaction strength.

We access the one-dimensional regime [Fis89, Bat02, Büc03b] using a non-isotropic optical lattice consisting of three mutually perpendicular standing waves. By choosing large potential depths in two axes we can selectively suppress tunneling and hopping is possible only along one dimension. Therefore an array of one-dimensional tubes with periodic modulation along their axis is formed. While the displayed phase diagram (figure 5.1) depicts the homogeneous case, the envelopes of the laser beams give rise to a harmonic trapping potential along the axial direction of the tubes. Consequently, the chemical potential decreases when moving away from the trap center. As a result, different phases are found, depending on the position. The green line in figure 5.1 shows the values the chemical potential can take at different positions when



$\mu_{center}/U \approx 2$ . In the center of the trap the gas is superfluid. Further out, the decreasing chemical potential favours a Mott insulating zone with  $\bar{n} = 2$ , followed by a superfluid region and another Mott insulating zone with  $\bar{n} = 1$  before the density goes to zero in the outer superfluid shell. The horizontal position  $zJ/U$  can be changed by adjusting the laser intensity for the standing wave along the axial direction.

## 5.2 Observing the superfluid to Mott insulator transition

The details of the experimental sequence and the setup are described in chapter 3.6.1. In brief, we produce an almost pure Bose-Einstein condensate of typically  $1.5 \times 10^5$   $^{87}\text{Rb}$  atoms in the  $|F = 2, m_F = +2\rangle$  hyperfine state and load the condensate into the ground state of the optical lattice. The intensities of the lasers are slowly increased to their final values using an exponential ramp with a time constant of 25 ms and a duration of 100 ms. The resulting optical potential depths  $V_{x,y,z}$  are proportional to the laser intensities and are expressed in terms of the recoil energy  $E_r$ . To prepare an array of one-dimensional tubes, two lattice axes are ramped to  $V_{\perp} \equiv V_x = V_z = 30 E_r$ . The third one is simultaneously ramped to a much lower value  $V_{ax,0} \equiv V_y$ . In this configuration, the transverse tunneling matrix elements  $J_x$  and  $J_z$  are small and contribute a correction of the order of  $J_{x,z}/\mu \ll 1$  to the one-dimensional characteristics of the individual tubes. The ratio between interaction and kinetic energy is controlled by choosing different lattice depths  $V_{ax,0}$ . In the following paragraphs this ratio will be given in terms of  $U/\tilde{J}$ , with  $\tilde{J} = 2(J_x + J_y + J_z)$  including the non-isotropic tunneling between all  $z = 2d$  next neighbour sites.

### 5.2.1 Excitation spectra

We study the excitation spectrum by modulating the amplitude of the axial lattice potential  $V_{ax}$  in order to perform two-photon Bragg spectroscopy [Ste99]. The lattice potential takes the form  $V_{ax}(y, t) = (V_{ax,0} + A_{mod} \sin(2\pi\nu_{mod}t)) \sin^2(ky)$ . The modulation with amplitude  $A_{mod}$  and frequency  $\nu_{mod}$  introduces two sidebands with frequencies  $\pm\nu_{mod}$  relative to the lattice laser frequency which define the energy  $h\nu_{mod}$  of the excitation. Due to the Bragg condition, atoms scattering two photons receive a momentum transfer of  $0\hbar k$  or  $2\hbar k$ . In contrast to applying a potential gradient across the lattice [Gre02], this method is not susceptible to effects like Bloch oscillations and Zener tunneling which occur for low axial lattice depths. Furthermore, the excitation energy is precisely determined and does not involve any parameters that need calibration.

After the excitation, the experimental sequence is continued by ramping down the lattice potentials linearly in 15 ms to  $V_{ax} = V_{\perp} = 4 E_R$  where the atoms are able to tunnel again in all three dimensions between the sites of the lattice. To allow for re-thermalisation of the system, the atoms are kept at this lattice depth for 5 ms. Then all optical and magnetic potentials are suddenly switched off. The resulting matter wave interference pattern is detected by absorption imaging after 25 ms of ballistic expansion. The width of the central momentum peak is taken as a measure of how much energy has been deposited in the sample by the excitation. If the energy increase is small, the peak is well fitted by a bimodal distribution. For resonant excitation there is only a single Gaussian component, reflecting that the temperature of the atoms has significantly increased. In order to be independent of the shape of the peak we use the full width at half maximum (FWHM) as a measure of the introduced energy. Although this underestimates small energy increases, the important resonances and features of the spectra are shown well.

The duration  $t_{mod} = 30$  ms and amplitude  $A_{mod} = 0.2V_{ax,0}$  of the modulation are chosen so that the resulting excitation of the condensate does not exhibit saturation effects for all measurements presented here. We have verified that all atoms remain in the lowest Bloch band by adiabatically switching off the lattice potentials [Gre01b] after the modulation. When we load a cold thermal cloud into the lowest Bloch band and apply our modulation scheme, we do not observe excitations.

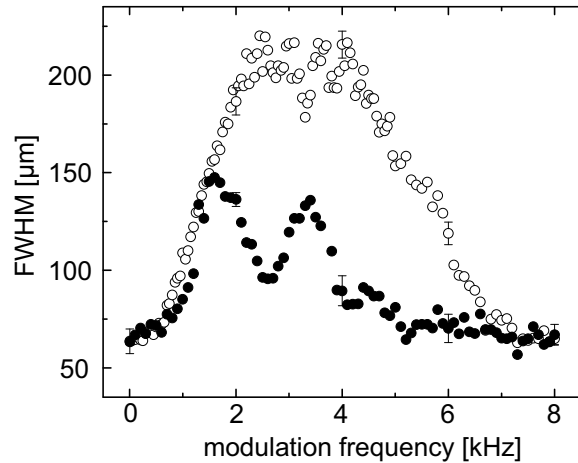


**Figure 5.2:** Spectroscopy of the 1D superfluid (open circles) and the Mott insulating phase (filled circles) with values of  $U/\tilde{J}$  of approximately 2.3 and 14 respectively. The error bars reflect the statistical error of 5 measurements.

Figure 5.2 displays the fundamental change in the excitation spectrum for a 1D Bose gas when the crossover from the superfluid to the Mott insulating phase occurs: the broad continuum of the superfluid contrasts with the discrete spectrum of the Mott insulator. One surprising feature is that we can excite the superfluid with our scheme at large  $\hbar\nu_{mod}$  contrary to predic-

tions for the weakly interacting superfluid in an optical lattice formed by a single standing wave [Men03]. In our experiment strong interactions lead to quantum depletion and higher order excitations beyond Bogoliubov theory become possible [Hug59]. In combination with the broken translational invariance in the inhomogeneous trap, this could explain the non-vanishing excitation probability observed in the experiment at  $2\hbar k$  and high energies [Büc03a]. In another explanation, the parametric excitation of the Bogoliubov mode at frequency  $\nu_{\text{mod}}/2$  and the ensuing nonlinear dynamics are held responsible for the broad continuum observed [Krä05, Toz05]. We have experimentally studied the issue in more detail in [Sch04].

A full series of spectra for different values of  $U/\tilde{J}$ , ranging from the superfluid via the crossover region to the Mott insulating phase, is shown in figure 5.3. We observe the appearance of the discrete structure between  $U/\tilde{J} \approx 4$  and  $U/\tilde{J} \approx 8$ , which is characteristic for the Mott insulating phase. Above  $U/\tilde{J} \approx 20$  there is no more background due to the superfluid. Our results are in accordance with the prediction of  $U/\tilde{J} \approx 5.8$  made by employing mean-field theory [Fis89, Jak98] for the borderline between superfluid and the  $n = 1$  Mott insulator. Calculations beyond the mean-field approach indicate an onset of the Mott insulating phase in the homogeneous 1D system at  $U/\tilde{J} \approx 1.8$  [Küh98]. However, the finite size of the trap prohibits a sharp transition [Bat02], so that the fraction of Mott insulating atoms increases gradually with increasing  $U/\tilde{J}$ .

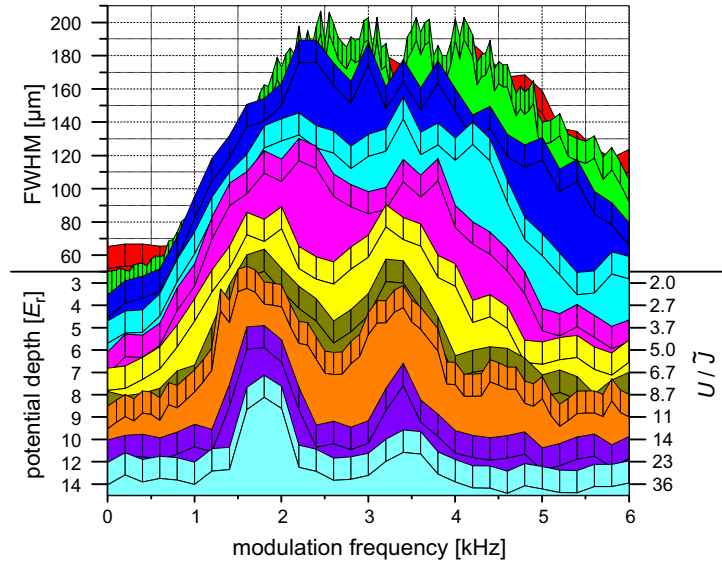


**Figure 5.3:** The measured excitation spectrum of an array of 1D gases is shown for different values of the lattice potential depth  $V_{\text{ax},0}$ . The corresponding ratios between interaction and kinetic energy  $U/\tilde{J}$  are calculated numerically using a band structure model in the tight-binding approximation, which is described in section 2.3.3.

For the superfluid we obtain spectra which differ significantly from the results of Greiner et

al. [Gre02], since the superfluid excitations decrease at higher energies. Our excitation scheme does not induce dephasing that occurs when the strongly interacting condensate is accelerated near the edge of the Brillouin zone [Bro01]. This dephasing might cause the broadening and the background in the tilted lattice experiments at high energies in ref. [Gre02]. The width of the superfluid spectra for the 1D gas is on the same order as twice the width of the lowest band for Bogoliubov excitations.

In the Mott insulating phase we find the first resonant peak for all data sets close to the calculated value of  $U$ . A second peak appears at  $(1.91 \pm 0.04)$  times the energy of the first resonance, slightly smaller than the value of 2 reported in [Gre02]. This resonance might be attributed to defects at positions where initially one site with  $n = 1$  atom is next to one with  $n = 2$  atoms. In the excited state the single atom has hopped onto the doubly occupied site. A much weaker resonance appears at  $(2.60 \pm 0.05)$  times the energy of the first resonance, which could indicate higher order processes of two atoms tunneling simultaneously.

### 5.2.2 Coherence properties

Compared to the superfluid properties, the coherence properties of the system provide complementary information about the state of the gas. They are probed by studying the matter wave interference pattern [Orz01, Gre02].

We first prepare the array of 1D systems as above but do not apply our excitation scheme. Instead, after holding the atoms at the final lattice depth for  $t_h = 30$  ms, we increase  $V_{ax}$  rapidly ( $< 40 \mu\text{s}$ ) to about  $25 E_R$  and then abruptly switch off all optical and magnetic trapping potentials. This procedure projects the different initial configurations onto the same Bloch state. To extract the number of coherent atoms  $N_{coh}$  from the interference pattern, the peaks at  $0\hbar k$ ,  $\pm 2\hbar k$  and  $\pm 4\hbar k$  are fitted by Gaussians (see figure 5.4 b). At  $V_{\perp} = 30 E_R$ , coherence between the individual 1D systems is lost after a few milliseconds. Thus perpendicular to the axis of the tubes the expansion of the ground state is Gaussian. Incoherent atoms give rise to a broad Gaussian background which dominates for higher  $V_{ax,0}$ . Taking this fit as a measure of the number of incoherent atoms  $N_{incoh}$ , we calculate the coherent fraction  $f_c = \frac{N_{coh}}{N_{coh} + N_{incoh}}$ . For comparison, we have performed the same experiment in three-dimensional isotropic geometry where  $V_{ax} = V_{\perp}$ . As shown in figure 5.4 a,  $f_c$  decreases slowly to zero for increasing values of  $U/\tilde{J}$  and appears to be almost independent of the dimensionality. This coincides with the prediction that for strongly interacting Bose gases in optical lattices the superfluid fraction can be significantly different from the coherent fraction, and that the decrease of  $f_c$  is not a sufficient signature of entering the Mott insulating phase [Rot03].

In figure 5.4 c we plot the width of the central peak of the interference pattern, which is a measure of the coherence length of the gas. An increasing width is a good indicator for

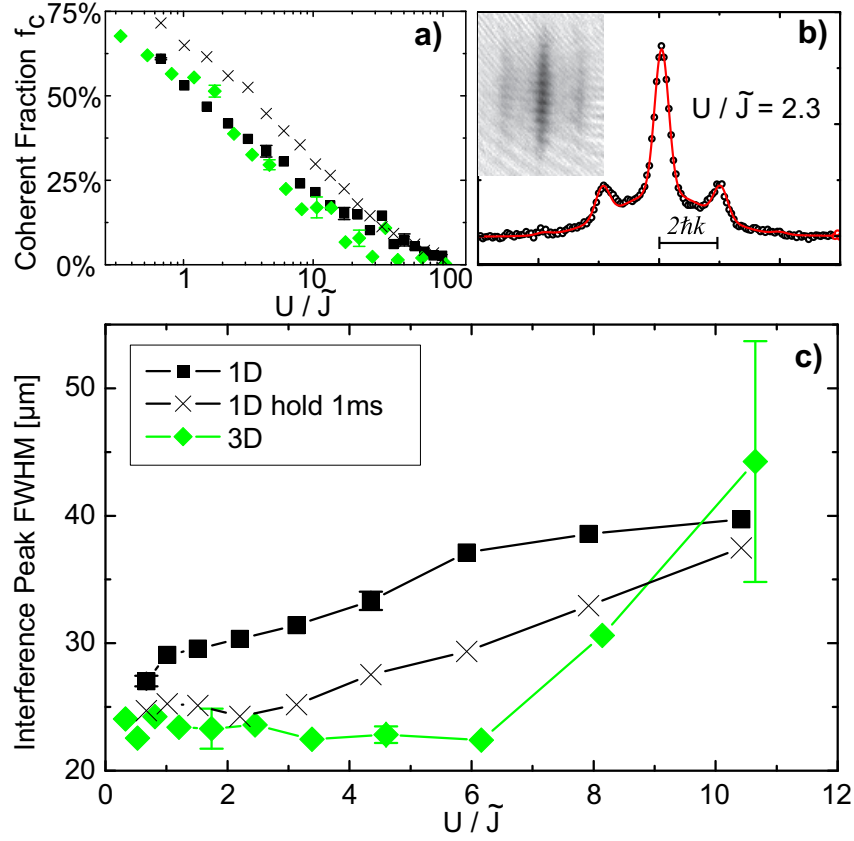


**Figure 5.4:** a) Coherent fraction vs.  $U/\tilde{J}$ . The error bars are determined by the statistical error of 4 measurements. b) The column sum of the optical density (circles) and the fits (solid line) from which the number of coherent and incoherent atoms is deduced for the 1D case. The inset shows the absorption image after 10 ms of time-of-flight (dimensions  $360 \mu\text{m} \times 467 \mu\text{m}$ ). c) Width of the central momentum peak vs.  $U/\tilde{J}$ .

the presence of a Mott insulating phase since even a small Mott insulating domain reduces the coherence length of the sample, as elucidated in numerical calculations [Kol04]. Our data show that the increase in width commences at much lower values of  $U/\tilde{J}$  for the 1D gas than for the 3D gas. This supports the expectation that due to the more pronounced quantum fluctuations in the 1D geometry the gas enters the Mott insulating state at lower values of  $U/\tilde{J}$  [Küh98, Bat02, Büc03b, Kol04]. Experimentally, thermal fluctuations may also contribute to the observed width. However, by comparing the width of the interference peak at different hold times ( $t_h = 1 \text{ ms}$  and  $t_h = 30 \text{ ms}$ ) we find that the primary effect of the additional heating is an overall increase of the width rather than a change of the slope of the curve.

### 5.3 A dimensional crossover

So far we have considered the gases in each tube of the lattice as entirely isolated systems because the tunneling time  $\hbar/J_{\perp}$  between the tubes exceeds the experiment duration. It is, however, very instructive to look at the effect that the tunneling between the tubes has on the ground state properties of the system.

For infinitely long tubes at zero temperature it has been shown that even an infinitesimally small tunneling drives the system into a three-dimensional superfluid state, provided there is no periodic potential along the tube axis [Efe75]. If such a periodic potential is present, the formation of Mott insulating domains competes with the tendency of the atoms to delocalise due to the tunneling between the tubes. This competition leads to a deconfinement transition between a 1D Mott insulator and a 3D superfluid [Ho04, Gan04] for densities commensurate with the lattice spacing. The corresponding phase diagram case is shown in figure 5.5.

The one-dimensional systems realised in this work are of finite size and harmonically trapped. Therefore the phase transitions described above are replaced by crossovers and the harmonic confinement gives rise to an inhomogeneous state with coexisting superfluid and Mott insulating phases. Moreover, the individual tubes can be treated as “atomic” quantum dots which have a finite “charging energy” representing the energy cost of adding one particle to the tube. This charging energy may play the same role as the interaction energy for a single site and drive a transition from a superfluid to a two-dimensional Mott insulator [Ho04, Gan04]. The tunneling between the tubes is suppressed by the charging energy and the 2D Mott insulator state is characterised by a fixed number of atoms per tube. Meanwhile, the state within an individual tube need not be Mott insulating. The new crossovers arising from the finite size have also been included in the phase diagram in figure 5.5.

It is now interesting to evaluate the relevance of this phase diagram to our experimental observations. The dashed green line in figure 5.5 indicates the range of the experimental parameters. To obtain these parameters the density in the mean-field regime was calculated using the theory presented in [Krä03], leading to a particle number of 150 atoms per tube. This particle number was then inserted into the formula 4.6 to yield the chemical potential  $\mu$  for small  $U/\tilde{J}$ . In the Mott insulator regime the particle number of the central sites was estimated to be  $\bar{n}=2$  by using the one-dimensional density in the mean-field regime. Therefore the chemical potential in the Mott insulator is approximately  $1.5 U$ . The other necessary parameter is the tunneling time at  $V_{\perp} = 30 E_r$ , which is  $\hbar/J_{\perp} = 110$  ms.

The comparison of the experimental parameters with the phase diagram suggests that the dimensional crossover from a one-dimensional Mott insulator to a three-dimensional superfluid should in principle be observable. For the experiment, however, one must bear in mind that the loading of the atoms into the two-dimensional lattice is not fully adiabatic for high lattice depths

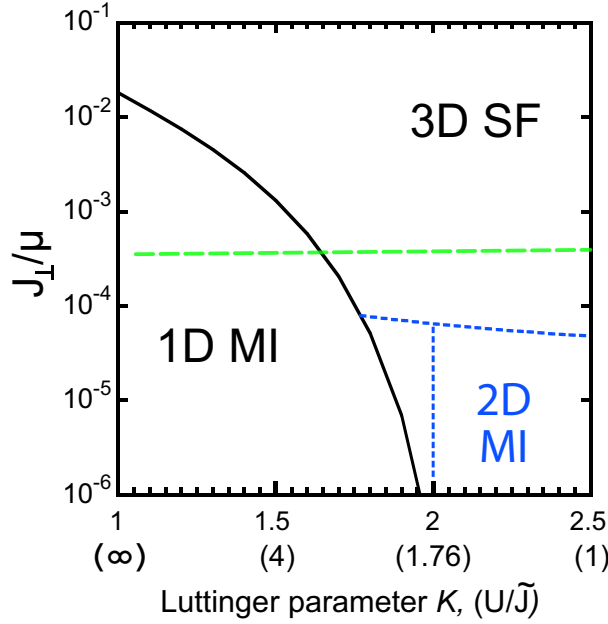


**Figure 5.5:** Phase diagram of an array of coupled tubes as a function of the tunneling between the tubes  $J_{\perp}$  and the effective interaction strength. The latter is given in terms of the Luttinger parameter  $K$  (for more information see [Gia04]). For convenience the corresponding values of our experimental parameter  $U/\tilde{J}$  are also given. The black lines illustrate the phase boundaries for the case of infinitely long tubes with a periodic potential along the direction of the tubes. In the case of harmonically confined system, the black lines show the corresponding crossovers. The additional blue dashed lines denote the crossover from the 2D Mott insulator to the 3D superfluid (horizontal) and from the 2D Mott insulator to the 1D Mott insulator (vertical), for a particle number of 100 atoms per finite tube. The regime of the experimental measurements in this chapter is indicated by the green dashed line. This figure is adapted from [Ho04] with kind permission of A. Ho.

due to the low tunneling rate between the tubes. Instead, the underlying harmonic potential will lead to a variation of the chemical potential between the tubes. The low tunneling rate  $J_{\perp}/\hbar$  is insufficient to counteract this difference and establish phase coherence between the tubes, as we have already observed in figure 5.4 b. Consequently, the observed crossover is between a strongly interacting one-dimensional superfluid and a one-dimensional Mott insulator.

## 5.4 Prospects for 1D Bose gases

In the experimental work described in the last two chapters one-dimensional Bose gases were created and brought into the strongly interacting regime for the first time. Several methods were developed which enabled these studies. The measurement of collective excitations proved to be

a sensitive tool to characterise the gas, drawing attention to the very low temperatures needed to achieve a one-dimensional Bose-Einstein condensate. Applying a periodic potential along the direction of motion increased the effective interaction strength and allowed us to study the superfluid to Mott insulator transition. The characteristic energy gap in the excitation spectrum was observed in a variation of two-photon Bragg spectroscopy. It became apparent, however, that the property most sensitive to the appearance of the Mott insulating regions is the coherence length.

Using these techniques we found indications that the quantum fluctuations inherent to one-dimensional systems shift the Mott insulator transition to lower values of  $U/\tilde{J}$  than in three-dimensional systems. However, further studies which pin down the transition region more accurately will be necessary to test the agreement between quantum Monte Carlo simulations and physical reality. A limiting factor is the trapping potential associated with the Gaussian envelope of the lattice lasers. In the confined system different phases can coexist in different regions of the trap. While it is impossible to realise unconfined systems, it seems feasible to create larger homogeneous regions. In such a set-up the curvature in the center of the trap would have to be compensated by the anti-trapping potential of a blue detuned laser. Due to its smaller spatial extent a bathtub potential would result.

Studies of the correlation functions could shed new light on the intriguing physics of strongly interacting 1D Bose gases. It has been predicted that the two and three body correlations are strongly reduced [Gan03, Khe03] and first evidence of this has been seen in three-body loss measurements in a gas with  $\gamma \approx 1$  [Tol04]. The two-body correlations might be measured by performing photoassociation in the lattice.



---

## 6 Confinement induced molecules in a 1D Fermi gas

Although it is conceptually simple, the scattering of two particles is of fundamental interest. It mediates interactions and can lead to the formation of molecules. The study of two particles forming a bound state has a long history both in physics and chemistry because it constitutes the most elementary chemical reaction. Cold atomic gases represent the ideal model system for these investigations as effects of temperature or the environment can be neglected, and the collisions are accurately described by standard quantum mechanics. For unconfined atoms undergoing *s*-wave interaction, a bound molecular state is only supported when the scattering length between the atoms is positive, whereas for negative scattering length the bound state is absent [Wig33].

Using optical lattices, we are in the unique position to be able to study scattering and molecule formation when motion is confined to one dimension. The strong confinement affects the two-particle physics fundamentally, provided that the scattering length and the size of the transverse ground state are similar [Ols98, Pet01, Ber03, Mor04]. We observe bound states irrespective of the sign of the scattering length, contrary to the situation in free space.

The experiments described in this chapter are performed with fermionic  $^{40}\text{K}$  atoms. Due to the Pauli principle, three-body collisions are suppressed and the weakly bound dimers are more stable than in comparable bosonic systems. Besides, the interactions are tunable because  $^{40}\text{K}$  features an easily accessible Feshbach resonance, which will be discussed in the next section. The strongly interacting one-dimensional Fermi gas which we create therefore represents the first realisation of a tunable atomic Luttinger liquid.

---

Parts of this chapter are published in [Mor05].

## 6.1 Scattering Theory

In ultracold atomic gases, the interaction strength can be changed by tuning the magnetic field to values in the vicinity of a Feshbach resonance [Tie93, Ino98]. The physical origin of such Feshbach resonances and their consequences on the scattering properties of atoms and on molecules formation will be discussed in this section. Further details can be found in [Sak94, Dal99] which feature comprehensive introductions to scattering theory, while Feshbach resonances are treated [Chi05, Szy05].

The interatomic potential which causes scattering stems from two main physical origins: strong repulsion at short distances caused by overlap of the two electron clouds and the van der Waals attraction at larger separations. Several minor effects such as spin-spin and spin-orbit interactions are usually neglected. In the low energy limit it is useful to expand the scattering wavefunction  $\psi_{\mathbf{k}}(\mathbf{r})$  into partial waves  $\psi_{\mathbf{k}}(\mathbf{r}) = Y_{lm}(\theta, \phi) R_l(r)$ , where the  $Y_{lm}(\theta, \phi)$  are spherical harmonics with the projection of the angular momentum  $l$  being  $m$  (not to be confused with the mass  $m$ ). The probability distribution in the radial direction is given by  $R_l(r)$  and obeys a modified 1D-Schrödinger equation

$$\left[ -\frac{\hbar^2}{2m} \left( \frac{d^2}{dr^2} + \frac{2}{r} \frac{d}{dr} \right) + V_{eff}(r) \right] R_l(r) = E R_l(r) \quad \text{with} \quad V_{eff}(r) = V(r) + \frac{l(l+1)}{r^2}. \quad (6.1)$$

For higher angular momenta the effective potential includes a centrifugal barrier as shown in figure 6.1 which prevents low energy particles from feeling the potential  $V(r)$ . Therefore usually only  $s$ -wave scattering is relevant, which is isotropic.

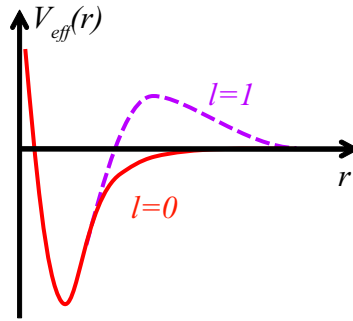


**Figure 6.1:** Effective interaction potential for  $s$ - and  $p$ -wave scattering.

The effect of the interaction is to give an extra phase  $\delta_s$  to the outgoing wavefunction, so that it becomes asymptotically proportional to  $r \cdot R_0(\mathbf{r}) \propto \sin(kr + \delta_s)$ . For cold atomic gases the deBroglie wavelength  $\lambda_{dB} = 2\pi/k \approx 1 \mu\text{m}$  greatly exceeds the extension of the interatomic potential of approximately 3 nm. Therefore the sine-function can be approximated by a straight

line at small distances. Within the interatomic potential the wavefunction is disturbed leading to the aforementioned asymptotic phase shift  $\delta_s$ , as demonstrated in figure 6.2. It is more convenient to parameterise the effect of the interaction by the intercept of the outside wavefunction with the  $x$ -axis. This yields the scattering length  $a$ .

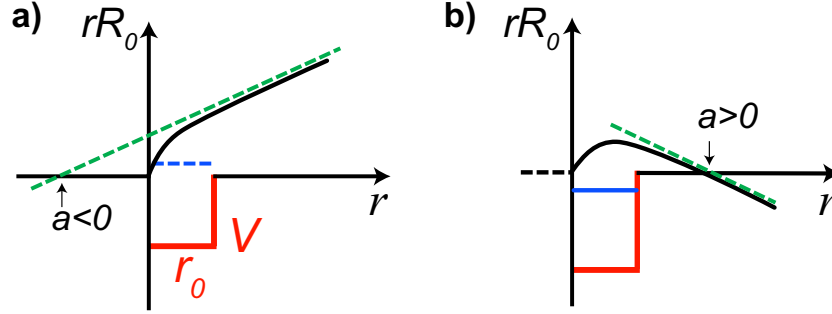


**Figure 6.2:** Scattering wavefunction  $rR_0$  in a simplified attractive potential. a) For a weak potential (red), the wavefunction (solid black) is modified only slightly. The asymptotic wavefunction, drawn in dashed green, intercepts the  $x$ -axis at negative  $a$ . b) The stronger potential with  $a > 0$  supports a true bound state (blue), in contrast to the quasi-bound state in a) (dashed blue).

As long as the potential is not deep enough to support a bound state, the wavefunction is only slightly modified and  $a < 0$  (see figure 6.2 a). Once the potential depth is sufficient for a bound state, the effect on the wavefunction is more pronounced (see figure 6.2 b). Instead of having a positive slope, the wavefunction is tilted downwards again resulting in a positive scattering length. The latter wavefunction is very similar to that of a bound state in the potential well. Indeed, when solving the Schrödinger equation (6.1) for a box potential with negligible radius  $r_0 \rightarrow 0$  (see e.g. [Sak94]), it is found to support a bound state for all positive  $a$  with binding energy

$$E_B = \frac{\hbar^2}{ma^2}. \quad (6.2)$$

For negative  $a$ , this equation can be used to define a quasi-bound state just above the continuum. The above formula is correct as long as the scattering length is much larger than the effective range  $r_0$  of the potential. For a square well potential with finite size  $r_0$ , the scattering length  $a$  in eq. (6.2) has to be replaced by  $a - r_0$ . For the more realistic van der Waals potential  $V_{vdW} = -C_6/r^6$ , the validity of the formula can be extended to lower values of  $a$  with the correction [Gri93]

$$E_B = \frac{\hbar^2}{m(a - \bar{a})^2} \quad \text{with } \bar{a} = \frac{\Gamma(3/4)}{2\Gamma(5/4)} \left( \frac{mC_6}{4\hbar^2} \right)^{1/4}. \quad (6.3)$$

In potassium, the “mean scattering length”  $\bar{a}$  as determined from  $C_6 = 3927 a_0$  [Tic04] is  $\bar{a} = 62.2 a_0$ .

### 6.1.1 Feshbach resonances

So far, we have had no reason to consider the internal states of the colliding atoms during the scattering process. However, if the two atoms with the quantum numbers  $|F_1, m_{F_1}\rangle$  and  $|F_2, m_{F_2}\rangle$ , which are good quantum numbers at large distances, approach each other the respective electron clouds overlap. The electron spins couple to each other and the exchange interaction  $\hat{S}_1 \cdot \hat{S}_2$  may become comparable to the hyperfine interaction. Looking at the spin-spin interaction as a perturbation, it couples channels with different total  $F_{\text{tot}} = F_1 + F_2$  of the unperturbed scattering Hamiltonian. The projection on the quantisation axis  $M_F = m_{F_1} + m_{F_2}$  has to be conserved for symmetry reasons.

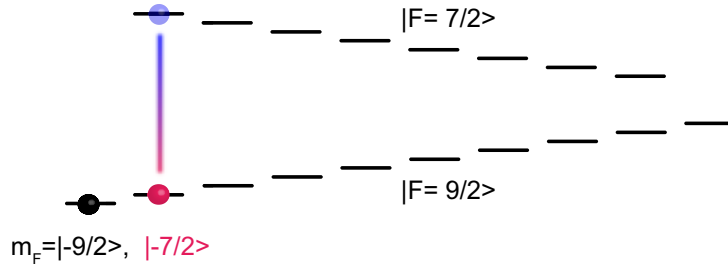


**Figure 6.3:** Level scheme of  $^{40}\text{K}$  at nonzero magnetic field. The  $m_F$ -number increases from left to right. The vertical line indicates the coupling between the different channels.

We are especially interested in collisions between the  $|9/2, -9/2\rangle$  and the  $|9/2, -7/2\rangle$  states of potassium  $^{40}\text{K}$ , because a Feshbach resonance is accessible at a moderate magnetic field. The only other combination with the same  $M_F$  is  $|9/2, -9/2\rangle$  and  $|7/2, -7/2\rangle$  (see Fig. 6.3). The former combination is called the open channel and the latter the closed channel. The two channels have different total magnetic moments and therefore their relative potential energy curves can be shifted against each other.

#### Bound states

Each potential curve of  $^{40}\text{K}$  supports approximately 40 deeply bound states, but we concentrate only on the highest vibrationally excited state of each channel. The background scattering length  $a_{bg}$  is given by the energy of the most weakly bound state in the open channel and is only valid if the coupling to the closed channel does not modify the scattering properties. The coupling to the closed channel becomes relevant if the closed channel has an energy level close to the collision energy of the two atoms. For realistic magnetic fields, this is only possible for the most weakly bound state of the closed channel.

When the molecular state of the closed channel is tuned close to resonance with the in-

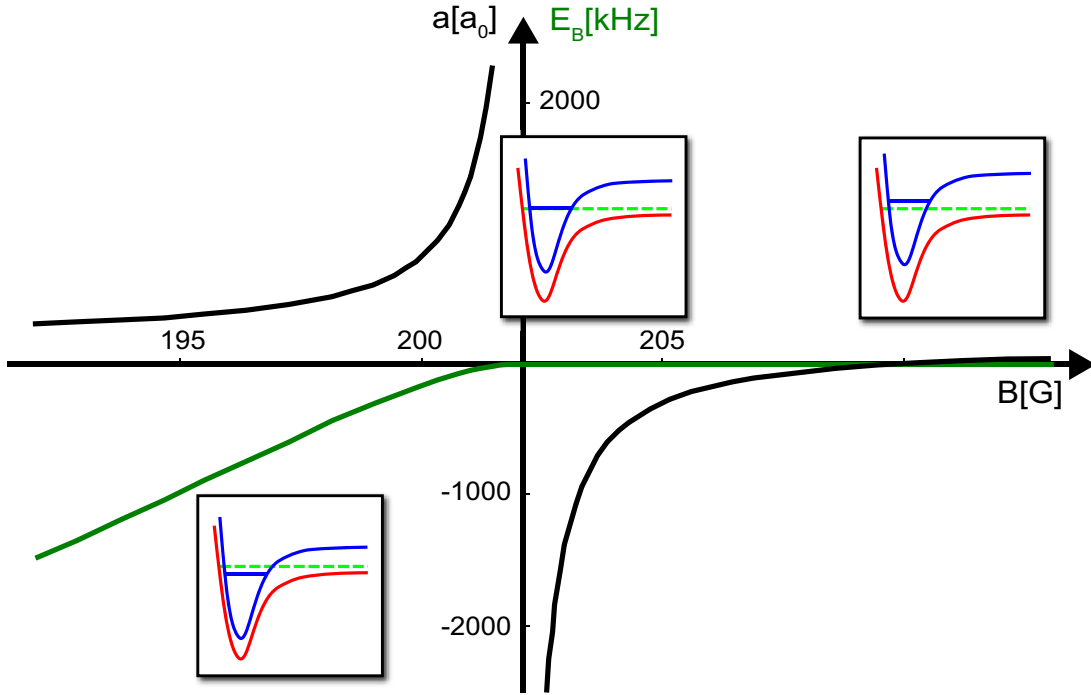


**Figure 6.4:** Resonant behaviour of the scattering length and formation of molecules of  $^{40}\text{K}$  atoms. The scattering length (in black) diverges at  $B_0 = 202.1$  Gauss [Reg04], and below this value, for positive scattering length, a bound state exists, the binding energy of which is shown in green. The insets demonstrate the qualitative evolution of the interaction potential curves of the open (red) and closed (blue) channel.

coming particle energy, second order processes during the scattering are enhanced, and virtual occupation of the closed channel becomes likely. The effective scattering potential is modified strongly and the scattering length diverges [Tie93]. Putting it another way, the coupled Hamiltonian has an eigenstate with the binding energy close to zero, so that the corresponding scattering length as given by equation (6.2) approaches infinity. The exact dependence of the scattering length on the magnetic field is given by [Moe95]

$$a(B) = a_{bg} \left( 1 - \frac{\Delta B}{B - B_0} \right), \quad (6.4)$$

where the width  $\Delta B$  and the position  $B_0$  parameterise the Feshbach resonance. In figure 6.4 the dependence of the scattering length, the binding energy and the separation of the two channels are depicted as functions of the magnetic field. For magnetic fields above the Feshbach resonance, no bound state exists and the scattering length is negative. The closed channel molecular state is above the continuum. At the Feshbach resonance itself, it crosses the continuum and the scattering length diverges, changing its sign in the process. As soon as the closed channel molecular state comes to lie below the continuum, a bound eigenstate develops.

### The Feshbach molecule

The resulting bound eigenstate is not identical with the molecular state of the closed channel. This is already obvious from the fact that the closed channel energy depends linearly on  $B$ , while the energy of the bound state is a quadratic function of  $B$ , as seen by inserting equation (6.4) into (6.2). The bound state is a solution of the coupled system, and the Feshbach molecule is a coherent mixture of the molecule in the closed channel and a long-range atom pair in the open channel.

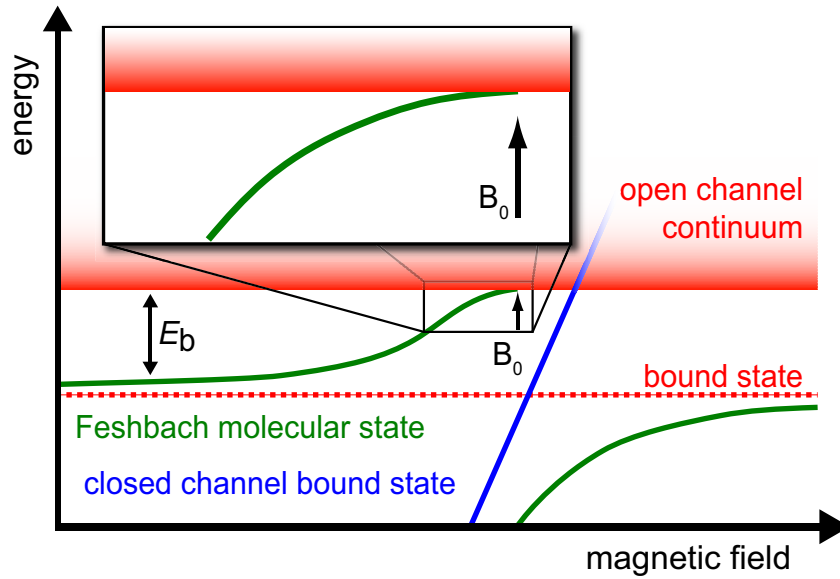


**Figure 6.5:** Evolution of the Feshbach molecule. The behaviour shown corresponds to the  $^{40}\text{K}$  Feshbach resonance and is not universal. The magnetic field dependence of the open channel has been subtracted, so that the continuum threshold is independent of  $B$ . The first bound state of the open channel (red dashed) is responsible for the positive background scattering length  $a_{bg}$ . The inset shows the quadratic dependence of the binding energy of the Feshbach molecule when it comes close to the continuum threshold (figure adapted from [Chi05, Szy05]).

To illustrate the exact nature of the bound state, a closer look at the coupling of the channels is necessary (see figure 6.5). The bound states of the closed and the open channel form an avoided crossing, as it is well known from two discrete coupled levels. As the upper branch of the avoided crossing approaches the open channel threshold, coupling to the continuum must be taken into account, which results in the quadratic dependence shown in the inset. For large negative detuning  $B - B_0$  from resonance, the  $^{40}\text{K}$  Feshbach molecule is not dominated by a large closed channel contribution, as one might expect, but instead approaches the open channel bound state. The closed channel admixture to the bound state never exceeds 8% [Szy05]. The Feshbach resonance in  $^{40}\text{K}$  qualifies as a "broad" resonance, which is dominated by the open channel.

### Experimental progress

Although Feshbach resonances were originally discussed in nuclear physics [Fes58], they have had great impact on experiments with ultracold quantum gases recently. After the first observation in a Bose-Einstein condensate in 1998 [Ino98] they were used to tune the interactions in Bose gases in various experiments. These studies include the implosion of a condensate [Don01], the formation of solitons [Str02, Kha02] and the observation of molecules [Don02, Chi03, Her03]. The first Feshbach molecules from fermionic atoms were created in the group of D. Jin [Reg03b], quickly followed by others [Str03, Cub03, Joc03a]. The composite fermions are much more stable against collisional relaxation of the vibrationally highly excited state than the bosons, because the Pauli principle suppresses the inelastic three-body collision [Pet04b]. Lifetimes up to 100 ms in  $^{40}\text{K}_2$  and 40 s in  $^6\text{Li}_2$  have been observed close to the Feshbach resonance. This enabled the Bose-Einstein condensation of molecules [Gre03, Joc03b].

The character of the pairs in a many-body system changes continuously with the magnetic field strength. Above resonance, no two particle bound state exists, but the fermionic atoms are expected to form a many-body BCS-like ground state with Cooper pairing which exhibits superfluidity. On the resonance, the scattering length diverges. The elastic collision cross section, on the other hand, is finite: The dependence on the relative wavevector of the scattering particles has the form [Dal99]

$$\sigma(k) = \frac{4\pi a^2}{1 + k^2 a^2}. \quad (6.5)$$

For  $ka \gg 1$  the cross section becomes universal and depends only on  $k$  as  $\sigma(k) = 4\pi/k^2$ . In this strongly interacting region the many-body ground state is notoriously hard to find theoretically. However, at sufficiently low temperatures vortices have been observed [Zwi05], which are a proof of superfluidity. Below resonance, the binding energy increases and the bosonic character of the molecules dominates. They can Bose condense and their size is approximately equal to the scattering length  $a$ .

#### 6.1.2 Molecule formation in the presence of 1D confinement

Tight radial confinement alters the scattering properties of two colliding atoms fundamentally: a bound state exists irrespective of the sign of the scattering length [Ber03]. Moreover, the interaction strength  $g_{1D}$  diverges when the scattering length approaches the transverse oscillator length  $a_r = \sqrt{\hbar/m\omega_r}$  [Ols98], with  $\omega_r$  being the radial trapping frequency. The actual scattering process is three-dimensional, because the effective range of the interatomic potential  $r_0$  is much smaller than the transverse oscillator length  $a_r$ . The asymptotic scattering states, on the other hand, are restricted to motion along the unconfined direction, and the radial wavefunction is given by the harmonic oscillator state of the waveguide potential.

The scattering properties under these circumstances are described by a short range potential  $g_{1D}\delta(z)$  and the interaction strength depends on the scattering length  $a$  in the following way [Ols98]:

$$g_{1D} = 2\hbar\omega_r \frac{a}{1 - Aa/a_r} \quad (6.6)$$

with  $A \simeq 1.0326$ . When  $a \rightarrow a_r/A$ , the interaction strength diverges in a one-dimensional system, in contrast to a gas without confinement, where the interaction strength becomes largest when  $a \rightarrow \infty$  (see figure 6.6).

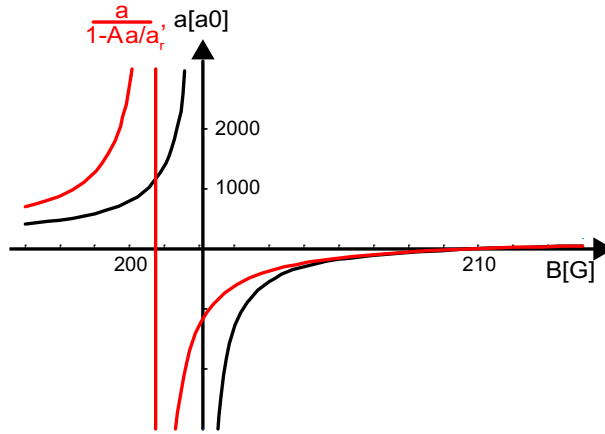


**Figure 6.6:** Comparison between confinement induced (red) and standard (black) Feshbach resonance in  $^{40}\text{K}$  centered around 202.1 G. The interaction strength is proportional to  $a/(1 - Aa/a_r)$  (eq. (6.6)) and  $a$  (eq. (2.12)) respectively. The confinement induced resonance is calculated for a harmonic oscillator length  $a_r = 62$  nm which corresponds to  $^{40}\text{K}$  in a  $25 E_R$  deep lattice.

The molecule formation under one-dimensional confinement is special: a bound state exists irrespective of the sign of the scattering length. This peculiar behaviour arises from the additional radial confinement which raises the continuum energy to the zero point energy of the confining potential, e. g. the two-dimensional harmonic oscillator ground state energy  $\hbar\omega_r$ . The energy of a bound or quasi-bound state remains nearly unaffected by the external confinement because the effective range of the interaction is small compared to the extension of the confined ground state. Therefore, a quasi-bound state, which for negative scattering length  $a$  lies above the continuum in free space, is below the new continuum in the confined system.

This explanation is instructive, but not numerically exact. The correct analysis which takes all excited harmonic oscillator states into account yields a binding energy  $E_b$  of the dimers of [Ber03]

$$\frac{a}{a_r} = -\frac{\sqrt{2}}{\zeta(1/2, -E_b/(2\hbar\omega_r))}, \quad (6.7)$$



where  $\zeta$  denotes the Hurwitz zeta function. For negative  $a$  and  $|a| \ll a_r$  a weakly bound state with  $E_b \approx m\omega_r^2 a^2$  exists which has a very anisotropic shape. The effective axial size is  $l_z \approx a_r^2/a$  as compared to the radial size  $a_r$  [Tok04]. In the limit  $|a| \gg a_r$  the binding energy takes the universal form  $E_b \approx 0.6 \hbar\omega_r$  and for positive  $a$  and  $a \ll a_r$  the usual 3D expression for the binding energy  $E_b = \hbar^2/(ma^2)$  is recovered with spherical molecules of size  $a$ .

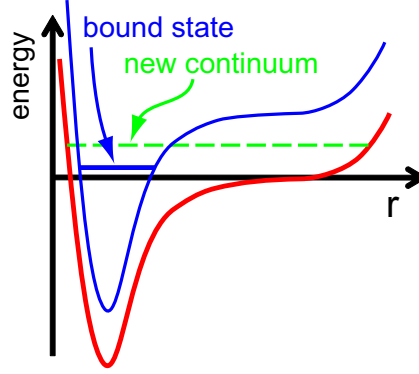


**Figure 6.7:** Interaction potential of the open (red) and closed (blue) channel in the presence of strong confinement. The continuum energy of the open channel is identical with the  $x$ -axis, provided that no confinement is present. The confinement, however, leads to the increase of the potential at larger distances and to a rise in the continuum energy. The new continuum is depicted with the green dashed line and lies above the bound state of the closed channel even for negative scattering length.

## 6.2 Preparation of the strongly interacting 1D gas

A trapped gas is kinematically one-dimensional if both the chemical potential and the temperature are smaller than the level spacing due to the transverse confinement (see chapter 4). For a harmonically trapped 1D Fermi gas the Fermi energy  $E_F = N \hbar\omega_z$  must be smaller than the energy gap to the first excited state in the transverse direction  $\hbar\omega_r$ . Here  $N$  denotes the number of particles and  $\omega_z$  is the trapping frequency along the weakly confining axis.

In our experiment we employ a two-dimensional optical lattice in order to create 1D Fermi gases. For atoms trapped in the intensity maxima of the two perpendicular standing wave laser fields, the radial confinement is only a fraction of the optical lattice period. The much weaker axial trapping is a consequence of the Gaussian intensity envelope of the lattice laser beams. The resulting aspect ratio  $\omega_r/\omega_z = \pi w/\lambda$  is determined by the waist  $w$  and the wavelength  $\lambda$  of the beams. The two-dimensional optical lattice creates an array of 1D tubes, approximately

$70 \times 70$  of which are occupied. For a noninteracting gas in the lattice trap we measure  $1/e^2$  cloud diameters of approximately  $60 \mu\text{m}$  along the tube axis and  $35 \mu\text{m}$  radially. This array fulfills the 1D condition  $N < \omega_r/\omega_z \approx 270$  in each tube while simultaneously providing a good imaging quality because we study many isolated 1D Fermi gases at the same time.

One-dimensional quantum systems have been realised with fermions, e. g. in semiconductor nanostructures [War86], and with bosons in ultracold atomic gases (see chapter 4 and [Mor03, Stö04, Tol04, Par04, Kin04b]) but so far the scattering length could not be tuned. We overcome this by using a Feshbach resonance between two different spin states of the atoms. This allows us to access any value of the scattering length and to study the predicted bound states in one dimension.

The precise experimental procedure to produce a quantum degenerate spin mixture of fermionic atoms in a two-dimensional optical lattice is described in chapter 3.6.2. In brief, we use bosonic  $^{87}\text{Rb}$  to sympathetically cool a spin-polarised gas of fermionic  $^{40}\text{K}$  atoms to quantum degeneracy. The potassium atoms are then transferred from the magnetic trap into an optical dipole trap where we prepare a spin mixture with  $(50 \pm 4)\%$  in each of the  $|F = 9/2, m_F = -9/2\rangle$  and  $|F = 9/2, m_F = -7/2\rangle$  spin states. After further evaporative cooling in the optical trap, we reach temperatures between  $T = 0.2 T_F$  and  $0.25 T_F$  with  $5 \times 10^4$  to  $2 \times 10^5$  particles, respectively. The spin mixture is then transferred into a two-dimensional optical lattice formed from beams along the  $y$ - and  $z$ -direction as described in chapter 3.6.2. This process takes place at a magnetic field of  $B = 210 \text{ G}$ , so that the  $s$ -wave scattering length between the two states vanishes. The magnetic field strength is calibrated by radio-frequency spectroscopy between different Zeeman levels of  $^{40}\text{K}$ , and the uncertainty is below  $0.1 \text{ G}$ .

### 6.3 Radio-frequency spectroscopy

We create molecules by ramping from the zero crossing of the scattering length at  $B = 210 \text{ G}$  in  $10 \text{ ms}$  to its desired value close to the Feshbach resonance. Depending on the final value of this magnetic field sweep the binding energy of the molecules varies according to equation (6.7). We measure the binding energy  $E_b$  of the dimers by radio-frequency (rf) spectroscopy [Reg03b]. The idea behind this method is explained in figure 6.8.

A pulse with a frequency  $\nu_{\text{rf}}$  and a duration of  $40 \mu\text{s}$  dissociates the molecules and transfers atoms into the initially unpopulated  $|-5/2\rangle$  state which does not exhibit a Feshbach resonance with the state  $|-9/2\rangle$  at this magnetic field. The power and duration of the pulse is optimised to constitute a  $\pi$ -pulse on the free atom transition. The number of atoms in each spin state is detected using absorption imaging after ballistic expansion. For this we ramp down the lattice exponentially with a duration of  $1 \text{ ms}$  and a time constant of  $0.5 \text{ ms}$  from the initial depth  $V_0$

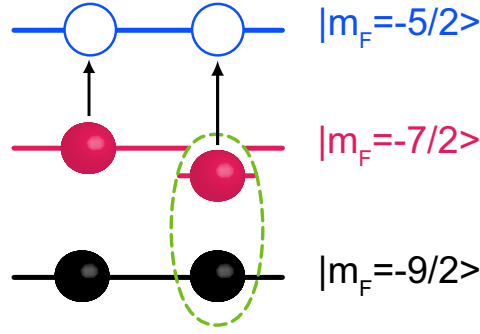


**Figure 6.8:** Scheme of the rf spectroscopy. An rf pulse with frequency  $\nu_{rf}$  is applied to the gas. Free atoms are transferred from the  $|m_F = -7/2\rangle$  state to the empty  $|m_F = -5/2\rangle$  by an rf photon resonant with the Zeeman level separation  $\nu_0$ . To break up molecules, the rf photon needs to bring an extra energy  $\hbar\delta > E_B$  along. Here the detuning is defined as  $\delta := \nu_{rf} - \nu_0$ . Excess rf energy is converted into kinetic energy of the fragments.

to  $5 E_r$ , in order to reduce the kinetic energy of the gas in the transverse directions, and then quickly turn off the trapping potential. The magnetic offset field is switched off rapidly at the start of the expansion, so that no molecules can be formed in the short time that the field passes the Feshbach resonance. We apply a magnetic field gradient during 3 ms of the total 7 ms of ballistic expansion in order to spatially separate the spin components.

Figure 6.9 shows rf spectra for one-dimensional gases with a potential depth of the optical lattice of  $V_0 = 25 E_r$ , which corresponds to  $\omega_r = 2\pi \times 69$  kHz. In figure 6.9 a the magnetic field is detuned to 0.57 G below the Feshbach resonance, i. e.  $a > 0$ . This spectrum exhibits two resonances: one corresponds to the  $|-7/2\rangle \rightarrow |-5/2\rangle$  transition for free atoms at  $\delta = 0$ , the other at  $\delta > 0$  corresponds to dissociated molecules. The constituent atoms of the dimers are observed in the  $|-9/2\rangle$  and  $|-5/2\rangle$  states. At this magnetic field, the molecules are not detected by our state-selective imaging procedure unless they are dissociated by an rf pulse. This is due to the fact that they are transformed into deeply bound molecules during the switch-off of the magnetic field. This explains the rise of the total atom number on the molecule dissociation peak.

## 6.4 Observation of confinement induced molecules

In figure 6.9 b the magnetic field is chosen 0.95 G above the resonance, i. e.  $a < 0$ . Again, the appearance of a second peak in the  $|-5/2\rangle$  atom number at  $\delta > 0$  demonstrates the existence of a bound state in our 1D geometry. These bound states are confinement induced since no molecules exist without confinement above the Feshbach resonance. They are only stabilised by the presence of the confining potential. Ramping down the lattice before detection dissoci-

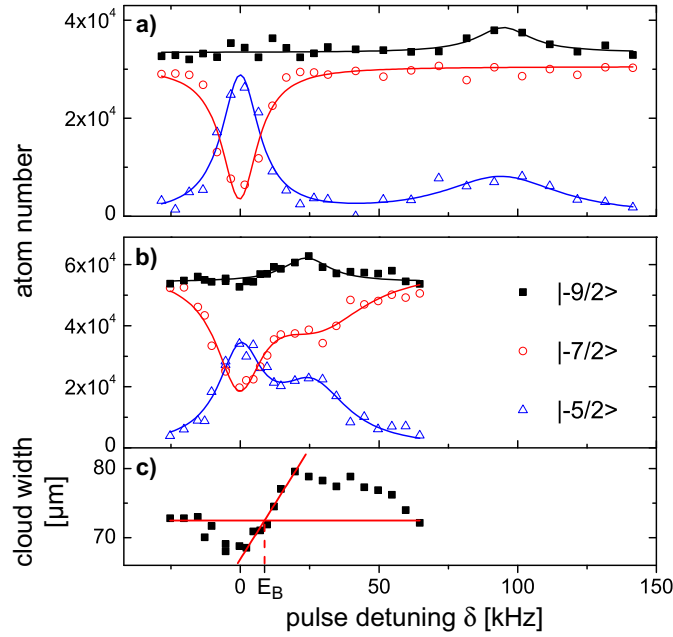


**Figure 6.9:** Radio-frequency spectroscopy of a one-dimensional gas at the magnetic fields 201.5 G (a) and 203.1 G (b, c) with respective scattering lengths  $2.5 \cdot 10^3 a_0$  (a) and  $-1.2 \cdot 10^3 a_0$  (b, c). The atom number in the respective spin states is plotted versus the detuning of the applied rf pulse in a) and b). The solid lines are single or double Lorentzian fits. c) shows the width of the  $|-9/2\rangle$  atom cloud along the 1D tube direction after 7 ms time-of-flight, obtained from a fit [DeM99a] to the atomic density distribution. The horizontal line marks the average width for an off-resonant rf pulse, the increase at the molecule dissociation threshold is fitted using a linear function. The decrease in width at higher detunings is due to a diminishing dissociation efficiency.

ates the dimers and therefore all atoms should be detected in the image, and the total particle number is expected to remain constant. This is reflected in our data, where the  $|-7/2\rangle$  atom number decreases upon dissociation while the  $|-5/2\rangle$  atom number increases. Incidentally, if the molecules are not dissociated by radio-frequency but by the lattice ramp-down, the total particle number is not absolutely constant but slightly reduced. The reason for this could be that a small fraction of molecules possibly forms again during the switch-off of the magnetic field.

To find out the exact binding energy it is not correct to take the difference between the molecular and the atomic peak position. The molecular peak position represents the detuning at which most molecules are dissociated. Its position depends on the exact Franck-Condon overlap between the bound state and the free atomic fragments and is therefore not the dissociation threshold. Instead, the binding energy is inferred from the kinetic energy of the dissociated fragments. The rf pulse not only breaks the pairs if the detuning  $\delta$  exceeds the binding energy

$E_b$ , but also imparts the kinetic energy  $\Delta E = h\delta - E_b$  to the fragments. In the 1D tubes only the kinetic energy along the tube axis increases because motion in the other direction is impossible for  $\Delta E < \hbar\omega_r$ . The position at which the kinetic energy starts to rise is the dissociation threshold. The cloud width shown in figure 6.9 c is extracted from the momentum distribution obtained from time-of-flight images. We find the binding energy by identifying the threshold position at which the cloud width exceeds that of a cloud without dissociation. The latter is determined by the Fermi statistics of the trapped atoms and the interaction of the  $|-9/2\rangle$  with the  $|-7/2\rangle$  atoms close to the Feshbach resonance. The decrease at  $\delta \approx 0$  is due to the particle transfer into the  $|-5/2\rangle$  state and an accordingly weaker interaction energy. Owing to this complication and to possible collisional shifts [Har02, Gup03] we estimate the systematic error of our binding energy measurements in all data sets to be 10 kHz.

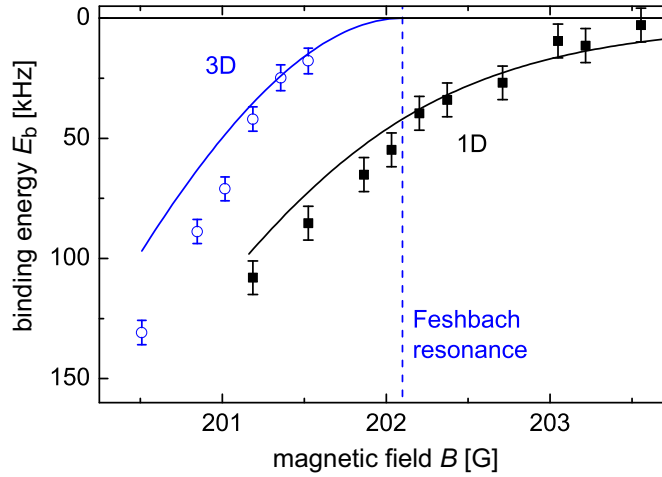


**Figure 6.10:** 1D and 3D molecules. Confinement induced molecules in the 1D geometry exist for both signs of the scattering length. The solid lines show the theoretical prediction of the binding energy with no free parameters (see text). In the 3D case we observed no bound states at magnetic fields above the Feshbach resonance (vertical dashed line). The error bars reflect the uncertainty in determining the position of the dissociation threshold.

We investigate the dependence of the binding energy of the 1D dimers on the magnetic field (figure 6.10), and we observe bound states for every examined magnetic field strength. The dimers at magnetic fields above the Feshbach resonance are induced by the confinement of the lattice. They are elongated, with the most weakly bound dimers having a calculated aspect ratio of up to  $l_z/a_r \approx 2.5$ . The data are in good agreement with the theoretical expectation calculated from equation (6.7) (solid black line) with no free parameters. For this calculation we compute the effective harmonic oscillator length  $a_r$  and the ground state energy  $\hbar\omega_r$  by minimising the energy of a Gaussian trial wavefunction in a single well of the lattice to account for the anharmonicity of the potential. To calculate the scattering length we use a width of

the Feshbach resonance of  $\Delta B = 7.8$  G [Reg03b] and the background scattering length  $a_{\text{bg}} = 174 a_0$  [Reg03a].

For a comparison with the situation in free space we create molecules in a crossed beam optical dipole trap without an optical lattice, where confinement effects are not relevant. The binding energy in 3D is measured with the same rf spectroscopy technique as for the 1D gas and we find molecules only for scattering lengths  $a > 0$ . The binding energy (solid blue) is calculated according to equation (6.3). The difference between the theory and the measured data for more deeply bound molecules is probably due to limitations of this single channel theory. A multi-channel calculation should be able to determine the binding energy more accurately.

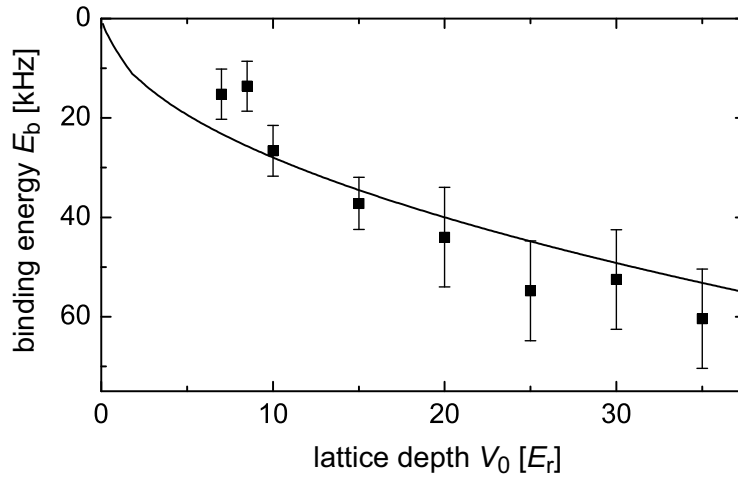


**Figure 6.11:** Changing the confinement. The spectra are taken very close to the Feshbach resonance at a magnetic field of  $B = 202.0$  G. The binding energy is measured by rf spectroscopy. For  $V_0 \geq 30 E_r$  no increase in kinetic energy can be detected and we use the rising edge in the  $|-5/2\rangle$  atom number in the spectrum to determine the binding energy. The error bars reflect the uncertainty in determining the position of the dissociation threshold. The solid line shows the theoretically expected value  $E_b = 0.6 \hbar \omega_r$ .

Exactly on the Feshbach resonance at which the scattering length diverges, the binding energy takes the universal form  $E_b \approx 0.6 \hbar \omega_r$  and is solely dependent on the external confinement. We vary the potential depth of the optical lattice and thereby the transverse confinement, and measure the binding energy. We find good agreement of our data with the theoretical prediction (see figure 6.11). For a very low depth of the optical lattice the measured data deviate from the 1D theory because the gas is not one-dimensional anymore.

## 6.5 Conclusion

To sum up, in the experiment described above we realised an interacting 1D Fermi gas in a two-dimensional optical lattice. Using a Feshbach resonance we created molecules and measured their binding energy. We found two-particle bound states for both signs of the scattering length, which in the case of negative scattering length are stabilised only by the tight transverse confinement. The binding energy measurements are in good agreement with theory describing two-particle physics. The strongly interacting 1D Fermi gas realises an atomic Luttinger liquid, and fascinating many-body phenomena are predicted in this system [Rec03, Ast04, Gia04].

Especially intriguing is the BCS-BEC crossover, which is exactly solvable in one dimension [Tok04, Fuc04]. For magnetic fields significantly below the confinement induced resonance the interaction strength is repulsive and the molecules are bosonic in character. The ground state is characterised by a molecular Bose-Einstein condensate. It is transformed to a Tonks-Girardeau gas on the confinement induced resonance. The interaction strength diverges, and the pairs behave like hard core bosons or equivalently like noninteracting fermions. Going to magnetic fields above the resonance, the attractive interaction strength diminishes and a weakly interacting Fermi gas results, featuring a BCS-like phase.

Another interesting feature of Luttinger liquids is the separation of “spin” and “charge” excitations, which in our context translate into excitations of the total density and into the density difference between the two spin states, respectively. Recent proposals show that it may be experimentally feasible to observe the different velocities of the spin and charge waves in our experimental setup [Rec03, Kol05].

The confinement induced resonance has yet to be observed. We have already tried to detect the corresponding mean-field shift by rf spectroscopy, but did not achieve the necessary resolution due to residual magnetic field fluctuations.





---

## 7 *p*-Wave interactions in low-dimensional Fermi gases

Ultracold fermionic atoms constitute a well-controllable many-body quantum system which provides access to fundamental concepts in physics. Using optical lattices, the atomic motion and the dimensionality of the trapping geometry can be controlled. Yet, it is the collisional interaction between atoms which opens up the path towards the physical richness of the strongly correlated regime [Hof02, Rig03, Jak05, Köh05a]. While the *s*-wave scattering examined in the last chapter is isotropic, *p*-wave interactions are particularly intriguing due to their anisotropic character. They are expected to give rise to fascinating phenomena such as *p*-wave superfluidity [Ho05, Che05, Gur05, Isk05] and the mapping of strongly interacting one-dimensional fermions to noninteracting bosons [Gra04, Che99] .

In contrast to the previous chapter, we turn to the study of spin-polarised fermions, whose spatial wavefunction must be anti-symmetric under the exchange of two particles. This allows for collisions with odd partial waves only, with the *p*-wave ( $\ell=1$ ) interaction having the lowest centrifugal barrier. The suppression of the collisional cross section at ultralow energies can be overcome by exploiting a *p*-wave Feshbach resonance [Reg03c, Zha04, Sch05]. The strong confinement available with the use of optical lattices allows us to realise one- and two-dimensional systems and restrict the asymptotic scattering states of atomic collisions. Examining the resonant behaviour of the atom losses as a function of magnetic field, we observe distinct structures depending on the dimensionality and the symmetry of the system.

---

Parts of this chapter are published in [Gün05].

## 7.1 *p*-Wave Feshbach resonance

In low energy scattering, nonzero angular momentum gives rise to a attractive potential with a centrifugal barrier which is much higher than the incident collision energy. Again, a closed channel exists, which can couple to the open channel through spin-spin interaction. In contrast to the *s*-wave Feshbach resonances discussed in section 6.1, the incoming atom must tunnel through the barrier in order to feel a perturbation by a closed channel bound state, which is necessarily short range (see figure 7.1). A *p*-wave Feshbach resonance exists at the magnetic field where the energy of a closed channel molecular state with  $\ell = 1$  coincides with the energy of two atoms with relative angular momentum  $\ell = 1$ . The scattering cross section is resonantly enhanced. If the collision energy is nonzero, a higher magnetic field is needed to tune the closed channel bound state in resonance. Due to the centrifugal barrier *p*-wave Feshbach resonances are very narrow and energy dependent. For thermal gases, this implies a broadening and a shift of the resonance with increasing temperature.

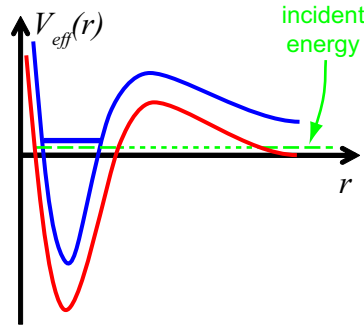


**Figure 7.1:** Effective interaction potentials for *p*-wave scattering with the centrifugal barrier.

### 7.1.1 Multiplet structure

In  $^{40}\text{K}$  a *p*-wave Feshbach resonance has been located for two atoms in the  $|9/2, -7/2\rangle$  state [Reg03c, Tic04]. At low temperatures it is split into two components, depending on the projection of the orbital angular momentum  $m_\ell$  on the magnetic field axis. This splitting is caused by the magnetic dipole-dipole interaction of the two valence electrons [Tic04]

$$H_{SS} = -\alpha^2 \frac{3(\hat{\mathbf{r}} \cdot \hat{S}_1)(\hat{\mathbf{r}} \cdot \hat{S}_2) - \hat{S}_1 \cdot \hat{S}_2}{r^3}, \quad (7.1)$$

where  $\alpha$  is the hyperfine structure constant,  $r$  the interatomic separation,  $\hat{\mathbf{r}}$  the unit vector along the interatomic axis and  $\hat{S}_i$  the spin of the valence electron of atom  $i$ . The spins in

the  $|9/2, -7/2\rangle$  state are nearly parallel to the magnetic field. The dipole-dipole interaction is attractive if they are lined up head to tail, whereas it is repulsive if they lie side by side. In order to see the origin of the multiplet structure it is illuminating to look at the relative motion of the atoms in the closed channel bound state as a classical orbit with relative angular momentum  $\ell = 1$  (see figure 7.2).

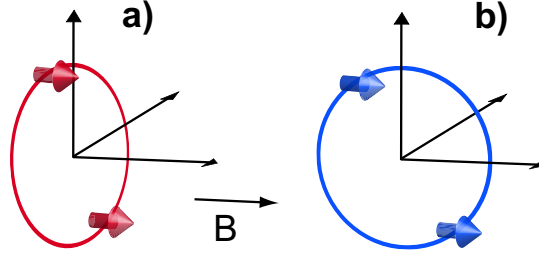


**Figure 7.2:** The electron spins describing classical orbits with (a)  $|m_\ell| = 1$  and (b)  $m_\ell = 0$ .

For  $|m_\ell| = 1$  the spins follow an orbit in the plane perpendicular to the magnetic field leading to repulsive mutual interaction. Conversely, for  $m_\ell = 0$ , the interaction alternates between attraction and repulsion, with the attraction dominating on average. Therefore the state with  $|m_\ell| = 1$  is at a higher energy and consequently resonant at lower field than the one with  $m_\ell = 0$ .

### 7.1.2 Scattering properties

In a similar fashion to characterisation of the  $s$ -wave scattering by the scattering length  $a$ , the  $p$ -wave scattering is parameterised by the scattering volume

$$V_p(k=0) := -\lim_{k \rightarrow 0} \frac{\tan(\delta_p(k))}{k^3}. \quad (7.2)$$

Here  $k$  is the collision wavevector and  $\delta_p(k)$  the phase shift introduced by the scattering potential (see also section 6.1). The scattering volume  $V_p(0)$  is magnetic field dependent and diverges on the Feshbach resonance. Furthermore, its energy dependence can be accounted for using an effective range expansion of the form [Tic04]

$$V_p(k) = (V_p(0)^{-1} + ck^2)^{-1}, \quad (7.3)$$

where the effective range coefficient  $c$  and the scattering volume are functions of the magnetic field. For  $^{40}\text{K}$  their dependence is tabulated in [Tic04]. The scattering volume is closely related to the three-body recombination rate  $K_3$  close to a Feshbach resonance, which is the quantity

we study experimentally. For small scattering volumes  $|V_p|$  for example, the recombination rate is found to depend on  $V_p$  as  $K_3 \propto |V_p|^{8/3}$  [Sun03].

When the atoms are confined to one-dimensional motion, the scattering resonance is shifted, similar to the case of the confinement induced resonance in  $s$ -wave scattering (see equation (6.6)). The exact value  $V_p^{\text{crit}}$  of the scattering volume at which the geometric resonance occurs depends on the collision energy  $E$  [Gra04]:

$$\frac{V_p^{\text{crit}}(E)}{a_r^3} = \left[ 12 \zeta \left( -\frac{1}{2}, \frac{3}{2} - \frac{E}{2\hbar\omega_r} \right) \right]^{-1}. \quad (7.4)$$

In general the shift is towards higher magnetic field.

## 7.2 Geometric suppression of collisions

The experiments reported in this chapter are performed with a spin-polarised Fermi gas in an optical lattice. The collisional properties in the vicinity of a  $p$ -wave Feshbach resonance are investigated by studying the resonant atom losses. Depending on the dimensionality and symmetry of the system, distinct structures are observed. For a three-dimensional gas a double-peaked structure appears, as has previously been reported by Ticknor *et al.* [Tic04]. It is caused by the magnetic dipole-dipole interaction discussed in section 7.1.1. This characteristic survives when the dimensionality is reduced to two dimensions but appears shifted in magnetic field. For one-dimensional geometries only a single shifted resonance peak is observed. All resonantly enhanced losses vanish when the spin-polarised gas is loaded into the lowest band of a three-dimensional optical lattice, in which each site can be regarded as a “zero-dimensional quantum dot”.

These observations can be qualitatively explained by considering the symmetry of the collisions, as illustrated in Fig. 7.3. The external magnetic field orients the polarisation of the atoms and may be chosen as the quantisation axis. In order to describe the atom-atom scattering with  $p$ -wave symmetry, the angular part of the corresponding asymptotic relative wavefunctions can be expressed in terms of spherical harmonics. Alignment of the scattering state parallel to the quantisation axis corresponds to the spherical harmonic  $Y_{\ell=1, m_\ell=0}$  and alignment in the plane perpendicular to the quantisation axis corresponds to superpositions of the spherical harmonics  $Y_{\ell=1, m_\ell=\pm 1}$ . In the two- and three-dimensional configurations both collisional channels are present, giving rise to the observed doublet feature (see Fig. 7.4 a and b). In one dimension, with the spin aligned orthogonal or parallel to the atomic motion, either the  $|m_\ell| = 1$  (see Fig. 7.4 c) or the  $m_\ell = 0$  (see Fig. 7.4 d) collisional channel is contributing, leading to a single peak. In zero dimensions – as realised in a three-dimensional optical lattice –  $p$ -wave collisions and the corresponding losses are absent (see Fig. 7.4 e).

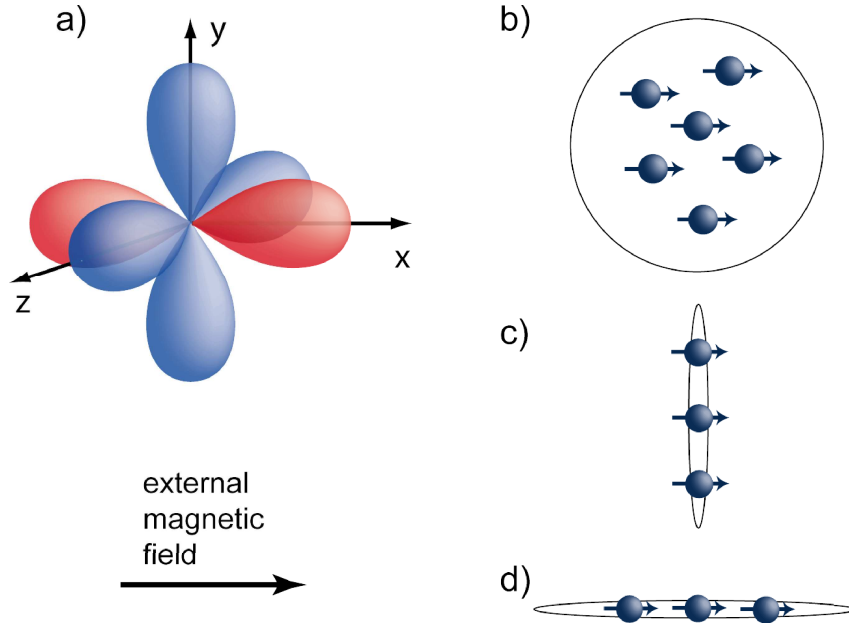


**Figure 7.3:** Spin-alignment dependent interactions in 1D and 2D. a) Depending on the projection of the angular momentum on the magnetic field, the angular part of the asymptotic scattering states is directed either along the  $x$ -axis for  $m_\ell = 0$  (red) or perpendicular to it for  $|m_\ell| = 1$  (blue). In the two-dimensional configuration of b) all projections of the angular momentum in the  $p$ -wave collision are present. c) and d) show a one-dimensional spin-polarised Fermi gas with the spins aligned orthogonal and parallel to the extension of the gas, respectively. In c) only the  $|m_\ell| = 1$  projection of the  $p$ -wave contributes to the scattering, in d) only the  $m_\ell = 0$  projection

One- and two-dimensional fermionic quantum systems have been realised in semiconductor nanostructures [Fow66, Fow82] and recently with noninteracting [Mod03] and interacting [Joc03b, Mor05] atomic gases in optical lattices. In these systems the strong confinement modifies the scattering properties of the particles: it stabilises molecular states and shifts the position of Feshbach resonances. This has been predicted for one- [Ols98, Ber03] and two-dimensional systems [Pet00a, Wou03] interacting via  $s$ -wave scattering, and confinement induced molecules have been observed in a 1D gas [Mor05]. Similarly, for spin-polarised fermions in one dimension a confinement induced shift of  $p$ -wave Feshbach resonances is predicted [Gra04].

### 7.2.1 Preparation of a spin-polarised 1D Fermi gas

The experimental procedure used to produce a degenerate Fermi gas has been described in detail in chapter 3.6.2. In brief, fermionic  $^{40}\text{K}$  atoms are sympathetically cooled by thermal contact with bosonic  $^{87}\text{Rb}$  atoms, the latter being subjected to forced microwave evaporation. The potas-

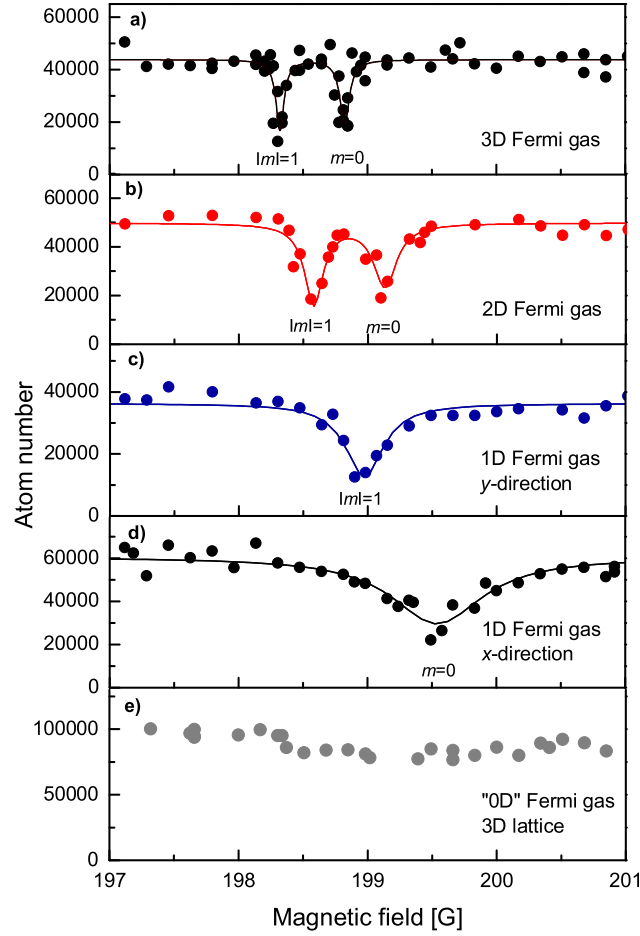


**Figure 7.4:** Loss measurements of the  $p$ -wave Feshbach resonance. a) Atoms are held in a crossed-beam optical dipole trap. b) Two-dimensional Fermi gas ( $V_z = 25 E_r$ ). c) One-dimensional Fermi gas with the motion confined orthogonal to direction of the magnetic field ( $V_z = V_x = 25 E_r$ ). d) One-dimensional Fermi gas with the motion confined parallel to the direction of the magnetic field ( $V_z = V_y = 25 E_r$ ). e) Fermi gas in a three-dimensional optical lattice ( $V_x = V_y = V_z = 25 E_r$ ). The solid lines are Lorentzian fits to the data from which we extract the position and the width of the resonance.

sium atoms are then transferred from the magnetic trap into an optical dipole trap consisting of two intersecting laser beams along the horizontal  $x$ - and  $y$ -directions.. In the optical trap we prepare the atoms in the  $|F = 9/2, m_F = -7/2\rangle$  spin state at a magnetic bias field of 232.9 G using two radio frequency (rf) sweeps. To remove residual atoms in the  $|F = 9/2, m_F = -9/2\rangle$  state we change the magnetic field within 100 ms to a value of 201.7 G, close to the  $s$ -wave Feshbach resonance between  $|F = 9/2, m_F = -9/2\rangle$  and  $|F = 9/2, m_F = -7/2\rangle$  [Lof02, Mor05],

where we encounter inelastic losses resulting in a pure spin-polarised Fermi gas. Subsequently we increase the magnetic field within 100 ms to 203.7 G. Then we evaporate atoms by lowering the optical trapping potential for 2.5 s to a final value of  $7 E_r$  in each of the two beams. The preparation of the gas is completed by rapidly ( $< 1$  ms) decreasing the magnetic field to 194.4 G, which is below the  $p$ -wave Feshbach resonance. We have calibrated the magnetic field by rf spectroscopy between Zeeman levels with an accuracy better than 100 mG, and we estimate the reproducibility of our magnetic fields to be better than 50 mG.

### 7.2.2 Three-dimensional Fermi gas

For comparison with the low-dimensional situations we first study the  $p$ -wave Feshbach resonance in the crossed-beam optical trap where motion in all three dimensions is possible. We sweep the magnetic field from its initial value of 194.4 G linearly to its final value in the vicinity of the Feshbach resonance within 1 ms. At this value the atoms are subject to inelastic losses [Reg03c]. After a hold time of 6.4 ms we switch off both the magnetic field and the optical trap and let the atomic cloud expand ballistically for 7 ms before taking an absorption image. From the image we extract the remaining number of atoms. In these data (see Fig. 7.4 a) we observe the doublet structure of the  $p$ -wave Feshbach resonance. The decay constant of the atom number close to the Feshbach resonance is on the order of 1 ms, which is comparable to the settling time of the magnetic field. Therefore we encounter a systematic shift of the magnetic field strength on the order of +0.1 G due to the direction of the magnetic field ramp. We have observed the opposite systematic shift when reversing the direction of the final sweep.

### 7.2.3 Two-dimensional Fermi gas

In a next step, we additionally apply a single optical standing wave along the vertical  $z$ -axis. The standing wave with a potential depth  $V_z$  creates a stack of two-dimensional Fermi gases in the horizontal  $x$ - $y$ -plane as shown in figure 7.3 b. The lattice laser intensity is increased using an exponential ramp with a time constant of 10 ms and a duration of 20 ms. The magnetic field is aligned along the horizontal  $x$ -axis. In the two-dimensional Fermi gas we have studied the  $p$ -wave Feshbach resonance analogous to the method described above, only the release process of the atoms is slightly altered: within 1 ms before the simultaneous switch-off of the magnetic and the optical potentials, we lower the lattice intensity to  $V_z = 5 E_r$  to reduce the kinetic energy. This results in a more isotropic expansion which allows to determine the atom number more precisely.

For the two-dimensional gas we observe a similar doublet structure of the Feshbach resonance but shifted towards higher magnetic field values with respect to the position without

strong confinement (see Fig. 7.4 b). The centrifugal barrier in a  $p$ -wave collision leads to a pronounced energy dependence of the scattering volume. In the confined gas the collision energy is modified by the motional ground state energy and the larger Fermi energy of the gas due to the confinement. Moreover, a confinement induced shift of the resonance could be envisaged, similar to what has been studied for  $s$ -wave interactions in two dimensions [Pet00a, Wou03].

We experimentally find that the shift of the resonance feature depends on the strength of the optical lattice. In Fig. 7.5 we compare the measured shift with a model in which we set the collision energy of the particles to be the sum of the Fermi energy and the ground state energy. We numerically calculate the Fermi energy for the noninteracting gas using a tight-binding model for the direction of the lattice laser and a harmonic oscillator potential in the transverse directions, corresponding to the experimental configuration. Using the parametrisation of the Feshbach resonance according to [Tic04], we obtain the shifted position of the resonance for a given lattice depth. For the  $|m| = 1$  branch of the resonance we find good agreement of the data with the theory whereas for the  $m = 0$  branch the observed shift is larger than predicted by our model. There may be an additional confinement induced shift of the  $p$ -wave resonance which depends on the quantum number  $m$  in the collision process [Gra04], however no quantitative theory is available.

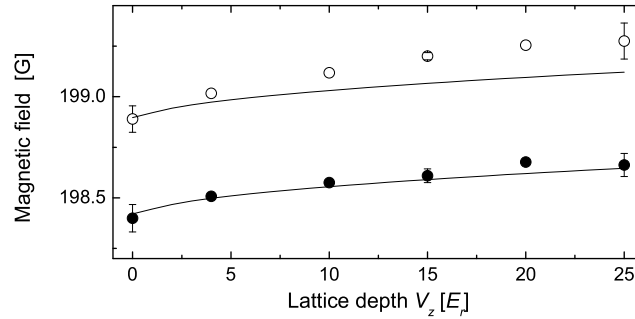


**Figure 7.5:** Shift of the Feshbach resonance position when tuning the gas from three to two dimensions. Open symbols indicate the position of the  $m = 0$  branch, solid symbols the  $|m| = 1$  branch of the resonance. The error bars denote the statistical error of 3 measurements. The solid lines show a calculation of the expected positions (see text).

## 7.2.4 One-dimensional Fermi gas

Reducing the dimensionality further, we study the effect of the alignment of the electronic spins on the  $p$ -wave interaction in a one-dimensional quantum gas. All spins are lined up either



orthogonal (see Fig. 7.3 c) or parallel (Fig. 7.3 d) to the orientation of the gas. We prepare one-dimensional Fermi gases by superimposing a second standing wave laser field onto the two-dimensional quantum gases [Mor05]. Either the  $x$ - or the  $y$ -direction of the optical dipole trap is slowly turned off and replaced by an optical lattice along the same direction and having the same beam geometry.

We now consider the orthogonal configuration where only collisions with  $|m| = 1$  are possible, and correspondingly we observe only this branch of the Feshbach resonance (see Fig. 7.4 c). To study the suppression of the  $m = 0$  branch quantitatively we create a two-dimensional optical lattice along the  $x$ - and the  $z$ -direction with  $V_z = 25 E_r$  and adjustable  $V_x$ . We measure the peak loss on the  $m = 0$  and the  $|m| = 1$  resonance position, respectively. In Fig. 7.6 a we plot the ratio of the peak loss versus the tunneling matrix element along the  $x$ -direction, i. e. between the tubes of the optical lattice. Without tunneling the one-dimensional gases are well isolated from each other and losses on the  $m = 0$  branch are completely suppressed. For larger tunneling rates hopping of atoms between the tubes is possible and the system is not kinematically one-dimensional anymore. Therefore collisions in the  $m = 0$  branch become possible which give rise to losses. The measurement directly verifies the suppressed tunneling between neighbouring lattice tubes and proves that the gases in the individual lattice tubes are kinematically one-dimensional. This method is complementary to the measurement of the collective oscillations in a one-dimensional gas (see chapter 4 and [Mor03]). Orienting the one-dimensional quantum gases parallel to the magnetic field axis, we observe the  $m = 0$  branch of the Feshbach resonance only (see Fig. 7.4 d).

For the one-dimensional Fermi gases we observe a further shift of the resonance position and a broadening of the loss feature as compared to the higher-dimensional configurations. A confinement induced shift of the  $p$ -wave resonance in one dimension for the  $m = 0$  branch has been predicted in addition to the increased ground state and Fermi energy (see equation (7.4) and [Gra04]). We numerically calculated the ground state and the Fermi energy for our trapping geometry and particle number and included the confinement induced shift according to equation (7.4). A comparison of the resulting shift with the experimental data is shown in Fig. 7.6 b. We note, however, that the confinement induced shift is relatively small as compared to the shift due to the increased collision energy. The increasing width of the loss feature is expected because the width of the Feshbach resonance also depends on the energy of the particles involved in the collision process [Tic04]. It appears that for the 1D data the  $m = 0$  resonance is wider than the  $|m| = 1$  resonance which could indicate that the Fermi gas is less cold in the former situation.

By using three orthogonal standing waves, we prepare a band-insulating state in a 3D optical lattice [Köh05a] where the atoms are localised in the potential wells with at most one atom per lattice site. In this "zero-dimensional" situation all  $p$ -wave scattering is completely inhibited (see Fig. 7.4 e).

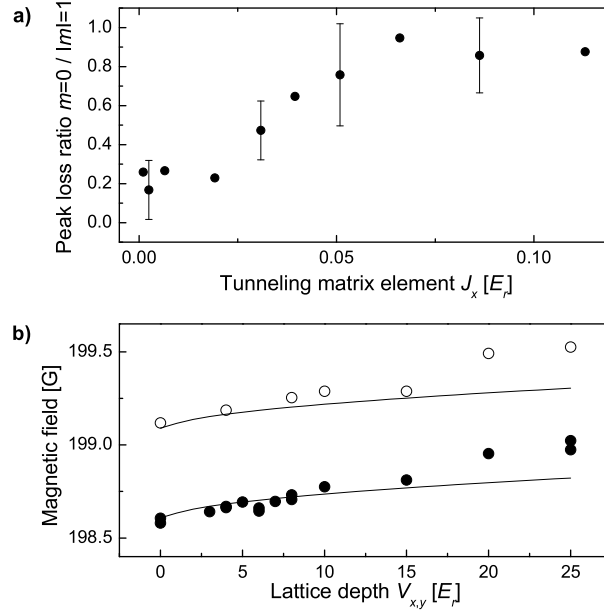


**Figure 7.6:** a) Suppression of collisional losses in the  $m = 0$  partial wave depending on the tunneling matrix element between the one-dimensional quantum gases. The error bars are determined from the fit to the loss peaks of two measurements. b) Shift of the Feshbach resonance position when tuning the gas from two to one dimensions. Open symbols indicate the position of the  $m = 0$  branch in the  $y$ - $z$ -lattice (see Fig. 7.3 d), the solid symbols the  $|m| = 1$  branch of the resonance in the  $x$ - $z$ -lattice (see Fig. 7.3 c). The solid lines show a calculation of the expected positions (see text).

In conclusion, we have studied spin-polarised interacting Fermi gases in low dimensions using a  $p$ -wave Feshbach resonance. We demonstrate that in reduced dimensions the direction of spin-alignment significantly influences the scattering properties of the particles. Moreover, we find a confinement induced shift of the resonance position and observe good agreement with a theoretical model. Strongly interacting low-dimensional Fermi gases offer a wealth of fascinating many-body phenomena. For one-dimensional systems the mapping of strongly interacting fermions to noninteracting bosons may be studied [Che99, Gra04] which resembles the inverse of the Tonks-Girardeau limit for strongly interacting bosons [Gir60]. The prospect of  $p$ -wave superfluidity [And61] appears very intriguing in cold atomic gases [Ho05, Che05] and especially in two-dimensional systems exotic phases are predicted [Gur05, Isk05] where the spin-alignment is essential.

---

## 8 Fermionic atoms in a three-dimensional lattice

The exploration of quantum degenerate gases of fermionic atoms is driven by the ambition to get deeper insight into long-standing problems of quantum many-body physics, such as high temperature superconductivity. Very recently, the cross-over regime between a strongly interacting two-component Fermi gas and a molecular Bose-Einstein condensate has been studied in harmonic traps [Reg04, Bar04, Zwi04, Kin04a, Bou04, Zwi05]. These experiments mark a milestone towards the understanding of superfluidity of fermionic atoms. However, the analogy to an electron gas in a solid is limited since there the electrons experience a periodic lattice potential. The lattice structure is in fact a key ingredient for most models describing quantum many-body phenomena in materials. It has been suggested that strongly interacting fermionic atoms in optical lattices could be employed for studies of high-Tc-superconductivity [Hof02], Mott-insulating phases [Rig03], Bose condensation of fermionic particle-hole pairs [Lee04], or interacting spin systems [San04].

Here we report on an experiment bridging the gap between current ultracold atom systems and fundamental concepts in condensed matter physics. A quantum degenerate Fermi gas of atoms is prepared in the crystal structure of a three-dimensional optical lattice potential created by three crossed standing laser waves. The unique control over all relevant parameters in this system allows us to carry out experiments which are not feasible with solid state systems. Direct imaging of the Fermi surface of the atoms in the lattice is demonstrated. Due to the confining potential gradual filling of the lattice transforms the system from a normal state into a band insulator. Using a Feshbach resonance the interactions between atoms in two different spin states are increased and induce a dynamical coupling between the lowest energy bands.

Conceptually, this chapter differs from the previous ones. It does not deal with a one-dimensional gas, but rather brings into focus the aspect that ultracold gases in optical lattices can serve as a model laboratory in which to simulate solid state systems. It is meant to broaden the scope of this thesis and point out capabilities of our setup which will be important for the future direction of research.

---

Parts of this chapter are published in [Köh05a].

## 8.1 Imaging the Fermi-surface

It was conceived by D. Jaksch et al. [Jak98] that ultracold atoms exposed to the periodic potential of an optical lattice are an almost ideal realisation of a Hubbard model (see also section 5.1). This model is elementary to describe the quantum physics of many electrons in a solid. It takes into account a single band of a static lattice potential and assumes the interactions to be purely local [Hub63]. Ultracold atoms in an optical lattice give a very direct access to the underlying physics. The fundamental parameters include the tunnel coupling between adjacent lattice sites, the atom-atom interactions and the dimensionality of the system. Previous experiments with far-detuned three-dimensional optical lattices [DeP99, Gre02, Stö04] were always carried out with bosonic atoms, and experiments with fermions were restricted to a single standing wave [Mod03]. In the latter situation many atoms can reside in each standing wave minimum but formation of a band insulator is prevented by the weak transverse confinement. The observed inhibition of transport [Pez04] is due to localised states and therefore differs qualitatively from the band insulator which we create in the three dimensional optical lattice.

The precise experimental procedure to produce a quantum degenerate spin mixture of fermionic atoms in a two-dimensional optical lattice is described in chapter 3.6.2. In brief, we use bosonic  $^{87}\text{Rb}$  to sympathetically cool a spin-polarised gas of fermionic  $^{40}\text{K}$  atoms to quantum degeneracy. The potassium atoms are then transferred from the magnetic trap into an optical dipole trap where we prepare a spin mixture with  $(50 \pm 4)\%$  in each of the  $|F = 9/2, m_F = -9/2\rangle$  and  $|F = 9/2, m_F = -7/2\rangle$  spin states. After further evaporative cooling in the optical trap, we reach temperatures between  $T = 0.2 T_F$  and  $0.25 T_F$  with  $5 \times 10^4$  to  $2 \times 10^5$  particles, respectively. The spin mixture is then transferred into a three-dimensional optical lattice as described in chapter 3.6.2. This process takes place at a magnetic field of  $B = 210 \text{ G}$ , so that the  $s$ -wave scattering length between the two states vanishes. The magnetic field strength is calibrated by radio-frequency spectroscopy between different Zeeman levels of  $^{40}\text{K}$ , and the uncertainty is below  $0.1 \text{ G}$ .

The potential created by the optical lattice results in a simple cubic crystal structure and the Gaussian intensity profiles of the lattice beams give rise to an additional confining potential which varies with the laser intensity. As a result, the sharp edges characterising the  $T = 0$  distribution function for the quasi momentum in the homogeneous case [Ash76] are expected to be rounded off. A quantitative picture can be obtained by considering a tight-binding Hamiltonian to describe noninteracting fermions in an optical lattice with an additional harmonic confinement [Rig04]. At  $T = 0$  the inhomogeneous system is characterised by the total atom number  $N$  and by the characteristic length  $\zeta$  over which the potential shift due to the harmonic confinement equals the tunnel coupling matrix element  $J$ . One finds  $\zeta_\alpha = \sqrt{2J/m\omega_\alpha^2}$ , with the frequencies of the external harmonic confinement given by  $\omega_\alpha$  ( $\alpha = x, y, z$ ). The density distri-

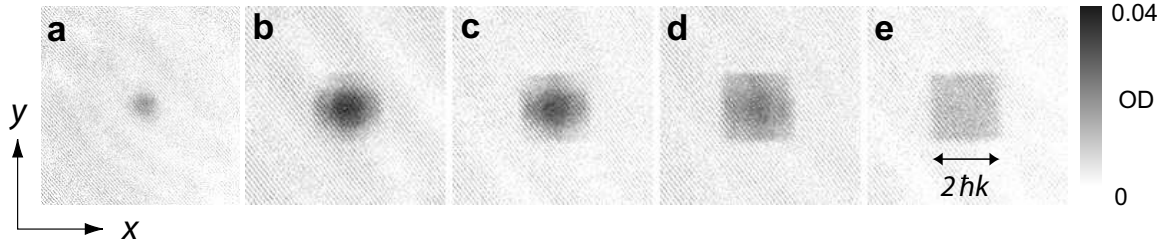


**Figure 8.1:** Observing the Fermi surface. Time-of-flight images obtained after adiabatically ramping down the optical lattice. The characteristic density increases from left to right. (a) 3500 atoms per spin states and a potential depth of the optical lattice of  $5 E_r$ . Images (b)-(e) were obtained with 15000 atoms per spin state. The potential depths of the optical lattices were  $5 E_r$  (b),  $6 E_r$  (c),  $8 E_r$  (d) and  $12 E_r$  (e). The images show the optical density (OD) integrated along the vertically oriented z-axis after 6 ms of ballistic expansion.

bution scaled by  $\zeta_\alpha$  and the momentum distribution of the atoms in the lattice only depend on the characteristic density  $\rho_c = \frac{Nd^3}{\zeta_x \zeta_y \zeta_z}$ , where  $d = \lambda/2$  is the lattice spacing [Rig03]. For a three-dimensional lattice with  $20 \times 20 \times 20$  sites we have numerically calculated the characteristic density for the onset of a band insulator to be  $\rho_c \simeq 60$ . For this value of  $\rho_c$  the occupation number at the center of the trap is larger than 0.99. It has recently been pointed out that a fermionic band insulator in an optical lattice with confining potential constitutes a high fidelity quantum register [Viv04].

In the experiment we probe the population within the first Brillouin zones by ramping down the optical lattice slowly enough for the atoms to stay adiabatically in the lowest band whilst quasimomentum is approximately conserved [Gre01b]. We lower the lattice potential to zero over a timescale of 1 ms. After 1 ms we switch off the homogeneous magnetic field and allow for 6 ms of ballistic expansion before we take an absorption image of the expanded atom cloud. The momentum distribution obtained from these time-of-flight images, shown in Fig. 8.1, reproduces the quasimomentum distributions of the atoms inside the lattice. With increasing characteristic density the initially circular shape of the Fermi surface develops extensions pointing towards the Bragg planes and finally transforms into a square shape completely filling the first Brillouin zone deeply in the band insulator. In Fig. 8.2 the experimental data for momentum distributions along the line with quasimomentum  $q_y = 0$  are compared to the results of numerical simulations using the same characteristic densities.

When imaging the cloud along the x-direction we find a homogeneous filling of the band in the vertical (z-) direction, probably due to the change in the harmonic confinement while loading the lattice combined with the presence of gravity. This asymmetry between the horizontal x-, y-, and the vertical z-directions vanishes when the gas approaches the band insulating regime. We have examined the level of adiabaticity of our loading scheme into the optical lattice by

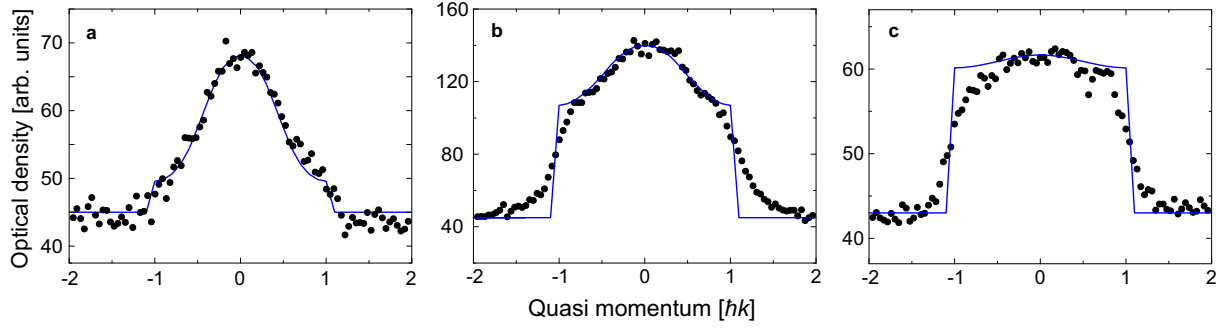


**Figure 8.2:** Analysis of the density distributions. The dots are cuts through the measured density distribution for quasi momentum  $q_y = 0$  after adiabatically ramping down the optical lattice. **(a)** Normal state with  $\rho_c = 14.5$ , **(b)** band insulator with  $\rho_c = 137$ , **(c)** band insulator with  $\rho_c = 2500$ . We have numerically calculated the momentum distribution function of fermions in the lowest band of a three-dimensional lattice with  $20 \times 20 \times 20$  sites and characteristic lengths  $\zeta_x/d = 3.2$ ,  $\zeta_y/d = 2.6$ ,  $\zeta_z/d = 2.5$  (**(a)** and **(b)**) and  $\zeta_x/d = 1$ ,  $\zeta_y/d = 0.8$ ,  $\zeta_z/d = 0.8$  (**(c)**), assuming zero temperature (solid lines). Experimental data of **(c)** are averaged over 5 images. Imperfect adiabaticity during the switch-off of the optical lattice may cause the rounding-off of the experimental data at the edge of the Brillouin zone in **(b)** and **(c)**. The calculated momentum distribution function is scaled to match the experimental data using identical scale factors for all graphs.

transferring the atoms from the band insulator back into the crossed beam dipole trap. There we find a temperature of  $0.35 T_F$  when the initial temperature prior to loading into the lattice was  $0.2 T_F$ .

## 8.2 Interaction-induced coupling between bands

We investigate the interacting regime in the lattice starting from a noninteracting gas deep in a band insulator with  $V_x = 12 E_r$  and  $V_y = V_z = 18 E_r$ . A short radio-frequency pulse is applied to transfer all atoms from the  $|F = 9/2, m_F = -7/2\rangle$  into the  $|F = 9/2, m_F = -5/2\rangle$  state, with the atoms in the  $|F = 9/2, m_F = -9/2\rangle$  remaining unaffected (see figure 8.3 a). The scattering length of the resulting mixture diverges at a Feshbach resonance located at  $B = 224.21 \text{ G}$  [Reg03a].

We ramp the magnetic field with an inverse sweep rate of  $12 \mu\text{s}/\text{G}$  to different final values around the Feshbach resonance (see Fig. 8.3). The sweep across the Feshbach resonance goes from the side of repulsive interactions towards the side of attractive interactions. When using this direction of the sweep there is no adiabatic conversion to molecules. After turning off the optical lattice adiabatically and switching off the magnetic field we measure the momentum

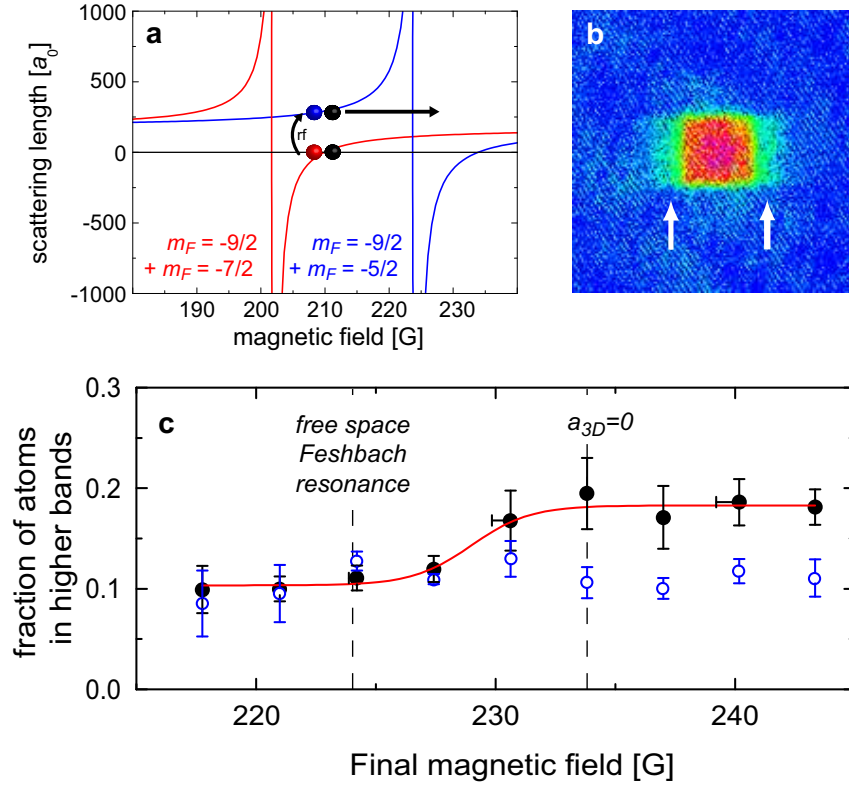


**Figure 8.3:** Interaction-induced transition between Bloch bands. (a) Experimental method: two Feshbach resonances between the  $|m_F = -9/2\rangle$  and  $|m_F = -7/2\rangle$  states (red) and the  $|m_F = -9/2\rangle$  and  $|m_F = -5/2\rangle$  states (blue) are exploited, where  $F = 9/2$  always. The first resonance allows loading at zero scattering length, while the second is needed to sweep the across a resonance from left to right. (b) Momentum distribution for a final magnetic field of  $B = 233$  G. Arrows indicate the atoms in the higher bands. (c) Fraction of atoms transferred into higher bands by a sweep across the resonance (filled symbols). The line shows a sigmoidal fit to the data. The open symbols show a repetition of the experiment with the atoms prepared in the spin states  $|F = 9/2, m_F = -9/2\rangle$  and  $|F = 9/2, m_F = -7/2\rangle$  where the scattering length is not sensitive to the magnetic field. The magnetic field uncertainty is dominated by eddy currents induced by the rapid field ramp which cause the field to lag behind its asymptotic value. The error bar represents the deviation of the magnetic field from the asymptotic value  $100\ \mu\text{s}$  after starting to ramp down the optical lattice, calibrated by rf spectroscopy between Zeeman levels. The vertical error bars show the statistical error of 4 repetitive measurements.

distribution. To see the effect of the interactions we determine the fraction of atoms transferred into higher bands. For final magnetic field values well above the Feshbach resonance we observe a significant increase in the number of atoms in higher bands along the weak axis of the lattice, demonstrating an interaction-induced coupling between the lowest bands.

Since the  $s$ -wave interaction is changed on a time scale short compared to the tunneling

time between adjacent potential minima, we may regard the band insulator as an array of harmonic potential wells. It has been shown that increasing the  $s$ -wave scattering length for two particles in a harmonic oscillator shifts the energy of the two-particle state upwards until the next oscillator level is reached [Bus98]. In our case this leads to a population of higher energy bands. The fraction of atoms transferred is limited by the number of doubly occupied lattice sites. Only about 40% of the atoms reside on doubly occupied sites, as has been determined by a study of molecule formation in the lattice [Stö05]. Moreover, the relatively fast tunneling in higher bands might lead to collisions and decay of the atoms in higher bands.

In addition, we observe a shift of the position of the Feshbach resonance from its value in free space to larger values of the magnetic field (see Fig. 8.3a), which has been predicted for tightly confined atoms in an optical lattice [Fed04]. This mechanism for a confinement induced resonance is related to the phenomenon predicted for one-dimensional quantum gases [Ols98] which has as yet escaped experimental observation. For a quantitative description of this strongly interacting Fermi gas on a lattice a multi-band Hubbard model is appropriate. Very recently, studies of this model, which include the effect of the Feshbach resonance, have been published [Car05, Die05, Dic05]. In particular, Diener et al. [Die05] calculate the number of particles that should be transferred into the next band, yielding 50% at  $T=0$ . However, only the 40% of atoms residing in doubly occupied sites are expected to experience the interaction. The resulting theoretically predicted fraction of 20% is compatible with our measurements.

In conclusion we have created a fermionic many-particle quantum system on a lattice. We have demonstrated the dynamical control over the parameters of the system such as filling and interactions which is not feasible in solid state systems. For the noninteracting regime we find good agreement between our measurements and a theoretical model. The strongly interacting case poses challenges for the present theoretical understanding of many-particle fermionic systems on optical lattices.



---

## 9 Conclusions and outlook

Optical lattices have put a new perspective on the research with ultracold quantum gases. They open up the path to low-dimensional systems and enable us to study solid state phenomena in a very pure model system. The experiments described in the thesis mark essential milestones on this path: the first one-dimensional Bose gas is created and characterised by means of measuring its collective oscillations. By applying an optical lattice along the axis of the one-dimensional gases, the strongly interacting regime is entered and the transition to a Mott insulator observed, a paradigm of strong correlations.

We have also realised the first one-dimensional atomic Fermi gas and used an  $s$ -wave Feshbach resonance to study the formation of confinement induced molecules. These bound states are a unique feature of low-dimensional systems and have no counterpart in the unconfined case. The effect of the confinement on the scattering properties was investigated using a  $p$ -wave Feshbach resonance, which is particularly exciting due to its anisotropic character. We observed that collisions with a particular projection of the angular momentum on the quantisation axis are completely suppressed in one dimension.

One-dimensional systems have some very intriguing properties. Their interaction strength increases with decreasing density and the clear distinction between bosonic and fermionic quantum statistics vanishes for strong interactions. Strongly interacting Bose gases acquire fermionic properties [Gir60] with the wavefunction given by that of noninteracting fermions  $\Psi_b = |\Psi_f|$ , whereas spin-polarised Fermi gases which interact strongly via  $p$ -wave interactions map to noninteracting Bose gases [Che99, Gra04]. While the bosonic Tonks gas has been recently realised [Par04, Kin04b], the fermionic counterpart has yet to be observed. Moreover, studies of two and three-body correlation functions [Gan03, Khe03] will shed new light on peculiar properties of the bosonic Tonks gas.

Both the one-dimensional Bose gas as well as the one-dimensional Fermi gas are examples of Luttinger liquids. This model describes the low energy behaviour of one-dimensional quantum liquids universally [Hal81] and features a variety of fascinating phenomena. Probably the most exciting prediction of the Luttinger liquid theory is the phenomenon of spin-charge separation. It is a feature unique to interacting Fermi gases in one dimension and manifests itself in the complete separation of the dynamics of spin and charge density waves. Analytical [Rec03] and numerical studies [Kol05] suggest that it should be feasible to observe the different velocities and behaviour of spin and charge density waves, which may be created by a local

perturbation such as a focused laser beam.

Feshbach resonances offer the opportunity to form weakly bound molecules in a one-dimensional gas. The transformation of weakly bound fermionic pairs to bosonic molecules, which is demonstrated in this thesis, has a profound influence on the many-body physics. When changing the interaction strength and molecular binding energy, the ground state of the gas is expected to undergo a BEC-BCS crossover. The BEC-BCS crossover has been an important issue in many-body physics for a long time and has regained a lot of attention recently because it can be studied in detail in cold atomic gases. The one-dimensional case is of particular interest as exactly solvable models exist [Fuc04, Tok04], in contrast to the three-dimensional case. Using the methods described in chapter 6, this crossover should be observable in our setup, provided that the temperature can be reduced further.

It is also conceivable to simultaneously trap fermionic and bosonic atoms in the same lattice and study Bose-Fermi mixtures in one dimension. Depending on the interspecies interaction strength and the density difference, the ground state of the system may display charge-density waves,  $p$ -wave pairing of fermionic polarons or phase separation [Caz03, Mat04]. Even more exotic phases might be observed when interspecies Feshbach resonances, which have already been observed in loss measurements [Ino04, Sta04], are used to create dipolar molecules.

Yet the setup described in this thesis is not limited to one-dimensional systems, as demonstrated in the experiments presented in chapter 8. By loading a Fermi gas into a three-dimensional lattice, a system is realised capable of simulating the Fermi-Hubbard model in two and three dimensions as well as in one. The Fermi-Hubbard model still poses many open questions on the theoretical side and has received renewed attention in recent years due to its relevance for the theory of high temperature superconductors. The repulsive case covers the Mott metal-insulator transition, the antiferromagnetic phase and  $d$ -wave superfluidity in two dimensional systems. The attractive case describes the BEC to BCS crossover of  $s$ -wave superfluidity. Detailed proposals discussing the realisation and observation of these phases in optical lattices have been published recently (see [Hof02, Rig04, Liu05, Wer05, Tre05]).

When a Feshbach resonance is present, the model describing the atoms in the lattice has to include the conversion of fermionic atoms into bosonic molecules. The regime of Fermi-Bose conversion is not accessible in standard condensed matter systems and only recently the first steps to understand this mixed world of fermions and bosons have been undertaken theoretically [Die05, Car05, Dic05]. New and exciting phenomena such as the transition from a fermionic band insulator to a Bose superfluid are to be expected.

The experiments demonstrate that the research in quantum gases has crossed the threshold to a new field with a unique range of possibilities. The two key technologies are optical lattices and Feshbach resonances, which are combined here for the first time. They enable the simulation of many-body Hamiltonians with an intrinsically pure system with the added benefit of direct and “in situ” control of dimensionality, interaction strength and filling.

# A Atomic properties

## A.1 $^{87}\text{Rb}$ data

Mass	86.9091835(27) u [NIS05]
Natural abundance	27.83(2)% [NIS05]
Nuclear spin $I$	3/2 [NIS05]
Nuclear $g_I$ -factor	-0.0009951414(10) [Ari77]
Landé $g_J$ -factor for $D$ transitions	2.00233113(20) [Ari77]
Hyperfine ground state splitting $\nu_{\text{hfs}}$	+6.83468261090429(9) GHz [Biz99]
Vacuum Wavelength $\lambda_{D1}$ ( $5^2S_{1/2} \rightarrow 5^2P_{1/2}$ )	794.9788509(8) nm [Ste01]
Natural line width $\Gamma_{D1}$ (FWHM)	$2\pi \times 5.746(8)$ MHz [Ste01]
Vacuum Wavelength $\lambda_{D2}$ ( $5^2S_{1/2} \rightarrow 5^2P_{3/2}$ )	780.241209686(13) nm [Ste01]
Natural line width $\Gamma_{D2}$ (FWHM)	$2\pi \times 6.065(9)$ MHz [Ste01]
Saturation intensity $I_{\text{sat}}$ $F = 2 \rightarrow F' = 3$ ( $\sigma^\pm$ -polarized light, $D_2$ -line)	1.669 mW/cm <sup>2</sup>
Resonant cross section $\sigma_0$ $F = 2 \rightarrow F' = 3$ ( $\sigma^\pm$ -polarized light, $D_2$ -line)	$2.907 \cdot 10^{-9}$ cm <sup>2</sup>
Saturation intensity $I_{\text{sat}}$ $F = 2 \rightarrow F' = 3$ (isotropically polarized light, $D_2$ -line)	3.576 mW/cm <sup>2</sup>
Resonant cross section $\sigma_0$ $F = 2 \rightarrow F' = 3$ (isotropically polarized light, $D_2$ -line)	$1.356 \cdot 10^{-9}$ cm <sup>2</sup>
Scattering length $a_S$ (singlet)	90(1) $a_0$ [Rob98]
Scattering length $a_T$ (triplet)	106(4) $a_0$ [Rob98]
van der Waals coefficient $C_6$	4691(23) $a_0^6 \alpha^2 m_e c^2$ [Der99]

**Table A.1:** Properties of  $^{87}\text{Rb}$ .

## A.2 $^{40}\text{K}$ data

Mass	39.96399867(29) u [NIS05]
Natural abundance	0.0117(1)% [NIS05]
Nuclear spin $I$	4 [NIS05]
Nuclear $g_I$ -factor	+0.000176490(34) [Ari77]
Landé $g_J$ -factor for $D$ transitions	2.00229421(24) [Ari77]
Hyperfine ground state splitting $\nu_{\text{hfs}}$	−1.285790(7) GHz [Ari77]
Vacuum Wavelength $\lambda_{D1}$ ( $4^2S_{1/2} \rightarrow 4^2P_{1/2}$ )	770.1098 nm [Wil97]
Natural line width $\Gamma_{D1}$ (FWHM)	$2\pi \times 6.0$ MHz [Wil97]
Vacuum Wavelength $\lambda_{D2}$ ( $4^2S_{1/2} \rightarrow 4^2P_{3/2}$ )	766.7017 nm [Wil97]
Natural line width $\Gamma_{D2}$ (FWHM)	$2\pi \times 6.09$ MHz [Gol02]
Saturation intensity $I_{\text{sat}}$ $F = 9/2 \rightarrow F' = 11/2$ ( $\sigma^\pm$ -polarized light, $D_2$ -line)	1.670 mW/cm <sup>2</sup>
Resonant cross section $\sigma_0$ $F = 9/2 \rightarrow F' = 11/2$ ( $\sigma^\pm$ -polarized light, $D_2$ -line)	$2.807 \cdot 10^{-9}$ cm <sup>2</sup>
Saturation intensity $I_{\text{sat}}$ $F = 9/2 \rightarrow F' = 11/2$ (isotropically polarized light, $D_2$ -line)	4.175 mW/cm <sup>2</sup>
Resonant cross section $\sigma_0$ $F = 9/2 \rightarrow F' = 11/2$ (isotropically polarized light, $D_2$ -line)	$1.123 \cdot 10^{-9}$ cm <sup>2</sup>
Scattering length $a_S$ (singlet)	104 $a_0$ [Tic04]
Scattering length $a_T$ (triplet)	174 $a_0$ [Tic04]
van der Waals coefficient $C_6$	$3927 a_0^6 \alpha^2 m_e c^2$ [Tic04]

**Table A.2:** Properties of  $^{40}\text{K}$ .

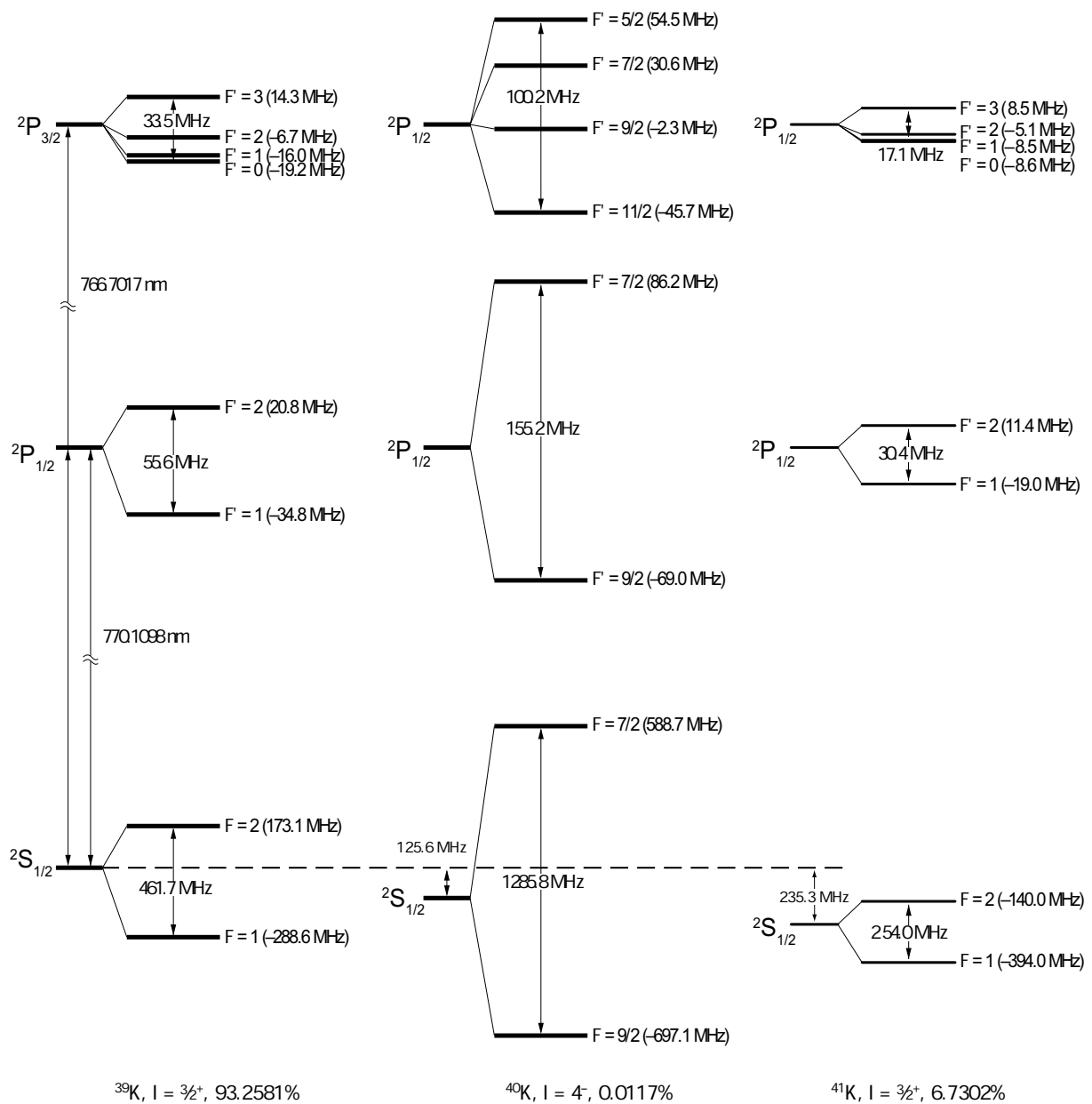


**Figure A.1:** The level structure of the potassium isotopes  $^{39}\text{K}$ ,  $^{40}\text{K}$  and  $^{41}\text{K}$ , adapted from [Wil97]. The levels of  $^{39}\text{K}$  without the hyperfine splitting form the reference points for the frequencies given in the brackets.

### A.3 Physical constants

In this thesis, the following physical constants are used:

Speed of light	$c$	$299792458 \text{ m s}^{-1}$
Planck constant	$h$	$6.6260693(11) \cdot 10^{-34} \text{ J s}$
Fine-structure constant	$\alpha$	$7.297352568(24) \cdot 10^{-3}$
Electric constant	$\epsilon_0$	$8.854187817 \cdot 10^{-12} \text{ F m}^{-1}$
Elementary charge	$e$	$1.60217653(14) \cdot 10^{-19} \text{ C}$
Electron mass	$m_e$	$9.1093826(16) \cdot 10^{-31} \text{ kg}$
Atomic mass constant	$u$	$1.66053886(28) \cdot 10^{-27} \text{ kg}$
Boltzmann constant	$k_B$	$1.3806505(24) \cdot 10^{-23} \text{ J K}^{-1}$
Bohr radius	$a_0$	$0.5291772108(18) \cdot 10^{-10} \text{ m}$
Bohr magneton	$\mu_B$	$9.27400949(80) \cdot 10^{-24} \text{ J T}^{-1}$
Nuclear magneton	$\mu_N$	$5.05078343(43) \cdot 10^{-27} \text{ J T}^{-1}$
Electron $g$ -factor	$g_e$	$2.0023193043718(75)$

**Table A.3:** Physical constants from CODATA [COD02].

## Bibliography

- [And61] P.W. Anderson and P. Morel, *Generalized bardeen-cooper-schrieffer states and the proposed low-temperature phase of liquid  $^3\text{He}$* , Physical Review **123**, 1911 (1961).
- [And66] P.W. Anderson, *Considerations on the flow of superfluid helium*, Review of Modern Physics **38**, 298 (1966).
- [And95] M.H. Anderson, J.R. Ensher, M.R. Matthews, C.E. Wieman, and E.A. Cornell, *Observation of Bose-Einstein condensation in a dilute atomic vapor*, Science **269**, 198 (1995).
- [And97] M.R. Andrews, C.G. Townsend, H.-J. Miesner, D.S. Durfee, D.M. Kurn, and W. Ketterle, *Observation of interference between two Bose condensates*, Science **275**, 637 (1997).
- [And98] B.P. Anderson and M.A. Kasevich, *Macroscopic quantum interference from atomic tunnel arrays*, Science **282**, 1686 (1998).
- [Ari77] E. Arimondo, M. Inguscio, and P. Violino, *Experimental determinations of the hyperfine structure in the alkali atoms*, Review of Modern Physics **49**, 31 (1977).
- [Ash76] N.W. Ashcroft and N.D. Mermin, *Solid state physics*, Harcourt College Publishers, 1976.
- [Ast04] G.E. Astrakharchik, D. Blume, S. Giorgini, and L.P. Pitaevskii, *Interacting fermions in highly elongated harmonic traps*, Physical Review Letters **93**, 050402 (2004).
- [Bar04] M. Bartenstein, A. Altmeyer, S. Riedl, S. Jochim, C. Chin, J. Hecker Denschlag, and R. Grimm, *Crossover from a molecular Bose-Einstein condensate to a degenerate Fermi gas*, Physical Review Letters **92**, 120401 (2004).
- [Bat90] G.G. Batrouni, R.T. Scalettar, and G.T. Zimanyi, *Quantum critical phenomena in one-dimensional Bose systems*, Physical Review Letters **65**, 1765 (1990).

- [Bat02] G.G. Batrouni, V. Rousseau, R.T. Scalettar, M. Rigol, A. Muramatsu, P.J.H. Denteener, and M. Troyer, *Mott domains of bosons confined on optical lattices*, Physical Review Letters **89**, 117203 (2002).
- [Ber03] T. Bergeman, M.G. Moore, and M. Olshanii, *Atom-atom scattering under cylindrical harmonic confinement: Numerical and analytic studies of the confinement induced resonance*, Physical Review Letters **91**, 163201 (2003).
- [Biz99] S. Bize, Y. Sortais, M.S. Santos, C. Mandache, A. Clairon, and C. Salomon, *High-accuracy measurement of the  $^{87}\text{Rb}$  ground-state hyperfine splitting in an atomic fountain*, Europhysics Letters **45**, 558 (1999).
- [Bjo83] G.C. Bjorklund, M.D. Levenson, W. Lenth, and C. Ortiz, *Frequency modulation (FM) spectroscopy*, Applied Physics B **32**, 145 (1983).
- [Blo00] I. Bloch, T.W. Hänsch, and T. Esslinger, *Measurement of the spatial coherence of a trapped Bose gas at the phase transition*, Nature **403**, 166 (2000).
- [Bog47] N.N. Bogoliubov, *On the theory of superfluidity*, Journal of Physics (USSR) **11**, 23 (1947).
- [Bos24] S.N. Bose, *Plancks Gesetz und Lichtquantenhypothese*, Zeitschrift für Physik **26**, 178 (1924).
- [Bou04] T. Bourdel, L. Khaykovich, J. Cubizolles, J. Zhang, F. Chevy, M. Teichmann, L. Tarruell, S.J.J.M.F. Kokkelmans, and C. Salomon, *Experimental study of the BEC-BCS crossover region in lithium 6*, Physical Review Letters **93**, 050401 (2004).
- [Bro01] J.C. Bronski, L.D. Carr, B. Deconinck, and J.N. Kutz, *Bose-Einstein condensates in standing waves: The cubic nonlinear Schrödinger equation with a periodic potential*, Physical Review Letters **86**, 1402 (2001).
- [Büc03a] H.P. Büchler and G. Blatter, *Signature of quantum depletion in the dynamic structure factor of atomic gases*, e-print cond-mat, 0312526 (2003).
- [Büc03b] H.P. Büchler, G. Blatter, and W. Zwerger, *Commensurate-incommensurate transition of cold atoms in an optical lattice*, Physical Review Letters **90**, 130401 (2003).
- [Bus98] T. Busch, B.-G. Englert, K. Rzazewski, and M. Wilkens, *Two cold atoms in a harmonic trap*, Foundation of Physics **28**, 549 (1998).
- [But97] D.A. Butts and D.S. Rokhsar, *Trapped Fermi gases*, Physical Review A **55**, 4346 (1997).



## BIBLIOGRAPHY

---

- [Car05] L.D. Carr and M.J. Holland, *Quantum phase transitions in the Fermi–Bose hubbard model*, Physical Review A **72**, 031604(R) (2005).
- [Cat01] F.S. Cataliotti, S. Burger, C. Fort, P. Maddaloni, F. Minardi, A. Trombettoni, A. Smerzi, and M. Inguscio, *Josephson junction arrays with Bose-Einstein condensates*, Science **293**, 843 (2001).
- [Caz03] M.A. Cazalilla and A.F. Ho, *Instabilities in binary mixtures of one-dimensional quantum degenerate gas*, Physical Review Letters **91**, 150403 (2003).
- [Che99] T. Cheon and T. Shigehara, *Fermion-boson duality of one-dimensional quantum particles with generalized contact interactions*, Physical Review Letters **82**, 2536 (1999).
- [Che02] F. Chevy, V. Bretin, P. Rosenbusch, K.W. Madison, and J. Dalibard, *Transverse breathing mode of an elongated Bose-Einstein condensate*, Physical Review Letters **88**, 250402 (2002).
- [Che05] C.H. Cheng and S.K. Yip, *Anisotropic Fermi superfluid via p-wave Feshbach resonance*, Physical Review Letters **95**, 070404 (2005).
- [Chi03] C. Chin, A.J. Kerman, V. Vuletić, and S. Chu, *Sensitive detection of cold cesium molecules formed on Feshbach resonances*, Physical Review Letters **90**, 033201 (2003).
- [Chi04] C. Chin, M. Bartenstein, A. Altmeyer, S. Riedl, S. Jochim, J. Hecker Denschlag, and R. Grimm, *Observation of the pairing gap in a strongly interacting Fermi gas*, Science **305**, 1128 (2004).
- [Chi05] C. Chin, *A simple model of Feshbach molecules*, e-print cond-mat, 0506313 (2005).
- [Chu86] S. Chu, J.E. Bjorkholm, A. Ashkin, and A. Cable, *Experimental observation of optically trapped atoms*, Physical Review Letters **57**, 314 (1986).
- [COD02] CODATA, *Codata recommended values*, 2002.
- [Cor00] S.L. Cornish, N.R. Claussen, J.L. Roberts, E.A. Cornell, and C.E. Wieman, *Stable  $^{85}\text{Rb}$  Bose-Einstein condensates with widely tunable interactions*, Physical Review Letters **85**, 1795 (2000).
- [Cub03] J. Cubizolles, T. Bourdel, S.J.J.M.F. Kokkelmans, G.V. Shlyapnikov, and C. Salomon, *Production of long-lived ultracold  $\text{Li}_2$  molecules from a Fermi gas*, Physical Review Letters **91**, 240401 (2003).

- 
- [Dah96] M.B. Dahan, E. Peik, J. Reichel, Y. Castin, and C. Salomon, *Bloch oscillations of atoms in an optical potential*, Physical Review Letters **76**, 4508 (1996).
  - [Dal99] J. Dalibard, *Collisional dynamics of ultra-cold atomic gases*, Bose-Einstein Condensation in Atomic Gases (M. Inguscio, S. Stringari, and C.E. Wieman, eds.), IOS Press, 1999.
  - [Dav95a] K.B. Davis, M.-O. Mewes, M.R. Andrews, N.J. van Druten, D.S. Durfee, D.M. Kurn, and W. Ketterle, *Bose-Einstein condensation of sodium atoms*, Physical Review Letters **75**, 3969 (1995).
  - [Dav95b] K.B. Davis, M.-O. Mewes, M.A. Joffe, M.R. Andrews, and W. Ketterle, *Evaporative cooling of sodium atoms*, Physical Review Letters **74**, 5202 (1995).
  - [DeM99a] B. DeMarco and D.S. Jin, *Onset of Fermi degeneracy in a trapped atomic gas*, Science **285**, 1703 (1999).
  - [DeM99b] B. DeMarco, H. Rohner, and D.S. Jin, *An enriched  $^{40}\text{K}$  source for fermionic atom studies*, Review of Scientific Instruments **70**, 1967 (1999).
  - [DeM01a] B. DeMarco, *Quantum behavior of an atomic Fermi gas*, Ph.D. thesis, University of Colorado, 2001.
  - [DeM01b] B. DeMarco, S.B. Papp, and D.S. Jin, *Pauli blocking of collisions in a quantum degenerate atomic Fermi gas*, Physical Review Letters **86**, 5409 (2001).
  - [DeP99] M.T. DePue, C. McCormick, S.L. Winoto, S. Oliver, and D.S. Weiss, *Unity occupation of sites in a 3D optical lattice*, Physical Review Letters **82**, 2262 (1999).
  - [Der99] A. Derevianko, W.R. Johnson, M.S. Safronova, and J.F. Babb, *High-precision calculations of dispersion coefficients, static dipole polarizabilities, and atom-wall interaction constants for alkali-metal atoms*, Physical Review Letters **82**, 3589 (1999).
  - [Dic05] D.B.M. Dickerscheid, U. Al Khawaja, D. van Oosten, and H.T.C. Stoof, *Feshbach resonances in an optical lattice*, Physical Review A **71**, 043604 (2005).
  - [Die05] R.B. Diener and T.L. Ho, *Fermions in optical lattices across Feshbach resonance*, e-print cond-mat, 0507253 (2005).
  - [Don01] E.A. Donley, N.R. Claussen, S.L. Cornish, J.L. Roberts, E.A. Cornell, and C.E. Wieman, *Dynamics of collapsing and exploding Bose-Einstein condensates*, Nature **412**, 295 (2001).

- [Don02] E.A. Donley, N.R. Claussen, S.T. Thompson, and C.E. Wieman, *Atom-molecule coherence in a Bose-Einstein condensate*, Nature **417**, 529 (2002).
- [Dun01] V. Dunjko, V. Lorent, and M. Olshanii, *Bosons in cigar-shaped traps: Thomas-Fermi regime, Tonks-Girardeau regime, and in between*, Physical Review Letters **86**, 5413 (2001).
- [Efe75] K.B. Efetov and A.I. Larkin, Sov. Phys. JETP **42**, 390 (1975).
- [Ein25] A. Einstein, *Quantentheorie des einatomigen idealen Gases. Zweite Abhandlung*, Sitzungsberichte der Preussischen Akademie der Wissenschaften, Physikalische Klasse, 3 (1925).
- [Ess98] T. Esslinger, I. Bloch, and T.W. Hänsch, *Bose-Einstein condensation in a quadrupole-Ioffe-configuration trap*, Physical Review A **58**, 2664 (1998).
- [Fed04] P.O. Fedichev, M.J. Bijlsma, and P. Zoller, *Extended molecules and geometric scattering resonances in optical lattices*, Physical Review Letters **92**, 080401 (2004).
- [Fes58] H. Feshbach, *A unified theory of nuclear reactions*, Annals of Physics **5**, 337 (1958).
- [Fis89] M.P.A. Fisher, P.B. Weichman, G. Grinstein, and D.S. Fisher, *Boson localization and the superfluid-insulator transition*, Physical Review B **40**, 546 (1989).
- [Fow66] A.B. Fowler, F.F. Fang, W.E. Howard, and P. J. Stiles, *Magneto-oscillatory conductance in silicon surfaces*, 901 (1966).
- [Fow82] A.B. Fowler, A. Hartstein, and R.A. Webb, *Conductance in restricted-dimensionality accumulation layers*, 196 (1982).
- [Fre94] J.K. Freericks and H. Monien, *Phase diagram of the Bose-Hubbard model*, Europhysics Letters **26**, 545 (1994).
- [Fuc03] J.N. Fuchs, X. Leyronas, and R. Combescot, *Hydrodynamic modes of a one-dimensional trapped Bose gas*, Physical Review A **68**, 043610 (2003).
- [Fuc04] J.N. Fuchs, A. Recati, and W. Zwerger, *Exactly solvable model of the BCS-BEC crossover*, Physical Review Letters **93**, 090408 (2004).
- [Gan03] D.M. Gangardt and G.V. Shlyapnikov, *Stability and phase coherence of trapped 1D Bose gases*, Physical Review Letters **90**, 010401 (2003).
- [Gan04] D.M. Gangardt, P. Pedri, L. Santos, and G.V. Shlyapnikov, *Mott-insulator phase of coupled 1D atomic gases in a 2D optical lattice*, e-print cond-mat, 0408437 (2004).

- 
- [Gia04] T. Giamarchi, *Quantum physics in one dimension*, Oxford University Press, 2004.
- [Gir60] M. Girardeau, *Relationship between systems of impenetrable bosons and fermions in one dimension*, Journal of Mathematical Physics **1**, 516 (1960).
- [Gir01] M. D. Girardeau, E. M. Wright, and J. M. Triscari, *Ground-state properties of a one-dimensional system of hard-core bosons in a harmonic trap*, Physical Review A **63**, 033601 (2001).
- [Gün05] K. Günter, T. Stöferle, H. Moritz, M. Köhl, and Tilman Esslinger, *p-wave interactions in low-dimensional Fermi gases*, e-print cond-mat, 0507632 (2005).
- [Gol02] J. Goldwin, S.B. Papp, B. DeMarco, and D.S. Jin, *Two-species magneto-optical trap with  $^{40}\text{K}$  and  $^{87}\text{Rb}$* , Physical Review A **65**, 021402(R) (2002).
- [Gör01] A. Görlitz, J. M. Vogels, A.E. Leanhardt, C. Raman, T. L. Gustavson, J.R. Abo-Shaeer, A. P. Chikkatur, S. Gupta, S. Inouye, T. Rosenband, and W. Ketterle, *Realization of Bose-Einstein condensates in lower dimensions*, Physical Review Letters **87**, 130402 (2001).
- [Gra04] B.E. Granger and D. Blume, *Tuning the interactions of spin-polarized fermions using quasi-one-dimensional confinement*, Physical Review Letters **92**, 133202 (2004).
- [Gre01a] M. Greiner, I. Bloch, T.W. Hänsch, and T. Esslinger, *Magnetic transport of trapped cold atoms over a large distance*, Physical Review A **63**, 031401 (2001).
- [Gre01b] M. Greiner, I. Bloch, O. Mandel, T.W. Hänsch, and T. Esslinger, *Exploring phase coherence in a 2D lattice of Bose-Einstein condensates*, Physical Review Letters **87**, 160405 (2001).
- [Gre02] M. Greiner, O. Mandel, T. Esslinger, T.W. Hänsch, and I. Bloch, *Quantum phase transition from a superfluid to a Mott insulator in a gas of ultracold atoms*, Nature **415**, 39 (2002).
- [Gre03] M. Greiner, C.A. Regal, and D.S. Jin, *Emergence of a molecular Bose-Einstein condensate from a Fermi gas*, Nature **426**, 537 (2003).
- [Gri93] G.F. Gribakin and V.V. Flambaum, *Calculation of the scattering length in atomic collisions using the semiclassical approximation*, Physical Review A **48**, 546 (1993).
- [Gri00] R. Grimm, M. Weidemüller, and Y.B. Ovchinnikov, *Optical dipole traps for neutral atoms*, Advances in Atomic, Molecular and Optical Physics **42**, 95 (2000).

- [Gro61] E.P. Gross, *Structure of a quantized vortex in boson systems*, Nuovo Cimento **20**, 454 (1961).
- [Gry93] G. Grynberg, B. Lounis, P. Verkerk, J.-Y. Courtois, and C. Salomon, *Quantized motion of cold cesium atoms in two- and three-dimensional optical potentials*, Physical Review Letters **70**, 2249 (1993).
- [Gup03] S. Gupta, Z. Hadzibabic, M.W. Zwierlein, C.A. Stan, K. Dieckmann, C.H. Schunck, E.G.M. van Kempen, B.J. Verhaar, and W. Ketterle, *Radio-frequency spectroscopy of ultracold fermions*, Science **300**, 1723 (2003).
- [Gur05] V. Gurarie, L. Radzihovsky, and A.V. Andreev, *Quantum phase transitions across a p-wave Feshbach resonance*, Physical Review Letters **94**, 230403 (2005).
- [Hal81] F.D.M. Haldane, *Effective harmonic-fluid approach to low-energy properties of one-dimensional quantum fluids*, Physical Review Letters **47**, 1840 (1981).
- [Har02] D.M. Harber, H.J. Lewandowski, J.M. McGuirk, and E.A. Cornell, *Effect of cold collisions on spin coherence and resonance shifts in a magnetically trapped ultracold gas*, Physical Review A **66**, 053616 (2002).
- [Hem93] A. Hemmerich and T.W. Hänsch, *Two-dimensional atomic crystal bound by light*, Physical Review Letters **70**, 410 (1993).
- [Her03] J. Herbig, T. Kraemer, M. Mark, T. Weber, C. Chin, H.-C. Nägerl, and R. Grimm, *Preparation of a pure molecular quantum gas*, Science **301**, 1510 (2003).
- [Ho99] T.-L. Ho and M. Ma, *Quasi 1D and 2D dilute Bose gas in magnetic traps: Existence of off-diagonal order and anomalous quantum fluctuations*, Journal of Low Temperature Physics **115**, 61 (1999).
- [Ho04] A.F. Ho, M.A. Cazalilla, and T. Giamarchi, *Deconfinement in a 2D optical lattice of coupled 1D boson systems*, Physical Review Letters **92**, 130405 (2004).
- [Ho05] T.L. Ho and R.B. Diener, *Fermion superfluids of nonzero orbital angular momentum near resonance*, Physical Review Letters **94**, 090402 (2005).
- [Hof02] W. Hofstetter, J.I. Cirac, P. Zoller, E. Demler, and M.D. Lukin, *High-temperature superfluidity of fermionic atoms in optical lattices*, Physical Review Letters **89**, 220407 (2002).
- [Hoh67] P. C. Hohenberg, *Existence of long-range order in one and two dimensions*, Physical Review Letters **158**, 383 (1967).

- [Hua95] K. Huang, *Bose-Einstein condensation and superfluidity*, Bose-Einstein Condensation (A. Griffin, D.W. Snoke, and S. Stringari, eds.), Cambridge University Press, 1995.
- [Hub63] J. Hubbard, *Electron correlations in narrow energy bands*, Proceedings of the Royal Society of London, Series A **276**, 238 (1963).
- [Hug59] N.M. Hugenholtz and D. Pines, *Ground-state energy and excitation spectrum of a system of interacting bosons*, Physical Review **116**, 489 (1959).
- [Ino98] S. Inouye, M.R. Andrews, J. Stenger, H.-J. Miesner, D.M. Stamper-Kurn, and W. Ketterle, *Observation of Feshbach resonances in a Bose-Einstein condensate*, Nature **392**, 151 (1998).
- [Ino04] S. Inouye, J. Goldwin, M.L. Olsen, C. Ticknor, J.L. Bohn, and D.S. Jin, *Observation of heteronuclear Feshbach resonances in a mixture of bosons and fermions*, Physical Review Letters **93**, 183201 (2004).
- [Isk05] M. Iskin and C.A.R. Sá de Melo, *Exotic p-wave superfluidity of single hyperfine state Fermi gases in optical lattices*, e-print cond-mat, 0502148 (2005).
- [Jak98] D. Jaksch, C. Bruder, J.I. Cirac, C.W. Gardiner, and P. Zoller, *Cold bosonic atoms in optical lattices*, Physical Review Letters **81**, 3108 (1998).
- [Jak05] D. Jaksch and P. Zoller, *The cold atom Hubbard toolbox*, Annals of Physics **315**, 52 (2005).
- [Joc03a] S. Jochim, M. Bartenstein, A. Altmeyer, G. Hendl, C. Chin, J. Hecker-Denschlag, and R. Grimm, *Pure gas of optically trapped molecules created from fermionic atoms*, Physical Review Letters **91**, 240402 (2003).
- [Joc03b] S. Jochim, M. Bartenstein, A. Altmeyer, G. Hendl, S. Riedl, C. Chin, J. Hecker-Denschlag, and R. Grimm, *Bose-Einstein condensation of molecules*, Science **302**, 2101 (2003).
- [Ket96] W. Ketterle and N.J. van Druten, *Bose-Einstein condensation of a finite number of particles trapped in one or three dimensions*, Physical Review A **54**, 656 (1996).
- [Köh01] M. Köhl, T.W. Hänsch, and T. Esslinger, *Measuring the temporal coherence of an atom laser beam*, Physical Review Letters **87**, 160404 (2001).
- [Kha02] L. Khaykovich, F. Schreck, G. Ferrari, T. Bourdel, J. Cubizolles, L.D. Carr, Y. Castin, and C. Salomon, *Formation of a matter-wave bright soliton*, Science **296**, 1290 (2002).

- [Khe03] K.V. Kheruntsyan, D.M. Gangardt, P.D. Drummond, and G.V. Shlyapnikov, *Pair correlations in a finite-temperature 1D Bose gas*, Physical Review Letters **91**, 040403 (2003).
- [Kin04a] J. Kinast, S.L. Hemmer, M.E. Gehm, A. Turlapov, and J. E. Thomas, *Evidence for superfluidity in a resonantly interacting Fermi gas*, Physical Review Letters **92**, 150402 (2004).
- [Kin04b] T. Kinoshita, T. Wenger, and D.S. Weiss, *Observation of a one-dimensional Tonks-Girardeau gas*, Science **305**, 1125 (2004).
- [Kit87] C. Kittel, *Quantum theory of solids*, John Wiley & Sons, 1987.
- [Köh04] M. Köhl, T. Stöferle, H. Moritz, C. Schori, and T. Esslinger, *1D Bose gases in an optical lattice*, Applied Physics B **79**, 1009 (2004).
- [Köh05a] M. Köhl, H. Moritz, T. Stöferle, K. Günter, and T. Esslinger, *Fermionic atoms in a three dimensional optical lattice: Observing Fermi surfaces, dynamics, and interactions*, Physical Review Letters **94**, 080403 (2005).
- [Köh05b] M. Köhl, H. Moritz, T. Stöferle, C. Schori, and T. Esslinger, *Superfluid to Mott insulator transition in one, two, and three dimensions*, Journal of Low Temperature Physics **138**, 635 (2005).
- [Kol04] C. Kollath, U. Schollwöck, J. von Delft, and W. Zwerger, *Spatial correlations of trapped one-dimensional bosons in an optical lattice*, Physical Review A **69**, 031601 (2004).
- [Kol05] C. Kollath, U. Schollwöck, and W. Zwerger, *Spin-charge separation in cold Fermi-gases: a real time analysis*, e-print cond-mat, 0504299 (2005).
- [Krä02] M. Krämer, L. Pitaevskii, and S. Stringari, *Macroscopic dynamics of a trapped Bose-Einstein condensate in the presence of 1D and 2D optical lattices*, Physical Review Letters **88**, 180404 (2002).
- [Krä03] M. Krämer, C. Menotti, L. Pitaevskii, and S. Stringari, *Bose-Einstein condensates in 1D optical lattices: Compressibility, Bloch bands and elementary excitations*, European Physics Journal D **27**, 247 (2003).
- [Krä05] M. Krämer, C. Tozzo, and F. Dalfovo, *Parametric excitation of a Bose-Einstein condensate in a one-dimensional optical lattice*, Physical Review A, 061602(R) (2005).

- 
- [Küh98] T.D. Kühner and H. Monien, *Phases of the one-dimensional Bose-Hubbard model*, Physical Review B **58**, R14741 (1998).
- [Lee04] C. Lee, *Bose-Einstein condensation of particle-hole pairs in ultracold fermionic atoms trapped within optical lattices*, Physical Review Letters **93**, 120406 (2004).
- [Leg91] A.J. Leggett and F. Sols, *On the concept of spontaneously broken gauge symmetry in condensed matter physics*, Foundations of Physics **21**, 353 (1991).
- [Leg95] A.J. Leggett, *Broken gauge symmetry in a Bose-Einstein condensate*, Bose-Einstein Condensation (A. Griffin, D.W. Snoke, and S. Stringari, eds.), Cambridge University Press, 1995, p. 452.
- [Leg01] A.J. Leggett, *Bose-Einstein condensation in the alkali gases: Some fundamental concepts*, Review of Modern Physics **73**, 307 (2001).
- [Let88] P.D. Lett, R.N. Watts, C.I. Westbrook, W.D. Phillips, P.L. Gould, and H.J. Metcalf, *Observation of atoms laser cooled below the doppler limit*, Physical Review Letters **61**, 169 (1988).
- [Lie63a] E.H. Lieb, *Exact analysis of an interacting Bose gas. II. The excitation spectrum*, Physical Review **130**, 1616 (1963).
- [Lie63b] E.H. Lieb and W. Liniger, *Exact analysis of an interacting Bose gas. I. The general solution and the ground state*, Physical Review **130**, 1605 (1963).
- [Lie03] E.H. Lieb, R. Seiringer, and J. Yngvason, *One-dimensional bosons in three-dimensional traps*, Physical Review Letters **91**, 150401 (2003).
- [Liu05] X.-J. Liu, P.D. Drummond, and H. Hui, *Signature of mott-insulator transition with ultracold fermions in a one-dimensional optical lattice*, Physical Review Letters **94**, 136406 (2005).
- [Lof02] T. Loftus, C.A. Regal, C. Ticknor, J.L. Bohn, and D.S. Jin, *Resonant control of elastic collisions in an optically trapped Fermi gas of atoms*, Physical Review Letters **88**, 173201 (2002).
- [Mat99] M.R. Matthews, B.P. Anderson, P.C. Haljan, D. S. Hall, C.E. Wieman, and E. A. Cornell, *Vortices in a Bose-Einstein condensate*, Physical Review Letters **83**, 2498 (1999).
- [Mat04] L. Mathey, D.-W. Wang, W. Hofstetter, M. D. Lukin, and Eugene Demler, *Luttinger liquid of polarons in one-dimensional boson-fermion mixtures*, Physical Review Letters **93**, 120404 (2004).



- [Men02] C. Menotti and S. Stringari, *Collective oscillations of a one-dimensional trapped Bose-Einstein gas*, Physical Review A **66**, 043610 (2002).
- [Men03] C. Menotti, M. Krämer, L. Pitaevskii, and S. Stringari, *Dynamic structure factor of a Bose-Einstein condensate in a one-dimensional optical lattice*, Physical Review A **67**, 053609 (2003).
- [Met99] H.J. Metcalf and P. van der Straten, *Laser cooling and trapping*, Springer, 1999.
- [Mew96] M.-O. Mewes, M.R. Andrews, N.J. van Druten, D.M. Kurn, D.S. Durfee, C.G. Townsend, and W. Ketterle, *Collective excitations of a Bose-Einstein condensate in a magnetic trap*, Physical Review Letters **77**, 988 (1996).
- [Mig85] A.L. Migdall, J.V. Prodan, W.D. Phillips, T.H. Bergeman, and H.J. Metcalf, *First observation of magnetically trapped neutral atoms*, Physical Review Letters **54**, 2596 (1985).
- [Mod02] G. Modugno, G. Roati, F. Riboli, F. Ferlaino, R.J. Brecha, and M. Inguscio, *Collapse of a degenerate Fermi gas*, Science **297**, 2240 (2002).
- [Mod03] G. Modugno, F. Ferlaino, R. Heidemann, G. Roati, and M. Inguscio, *Production of a Fermi gas of atoms in an optical lattice*, Physical Review A **68**, 011601(R) (2003).
- [Moe95] A.J. Moerdijk, B.J. Verhaar, and A. Axelsson, *Resonances in ultracold collisions of  $^6\text{Li}$ ,  $^7\text{Li}$ , and  $^{23}\text{Na}$* , Physical Review A **51**, 4852 (1995).
- [Mor03] H. Moritz, T. Stöferle, M. Köhl, and T. Esslinger, *Exciting collective oscillations in a trapped 1D gas*, Physical Review Letters **91**, 250402 (2003).
- [Mor04] C. Mora, R. Egger, A.O. Gogolin, and A. Komnik, *Atom-dimer scattering for confined ultracold fermion gases*, Physical Review Letters **93**, 170403 (2004).
- [Mor05] H. Moritz, T. Stöferle, K. Günter, M. Köhl, and T. Esslinger, *Confinement induced molecules in a 1D Fermi gas*, Physical Review Letters **94**, 210401 (2005).
- [NIS05] NIST, *Physical reference data*, 2005.
- [Ols98] M. Olshanii, *Atomic scattering in the presence of an external confinement and a gas of impenetrable bosons*, Physical Review Letters **81**, 938 (1998).
- [Orz01] C. Orzel, A.K. Tuchman, M.L. Fenselau, M. Yasuda, and M.A. Kasevich, *Squeezed states in a Bose-Einstein condensate*, Science **291**, 2386 (2001).

- 
- [Ott04] H. Ott, E. de Mirandes, F. Ferlaino, G. Roati, V. Türeċk, G. Modugno, and M. Inguscio, *Collisionally induced transport in periodic potentials*, Physical Review Letters **92**, 160601 (2004).
  - [Par04] B. Paredes, A. Widera, V. Murg, O. Mandel, S. Fölliing, I. Cirac, G.V. Shlyapnikov, T.W. Hänsch, and I. Bloch, *Tonks-Girardeau gas of ultracold atoms in an optical lattice*, Nature **429**, 277 (2004).
  - [Ped03] P. Pedri and L. Santos, *Three-dimensional quasi-Tonks gas in a harmonic trap*, Physical Review Letters **91**, 110401 (2003).
  - [Pen56] O. Penrose and L. Onsager, *Bose-einstein condensation and liquid helium*, Physical Review **104**, 576 (1956).
  - [Pet00a] D.S. Petrov, M. Holzmann, and G.V. Shlyapnikov, *Bose-Einstein condensation in quasi-2D trapped gases*, Physical Review Letters **84**, 2551 (2000).
  - [Pet00b] D.S. Petrov, G.V. Shlyapnikov, and J.T.M. Walraven, *Regimes of quantum degeneracy in trapped 1D gases*, Physical Review Letters **85**, 3745 (2000).
  - [Pet01] D.S. Petrov and G.V. Shlyapnikov, *Interatomic collisions in a tightly confined Bose gas*, Physical Review A **64**, 012706 (2001).
  - [Pet02] C.J. Pethick and H. Smith, *Bose-Einstein condensation in dilute gases*, Cambridge University Press, 2002.
  - [Pet04a] D.S. Petrov, D. Gangardt, and G.V. Shlyapnikov, *Low-dimensional trapped gases*, Journal de Physique IV **116**, 5–44 (2004).
  - [Pet04b] D.S. Petrov, C. Salomon, and G.V. Shlyapnikov, *Weakly bound dimers of fermionic atoms*, Physical Review Letters **93**, 090404 (2004).
  - [Pez04] L. Pezzè, L. Pitaevskii, A. Smerzi, S. Stringari, G. Modugno, E. de Mirandes, F. Ferlaino, H. Ott, G. Roati, and M. Inguscio, *Insulating behavior of a trapped ideal Fermi gas*, Physical Review Letters **93**, 120401 (2004).
  - [Phi98] W. D. Phillips, *Laser cooling and trapping of neutral atoms*, Review of Modern Physics **70**, 721 (1998).
  - [Pit61] L.P. Pitaevskii, *Vortex lines in an imperfect Bose gas*, Soviet Physics JETP **13**, 451 (1961).
  - [Pit03] L. Pitaevskii and S. Stringari, *Bose-Einstein condensation*, Oxford University Press, 2003.

- [Raa87] E.L. Raab, M. Prentiss, A. Cable, S. Chu, and D.E. Pritchard, *Trapping of neutral sodium atoms with radiation pressure*, Physical Review Letters **59**, 2631 (1987).
- [Rec03] A. Recati, P.O. Fedichev, W. Zwerger, and P. Zoller, *Spin-charge separation in ultracold quantum gases*, Physical Review Letters **90**, 020401 (2003).
- [Reg03a] C.A. Regal and D.S. Jin, *Measurement of positive and negative scattering lengths in a Fermi gas of atoms*, Physical Review Letters **90**, 230404 (2003).
- [Reg03b] C.A. Regal, C. Ticknor, J.L. Bohn, and D.S. Jin, *Creation of ultracold molecules from a Fermi gas of atoms*, Nature **424**, 47 (2003).
- [Reg03c] C.A. Regal, C. Ticknor, J.L. Bohn, and D.S. Jin, *Tuning p-wave interactions in an ultracold Fermi gas of atoms*, Physical Review Letters **90**, 053201 (2003).
- [Reg04] C.A. Regal, M. Greiner, and D.S. Jin, *Observation of resonance condensation of fermionic atom pairs*, Physical Review Letters **92**, 040403 (2004).
- [Ric95] L. Ricci, M. Weidemüller, T. Esslinger, A. Hemmerich, C. Zimmermann, V. Vuletic, W. König, and T.W. Hänsch, *A compact grating-stabilized diode laser system for atomic physics*, Optics Communications **117**, 541 (1995).
- [Rig03] M. Rigol, A. Muramatsu, G.G. Batrouni, and R.T. Scalettar, *Local quantum criticality in confined fermions on optical lattices*, Physical Review Letters **91**, 130403 (2003).
- [Rig04] M. Rigol and A. Muramatsu, *Quantum Monte Carlo study of confined fermions in one-dimensional optical lattices*, Physical Review A **69**, 053612 (2004).
- [Roa04] G. Roati, E. de Mirandes, F. Ferlaino, H. Ott, G. Modugno, and M. Inguscio, *Atom interferometry with trapped Fermi gases*, Physical Review Letters **92**, 230402 (2004).
- [Rob98] J.L. Roberts, N.R. Claussen, Jr. J.P. Burke, C.H. Greene, E.A. Cornell, and C.E. Wieman, *Resonant magnetic field control of elastic scattering in cold  $^{85}\text{Rb}$* , Physical Review Letters **81**, 5109 (1998).
- [Rot03] R. Roth and K. Burnett, *Superfluidity and interference pattern of ultracold bosons in optical lattices*, Physical Review A, 031602(R) (2003).
- [Sak94] J.J. Sakurai, *Modern quantum mechanics*, Addison-Wesley, 1994.

- 
- [San04] L. Santos, M.A. Baranov, J.I. Cirac, H.-U. Everts, H. Fehrmann, and M. Lewenstein, *Atomic quantum gases in Kagomé lattices*, Physical Review Letters **93**, 030601 (2004).
  - [Sch99] U. Schünemann, H. Engler, R. Grimm, M. Weidemüller, and M. Zielonkowski, *Simple scheme for tunable frequency offset locking of two lasers*, Review of Scientific Instruments **70**, 242 (1999).
  - [Sch01] F. Schreck, L. Khaykovich, K.L. Corwin, G. Ferrari, T. Bourdel, J. Cubizolles, and C. Salomon, *Quasipure Bose-Einstein condensate immersed in a Fermi sea*, Physical Review Letters **87**, 080403 (2001).
  - [Sch04] C. Schori, T. Stöferle, H. Moritz, M. Köhl, and T. Esslinger, *Excitations of a superfluid in a three-dimensional optical lattice*, Physical Review Letters **93**, 240402 (2004).
  - [Sch05] C.H. Schunck, M.W. Zwierlein, C.A. Stan, S.M.F. Raupach, W. Ketterle, A. Simoni, E. Tiesinga, C.J. Williams, , and P.S. Julienne, *Feshbach resonances in fermionic  $^6\text{Li}$* , Physical Review A **71**, 045601 (2005).
  - [Sta04] C.A. Stan, M.W. Zwierlein, C.H. Schunck, S.M.F. Raupach, and W. Ketterle, *Observation of Feshbach resonances between two different atomic species*, Physical Review Letters **93**, 143001 (2004).
  - [Ste99] J. Stenger, S. Inouye, A.P. Chikkatur, D.M. Stamper-Kurn, D.E. Pritchard, and W. Ketterle, *Bragg spectroscopy of a Bose-Einstein condensate*, Physical Review Letters **82**, 4569 (1999).
  - [Ste01] D.A. Steck, *Rubidium 87 D line data*, Tech. report, Los Alamos National Laboratory, 2001.
  - [Sto96] H.T.C. Stoof, M. Houbiers, C.A. Sackett, and R.G. Hulet, *Superfluidity of spin-polarized  $^6\text{Li}$* , Physical Review Letters **76**, 10 (1996).
  - [Stö04] T. Stöferle, H. Moritz, C. Schori, M. Köhl, and Tilman Esslinger, *Transition from a strongly interacting 1D superfluid to a Mott insulator*, Physical Review Letters **92**, 130403 (2004).
  - [Stö05] T. Stöferle, H. Moritz, K. Günter, M. Köhl, and Tilman Esslinger, *Molecules of fermionic atoms in an optical lattice*, e-print cond-mat, 0509211 (2005).
  - [Str96] S. Stringari, *Collective excitations of a trapped Bose-condensed gas*, Physical Review Letters **77**, 2360 (1996).

- [Str02] K.E. Strecker, G. Partridge, A. Truscott, and R. Hulet, *Formation and propagation of matter-wave soliton trains*, Nature **417**, 150 (2002).
- [Str03] K.E. Strecker, G.B. Partridge, and R.G. Hulet, *Conversion of an atomic Fermi gas to a long-lived molecular Bose gas*, Physical Review Letters **91**, 080406 (2003).
- [Sun03] H. Suno, B.D. Esry, and C.H. Greene, *Recombination of three ultracold fermionic atoms*, Physical Review Letters **90**, 053202 (2003).
- [Szy05] M.H. Szymańska, K. Góral, T. Köhler, and K. Burnett, Physical Review A **72**, 013610 (2005).
- [Tic04] C. Ticknor, C.A. Regal, D.S. Jin, and J.L. Bohn, *Multiplet structure of Feshbach resonances in nonzero partial waves*, Physical Review A **69**, 042712 (2004).
- [Tie93] E. Tiesinga, B.J. Verhaar, and H.T.C. Stoof, *Threshold and resonance phenomena in ultracold ground-state collisions*, Physical Review A **47**, 4114 (1993).
- [Tok04] I.V. Tokatly, *Dilute Fermi gas in quasi-one-dimensional traps: From weakly interacting fermions via hard core bosons to a weakly interacting Bose gas*, Physical Review Letters **93**, 090405 (2004).
- [Tol04] B. Laburthe Tolra, K.M. O'Hara, J.H. Huckans, W.D. Phillips, S.L. Rolston, and J.V. Porto, *Observation of reduced three-body recombination in a correlated 1D degenerate Bose gas*, Physical Review Letters **92**, 190401 (2004).
- [Toz05] C. Tozzo, M. Krämer, and F. Dalfovo, *Dilute Fermi gas in quasi-one-dimensional traps: From weakly interacting fermions via hard core bosons to a weakly interacting Bose gas*, Physical Review A **72**, 023613 (2005).
- [Tre05] S. Trebst, U. Schollwöck, M. Troyer, and P. Zoller, *d-wave resonating valence bond states of fermionic atoms in optical lattices*, e-print cond-mat, 0506809 (2005).
- [Tru01] A.G. Truscott, K.E. Strecker, W.I. McAlexander, G.B. Partridge, and R.G. Hulet, *Observation of Fermi pressure in a gas of trapped atoms*, Science **291**, 2570 (2001).
- [Viv04] L. Viverit, C. Menotti, T. Calarco, and A. Smerzi, *Efficient and robust initialization of a qubit register with fermionic atoms*, Physical Review Letters **93**, 110401 (2004).
- [War86] A.C. Warren, D.A. Antoniadis, and H.I. Smith, *Quasi one-dimensional conduction in multiple, parallel inversion lines*, Physical Review Letters **56**, 1858 (1986).

- [Wer05] F. Werner, O. Parcollet, A. Georges, and S. R. Hassan, *Interaction-induced adiabatic cooling and antiferromagnetism of cold fermions in optical lattices*, Physical Review Letters **95**, 056401 (2005).
- [Wig33] E. Wigner, *Über die Streuung von Neutronen an Protonen*, Zeitschrift für Physik **83**, 253 (1933).
- [Wil97] R.S. Williamson, *Magneto-optical trapping of potassium isotopes*, Ph.D. thesis, University of Wisconsin - Madison, 1997.
- [Wou03] M. Wouters, J. Tempere, and J. T. Devreese, *Feshbach resonances in a quasi-two-dimensional atomic gas*, Physical Review A **68**, 053603 (2003).
- [Zha04] J. Zhang, E.G.M. van Kempen, T. Bourdel, L. Khaykovich, J. Cubizolles, F. Chevy, M. Teichmann, L. Tarruell, S.J.J.M.F. Kokkelmans, and C. Salomon, *p-wave Feshbach resonances of ultracold  $^6\text{Li}$* , Physical Review A **70**, 030702 (2004).
- [Zwe03] W. Zwerger, *Mott-Hubbard transition of cold atoms in optical lattices*, Journal of Optics B **5**, S9 (2003).
- [Zwi04] M.W. Zwierlein, C.A. Stan, C.H. Schunck, S.M.F. Raupach, A.J. Kerman, and W. Ketterle, *Condensation of pairs of fermionic atoms near a Feshbach resonance*, Physical Review Letters **92**, 120403 (2004).
- [Zwi05] M.W. Zwierlein, J.R. Abo-Shaeer, A. Schirotzek, C.H. Schunck, and W. Ketterle, *Vortices and superfluidity in a strongly interacting Fermi gas*, Nature **435**, 1047 (2005).

---

# Publications during the PhD work

1. ***Exciting Collective Oscillations in a Trapped 1D Gas***  
H. Moritz, T. Stöferle, M. Köhl, and T. Esslinger  
Physical Review Letters **91**, 250402 (2003).
2. ***Transition from a Strongly Interacting 1D Superfluid to a Mott Insulator***  
T. Stöferle, H. Moritz, C. Schori, M. Köhl, and T. Esslinger  
Physical Review Letters **92**, 130403 (2004).
3. ***1D Bose Gases in an Optical Lattice***  
M. Köhl, T. Stöferle, H. Moritz, C. Schori, and T. Esslinger  
Applied Physics B **79**, 1009 (2004).
4. ***Excitations of a Superfluid in a Three-Dimensional Optical Lattice***  
C. Schori, T. Stöferle, H. Moritz, M. Köhl, and T. Esslinger  
Physical Review Letters **93**, 240402 (2004).
5. ***Superfluid to Mott Insulator Transition in One, Two, and Three Dimensions***  
M. Köhl, H. Moritz, T. Stöferle, C. Schori, and T. Esslinger  
Journal of Low Temperature Physics **138**, 635 (2005).
6. ***Fermionic Atoms in a Three-Dimensional Optical Lattice: Observing Fermi Surfaces, Dynamics, and Interactions***  
M. Köhl, H. Moritz, T. Stöferle, K. Günter, and T. Esslinger  
Physical Review Letters **94**, 080403 (2005).
7. ***Confinement Induced Molecules in a 1D Fermi Gas***  
H. Moritz, T. Stöferle, K. Günter, M. Köhl, and T. Esslinger  
Physical Review Letters **94**, 210401 (2005).
8. ***p-Wave Interactions in Low-Dimensional Fermi gases***  
K. Günter, T. Stöferle, H. Moritz, M. Köhl and Tilman Esslinger  
Physical Review Letters **95**, 230401 (2005).
9. ***Molecules of Fermionic Atoms in an Optical Lattice***  
T. Stöferle, H. Moritz, K. Günter, M. Köhl and Tilman Esslinger  
Physical Review Letters **96**, 030401 (2006).





---

# Curriculum vitae



## Henning Moritz

Born 25.10.1974 in Bruchsal, Germany

German citizen, married

ETH Zürich

HPF D25

8093 Zürich

Tel.: 044 / 633 3954

Fax: 044 / 633 1254

Email: moritz@phys.ethz.ch

Schneebelistrasse 2  
8048 Zürich

## Education

- 1981 – 1985 Primary school in Holzkirchen, Germany
- 1985 – 1994 Secondary school and Abitur at the Gymnasium Tegernsee, Germany
- 1994 – 1995 Army service
- 1995 – 1997 Undergraduate studies of physics at the University of Heidelberg, Germany
- 1997 – 1998 Rotary scholar at the University of Cambridge, England
- 1998 – 2001 Graduate Studies at the University of Heidelberg  
Diploma Thesis: “Fermionic Lithium in a Resonator Dipole Trap”  
under the supervision of Prof. Weidemüller and Prof. Grimm
- 06/2001 Diploma in physics
- 2001 – 2005 PhD student at the Swiss Federal Institute of the Technology, Zürich,  
under the supervision of Prof. Dr. T. Esslinger
- 11/2005 PhD thesis: “One-dimensional Atomic Gases“



---

# Danksagung

Die letzten vier Jahre waren eine Zeit, in der ich viel gelernt und die ich sehr genossen habe. Dies liegt an einer Reihe von Personen, ohne die diese Arbeit nicht denkbar gewesen wäre und bei denen ich mich ganz herzlich bedanken möchte.

Zu Dank bin ich vor allem **Tilman Esslinger**, **Thilo Stöferle** und **Michael Köhl** verpflichtet. **Tilman** schon allein dafür, daß er mir die Möglichkeit gegeben hat, diese Arbeit unter seiner Aufsicht durchzuführen. Seine persönliche Integrität und natürliche Autorität haben mich immer wieder beeindruckt und in Verbindung mit seiner fröhlichen und positiven Art hat er ein Klima in unserer Gruppe geschaffen, wie ich es mir besser nicht hätte wünschen können. Besonders bin ich ihm auch für die verständnisvolle Unterstützung in persönlich schwierigen Situationen dankbar.

**Michael** und Tilman haben sich das Forschungsprojekt ausgedacht und dabei ein bemerkenswertes Gespür bewiesen, das richtige Thema zur richtigen Zeit anzugehen. Ihre intensive Betreuung sowie ihr tiefes physikalisches Verständnis waren für den Erfolg entscheidend. Ich möchte mich bei Michael besonders bedanken für seine Hilfsbereitschaft und die viele Zeit, die er sich einerseits dafür genommen hat, meine Fragen zu beantworten, und die er andererseits im Labor verbracht hat. Dabei hat mich stets fasziniert, wie schnell er schwierige Probleme einfach gelöst hat.

**Thilo** war mein Mitstreiter vom ersten Tage an und wir sind gemeinsam mit Michael den langen Weg von leeren Räumen zu einer funktionierenden Apparatur mit Fermionen im optischen Gitter gegangen. Thilo ist hilfsbereit in einer Weise, die einen oft schon fast beschämen kann und ich hätte mir keinen besseren Kollegen vorstellen können. Ich habe viel von ihm gelernt, einerseits von seinem großen experimentellen Geschick, vor allem aber von der Professionalität, mit der er jede Aufgabe angeht und löst.

Zum Erfolg der Arbeit haben auch **Kenneth Günter** und **Christian Schori** entscheidend beigetragen. Ken ist vor einem Jahr zu unserem Team gestoßen, während Christian nun nach zwei Jahren als Postdoc wieder nach Dänemark zurückgekehrt ist. Die Zusammenarbeit mit ihnen hat grossen Spass gemacht, wir haben gemeinsam viele Stunden im Labor verbracht und viel über Physik diskutiert und gelernt.

---

Für die nette Stimmung, viele ausgeliehene Geräte und gute Diskussionen möchte ich mich bei den Labornachbarn **Stephan Ritter**, **Toni Öttl**, **Tobias Donner** und **Thomas Bourdel** bedanken ebenso wie bei unserem neuen Doktoranden **Bruno Zimmermann**.

**Alexander Frank** hat sehr professionelle Geräte für unsere Experimente gebaut und mir jede meiner oft dummen Fragen zu den Mysterien elektronischer Schaltungen beantwortet. Währenddessen hat **Veronica Bürgisser**, der „gute Geist“ der Gruppe, dafür gesorgt, daß die vielen Rechnungen bezahlt wurden und war nebenbei auch noch bei privaten Anliegen, wie z.B. der Wohnungssuche, mit Rat und Tat zur Stelle.

An dieser Stelle möchte ich auch **Markus Greiner** nochmals für die Pläne seiner Apparatur danken, von denen wir sehr profitiert haben, ebenso wie **Hans-Peter Bächler**, **Wilhelm Zwerger**, **Paivi Törmä**, **Selim Jochim** und vielen anderen für stimulierende Diskussionen und Erklärungen. Ich bin den Werkstätten der ETH sehr dankbar für ihre professionelle Unterstützung genauso wie **Jean-Pierre Stucki**, **Paul Herrmann** und **Hans-Jürg Gübeli** für ihre Hilfe bei der Laboreinrichtung.

Zuletzt und vor allem aber geht mein Dank an **Alexandra** und **meine Eltern** für ihre Unterstützung, Geduld und Anteilnahme.